Surface-dependent biodistribution and proinflammatory properties of semiconductor quantum dots

Marc Praetner
2014

Aus dem
Walter-Brendel-Zentrum für Experimentelle Medizin
der Ludwig-Maximilians-Universität München
Vorstand: Prof. Dr. med. Ulrich Pohl

Surface-dependent biodistribution and proinflammatory properties of semiconductor quantum dots

DISSERTATION

zum Erwerb des Doktorgrades der Medizin an der Medizinischen Fakultät
der
Ludwig-Maximilians-Universität zu München

vorgelegt von
Marc Praetner
aus München
2014

Mit Genehmigung der Medizinischen Fakultät der Universität München

1. Berichterstatter:	Prof. Dr. F. Krombach
Mitberichterstatter:	Prof. Dr. C. Kupatt Prof. Dr. D. Teupser Prof. Dr. J. Waschke
Mitbetreuung durch den promovierten Mitarbeiter:	PD Dr. M. Rehberg
Dekan:	Prof. Dr. med. Dr. h.c. M. Reiser, FACR, FRCR
Tag der mündlichen Prüfung:	20.11.2014

Summary

Methods based on nanotechnologies play a growing role in biomedical research. Quantum dots (QDs) are a group of engineered fluorescent nanoparticles suited for advanced imaging applications. The substitution of the particle's surface with defined molecular structures could enable the adoption as targeted contrast agents or therapeutic devices for a variety of clinical approaches. However, important aspects such as the basic surface-dependent behavior of non-targeted QDs in the organism and arising health effects upon systemic administration remain incompletely understood. Acute inflammatory effects for instance are often initiated on the microcirculatory level and are probably relevant for cardiovascular pathologies observed in epidemiologic and experimental studies of certain nanoparticles. Most *in vitro* studies show that the surface structures of QDs and other nanoparticles seem to be predominantly accountable for different cytotoxic effects and a variable potential to liberate proinflammatory cytokines. Currently, no systematic *in vivo* studies have addressed surface-dependent interactions of QDs on the level of the microcirculation and assessed the resulting impact on biokinetics as well as on proinflammatory parameters. Thus, this thesis aimed to i) analyze the incidence of QD-surface-dependent acute microvascular interactions and their influence on key biokinetic parameters and ii) investigate acute immunomodulatory effects on the multistep process of leukocyte recruitment *in vivo*. For this, three types of commercially available QDs with different surface modifications: carboxyl-QDs, amine- and polyethylene glycol-QDs (amine-QDs) and polyethylene glycol-QDs (PEG-QDs) were used. The physicochemical characterization was done by dynamic light scattering (DLS) analysis and microscale thermophoresis. In a first set of experiments, circulating half-lives, tissue distribution in different organs, and hepatic as well as renal clearance were measured. *Ex vivo* analysis of QD tissue distribution was performed on selected tissue samples via transmission electron microscopy (TEM) and two-photon microscopy. By combining *reflected-light oblique transillumination* (RLOT) and fluorescence *in vivo* microscopy of the murine *M. cremaster*, interactions of QDs with components of the microcirculation as well as leukocyte migration parameters were visualized and quantified. The extreme short circulating half-life of anionic carboxyl-QDs was related to pronounced clearance by the mononuclear phagocyte system. Beyond this, further investigations showed, for the first time, that the continuous capillary endothelium of skeletal and heart muscle tissue has the capacity to directly extract carboxyl-QDs from the circulation by means of caveolae-mediated endocytosis. Carboxyl-QDs were also taken up by perivascular macrophages in

the surgically exposed but not in the native *M. cremaster* and led to a significant increase of adherent and (subsequently) transmigrated leukocytes in this model. Further experiments provided evidence for a probable involvement of mast cells in the intercellular adhesion molecule-1 (ICAM-1)- and endothelial (E)-selectinmediated modulation of leukocyte recruitment. This process is most likely initiated by the endocytosis of carboxyl-QDs through activated perivascular macrophages. The primary activation of tissue-resident perivascular macrophages seems to be the consequence of tissue damage related to the surgical preparation of the cremaster muscle. This is supposedly a prerequisite for the endocytosis of carboxyl-QDs whereupon endothelial and mast cells seem to be secondarily activated in a paracrine fashion that then leads to an increase in leukocyte recruitment.

Zusammenfassung

Auf Nanotechnologien basierende Methoden spielen eine zunehmende Rolle in der biomedizinischen Forschung. Quantum dots (QDs) sind eine Gruppe künstlich hergestellter Nanopartikel mit speziellen Fluoreszenzeigenschaften, die im Rahmen zahlreicher bildgebender Verfahren eingesetzt werden können. Die Substitution der Partikeloberflächen mit definierten molekularen Strukturen könnte den Einsatz als zielgerichtete Kontrastsubstanzen oder Therapeutika im Hinblick auf eine Vielzahl klinischer Anwendungen ermöglichen. Unklar hingegen bleiben derzeit für den klinischen Einsatz wichtige Aspekte, wie etwa das prinzipielle oberflächenabhängige Verhalten von unspezifisch oberflächenmodifizierten, nicht auf distinkte molekulare Ziele ausgerichteten QDs im Organismus sowie mögliche gesundheitliche Folgen, die nach einer systemischen Applikation auftreten können. So liegen möglicherweise den durch gewisse Nanopartikel in epidemiologischen und experimentellen Studien beobachteten kardiovaskulären Pathologien unter anderem akute inflammatorische Effekte zugrunde, welche oftmals auf der Ebene der Mikrozirkulation initiiert werden. Die meisten *in vitro* Studien zeigen, dass insbesondere die Oberflächenstrukturen von QDs und anderen Nanopartikeln für unterschiedlich zytotoxische Effekte sowie ein variables Potential zur Freisetzung proinflammatorischer Zytokine verantwortlich zu sein scheint. Systematische *in vivo* Untersuchungen zu oberflächenabhängigen Wechselwirkungen systemisch applizierter QDs und proinflammatorischer Effekten auf Ebene der Mikrozirkulation und deren Bedeutung für biokinetische Größen liegen derzeit nicht vor. Die Ziele der vorliegenden Arbeit waren daher i) das Auftreten und die Bedeutung oberflächenabhängiger mikrovaskulärer Interaktionen von QDs und deren Beeinflussung biokinetischer Größen zu analysieren und ii) immunmodulatorische Effekte auf einzelne Schritte des mehrstufigen Prozesses der Leukozytenrekrutierung *in vivo* zu untersuchen. Hierzu wurden drei Typen kommerziell erhältlicher QDs mit jeweils unterschiedlichen Oberflächenmodifikationen (carboxylQDs, amine- und Polyethylenglykol-QDs (amine-QDs) und Polyethylenglykol-QDs (PEG-QDs) verwendet. Die physikochemische Charakterisierung der QD-Spezies erfolgte über die Analysetechniken der dynamische Lichtstreuung (DLS) sowie der mikroskalaren Thermopherese. In einer ersten Versuchsreihe wurden die Halbwertszeit im peripheren Blut, die Gewebeakkumulation in verschiedenen Organen sowie die hepatische und renale Ausscheidung quantifiziert. *Ex vivo* wurde die Verteilung der QD-Typen in verschiedenen Gewebeproben durch transmissionselektronenmikroskopische (TEM)

sowie 2-photonenmikroskopische Aufnahmen untersucht. Durch eine Kombination aus *reflected-light oblique transillumination* (RLOT)- und Fluoreszenz-Intravitalmikroskopie am murinen *M. cremaster* wurden in unterschiedlichen Versuchsansätzen die Interaktionen von QDs mit Komponenten der Mikrozirkulation sowie leukozytäre Migrationsparameter visualisiert und quantifiziert. Die extrem kurze Verweildauer von anionischen carboxyl-QDs in der systemischen Zirkulation stand mit einer ausgeprägten Clearance durch das mononukleäre Phagozytensystem in Zusammenhang. Darüber hinaus konnte in weiteren Untersuchungen erstmalig gezeigt werden, dass das kontinuierliche Endothel kapillärer Netzwerke in Skelett- und Herzmuskelgewebe die Kapazität zur direkten Aufnahme zirkulierender carboxyl-QDs in Form Caveolae-vermittelter Endozytose besitzt. Am präparierten aber nicht am nativen *M. cremaster* führte die Applikation von carboxylQDs zu deren Anreicherung in perivaskulären Makrophagen und einer signifikanten Zunahme adhärenter sowie (subsequent) transmigrierter Leukozyten. Weitere Versuchsreihen legen eine wahrscheinliche Beteiligung von Mastzellen an der intercellular adhesion molecule-1 (ICAM-1)- und endothelialen (E)-Selektinvermittelten Modulation der Leukozytenrekrutierung nahe. Höchstwahrscheinlich wird dieser Prozess durch die Endozytose der carboxyl-QDs durch perivaskuläre Makrophagen initiiert. Vermutlich ist die primäre Aktivierung perivaskulärer gewebeständiger Makrophagen eine Konsequenz der präparationsbedingten Gewebeschädigung des *M. cremaster*. Dies scheint eine Voraussetzung für die endozytotische Aufnahme der carboxyl-QDs zu sein, woraufhin Endothel- und Mastzellen sekundär infolge parakriner Mechanismen aktiviert werden, was eine gesteigerte Leukozytenrekrutierung zur Folge hat.

Table of figures

Eidesstattliche Versicherung

Praetner, Marc

Name, Vorname

Ich erkläre hiermit an Eides statt,

dass ich die vorliegende Dissertation mit dem Thema

SURFACE-DEPENDENT BIODISTRIBUTION AND PROINFLAMMATORY PROPERTIES OF SEMICONDUCTOR QUANTUM DOTS

selbständig verfasst, mich außer der angegebenen keiner weiteren Hilfsmittel bedient und alle Erkenntnisse, die aus dem Schrifttum ganz oder annähernd übernommen sind, als solche kenntlich gemacht und nach ihrer Herkunft unter Bezeichnung der Fundstelle einzeln nachgewiesen habe.

Ich erkläre des Weiteren, dass die hier vorgelegte Dissertation nicht in gleicher oder in ähnlicher Form bei einer anderen Stelle zur Erlangung eines akademischen Grades eingereicht wurde.

Ort, Datum

Unterschrift Doktorandin/Doktorand

I. INTRODUCTION

1. Background

The physicochemical properties of any given material may undergo quantitative as well as qualitative changes in a nonlinear fashion when a certain reduction in volume expansion is reached [1]. Despite advantages nanoparticulate substances can entail, concerns arose regarding the yet fragmentary understood behavior and potential toxicity within an environmental, therapeutic/diagnostic or occupational context [2-4]. Amongst other engineered nanoparticles, the classes of semiconductor quantum dot (QD) nanocrystals have attracted high scientific interest in multiple areas of basic as well as clinically oriented biomedical research [5].

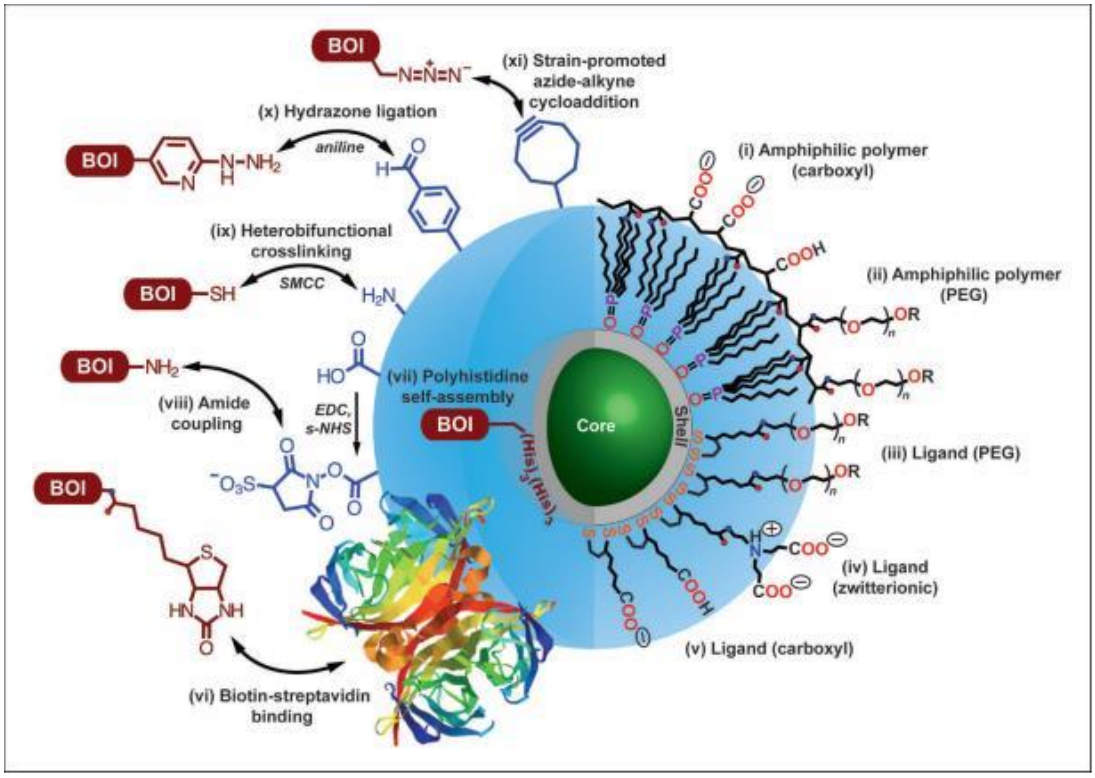

Figure 1 Illustrative overview of the chemistry of core-shell QDs

Coatings for aqueous solubility are as follows: (i) amphiphilic polymer coating with carboxyl(ate) groups; (ii) amphiphilic polymer coating with PEG oligomers; (iii) dithiol ligand with a distal PEG oligomer; (iv) dithiol ligand with a distal zwitterionic functionality; and (v) dithiol ligand with a distal carboxyl(ate) group. Common R groups include carboxyl, amine, and methoxy, although many others can be introduced (e.g., see vi, x, xi). Methods for conjugating biomolecules of interest (BOI) are as follows: (vi) biotin-streptavidin binding; (vii) polyhistidine self-assembly to the inorganic shell of the QD; (viii) amide coupling using EDC/s-NHS activation; (ix) heterobifunctional crosslinking using succinimidyl-4-(N-maleimidomethyl)cyclohexane-1-carboxylate (SMCC; structure not shown); (x) aniline-catalyzed hydrazone ligation; and (xi) strain-promoted azide–alkyne cycloaddition. The double arrows are intended to represent conjugation between the functional groups and, in principle, their interchangeability (not reaction mechanisms or reversibility). Not drawn to scale. **Figure and appending caption directly adapted from Petryayeva et al. [6].**

Prototypic QDs consist of a semiconductor nanocrystaline metalloid core structure in the size range of 1 to 10 nm which is capped by an additional semiconductor shell. The

wavelengths of emitted photons are a direct function of the nanoparticle size [7]. QDs display wide absorption and narrow size-tunable emission spectra, considerably high quantum yield and fluorescence values, pronounced photostability [8] and are significantly more resistant to photobleaching and chemical degradation [9] than conventional fluorescent dyes [10]. Target-oriented biological activation is enabled by modifying the particle surface. Additionally decorating the particle surface with basic functional chemical groups can enhance the solubility in aqueous media [11] and is the precondition for further linkage with selective bioactive molecules [12]. The broad use of QDs as fluorescent probes for biomedical applications in *in vivo* imaging derives from their superior optophysical performance for deep-tissue imaging compared to classic fluorophores [13, 14]. Abundant biological components strongly interfere with conventional fluorescence imaging by producing tissue autofluorescence, light absorption and light scattering, thereby impairing resolution, signal intensity, and the optical depth of penetration [15]. By the utilization of near-infrared emitting QDs, autofluorescence phenomena can be minimized and allow high signal-to-background [16]. A growing body of *in vitro* data suggests that unspecific low-molecular surface modifications alone can facilitate the activation of otherwise specific receptor-mediated pathways upon cellular contact *in vivo.* It is not always predictable how much of the particle-surface is still accessible to inadvertently occurring molecular interactions, even if the secondary targeting substance has been linked to the particle-surface. Under circumstances of insufficient conjugation or rapid degradation of the secondary targeting substance upon cellular ingestion and endolysosomal processing, QDs could exert unwanted or even adverse effects [17]. Nanoparticles immediately adsorb proteins in biological media, thereby forming a dynamic protein corona: a dynamic function of physicochemical particle characteristics and the surrounding biological environment [18]. However, when QDs are used as vascular contrast agents or for labeling of biological structures for *in vivo* imaging, they usually need to be directly injected into the blood stream [19-21]. The systemic administration of QDs for various purposes in a biomedical context inevitably subjects the vascular compartment with an initially high fraction of the applied dose [22]. Since the large internal surface area of the vascular system is mainly provided by the endothelial lining of the microcirculation, circulating QDs are particularly likely to interact with components of microvascular networks. As inflammatory reactions may play a central role in many nanoparticle-elicited cardiovascular effects observed after occupational or experimental exposure and given the fact that inflammatory reactions are often triggered on the level of the microcirculation [23], microvessels themselves are

eventually a critical anatomical location at which circulating or accumulated nanoparticles exert (adverse) biological responses [24].

2. Results and discussion

2.1. Physicochemical characterization and protein binding of QDs

Three types of commercially available QDs with a differently functionalized surface coating (Qdot® ITK™ carboxyl, Qdot® ITK™ amine (PEG), and Qdot® ITK™ nontargeted (PEG) (655 nm fluorescence peak emission) were chosen. The three subtypes investigated have an identical nuclear composition, a CdSe core ensheathed by an inner layer of ZnS. The outer layer and hence the particle-surface is provided by the respective chemical surface modification linked to the ZnS shell. According to the manufacturer, the QDs used in our studies all share an identical ellipsoid inorganic core with diameters of 6 nm (minor axis) by 12 nm (major axis) [25]. Using DLS and microscale thermophoresis, hydrodynamic diameters, polydispersity indices, and zeta potentials of each QD species in different solutions were measured. DLS calculates the hydrodynamic diameter of a given particle in aqueous solution by correlating detected dynamic changes in light scattering as a result of Brownian particle motion. So, mean values of hydrodynamic parameter, hydrodynamic peak distribution values, and the polydispersity index of the respective particle in solution can be determined [26]. This method is regularly used for particle characterization of QDs in aqueous media [27-32]. On the other hand, some investigators have questioned the accuracy of DLS for determination of physicochemical parameters of QDs, as engineered constructs with different constituents could influence the data obtained [17, 33]. In addition to that, DLS routinely uses the Stokes-Einstein equation to determine the diffusion coefficient of a spherical particle in aqueous solution. As QDs used in this study had a more elliptical configuration, confirmed by high-resolution transmission electron microscopy, the validity of this approximated formula on the accuracy of our measurements obtained by DLS was tested by additionally employing the method of Microscale Thermopheresis [34, 35]. This approach utilizes local mobility changes of QD concentrations in free solution upon the stimulation with an infra-red laser [35]. Hydrodynamic diameters measured with both methods are in good accordance with each other [28, 29]. The physicochemical values obtained here confirm the particle characterization measurements done by Zhang and Monteiro-Riviere, where QDs were scaled via size exclusion chromatography on high-performance liquid chromatography [17]. As a measure of unspecific protein binding affinity, hydrodynamic diameters of QDs were also assessed in protein-containing media (PBS + mouse serum) which approximate

the physiological environment QDs will encounter upon systemic administration. A gain in hydrodynamic diameter in mouse serum is interpreted to mirror the quantitative amount of protein adsorption on a particles' surface. PEGylation has been repeatedly shown to significantly reduce the amount of unspecific protein binding [36]. As expected, PEGQDs showed the lowest increase in hydrodynamic diameter. Carboxyl-QDs displayed the highest tendency to bind serum proteins. This also resulted in a reduction of absolute zeta potential negativity, possibly a consequence of protein shielding. Although the zeta potential, a "(…) measurable quantity used to control the intensity of the repulsive electrostatic interaction between the charged colloidal particles (…)" [37] is also related to the actual surface charge, those terms are not synonymous. This, as well as the fact that the effective number of terminal located positively charged amino-groups on amine-QDs might be reduced due to PEG-chain-entanglement, as hypothesized by Kelf et al. [38] can explain the moderately negative zeta potential values of amine QDs, similar to those of PEG-QDs. Quantitative and qualitative characteristics of the socalled protein corona built up around nanoparticles in biological media are thought to be chiefly involved in mediating particle behavior and biological impact [39].

2.2 Semiquantitative assessment of organ distribution and blood kinetics

Semiquantitative assessment of organ distribution and blood kinetics was done by establishing calibration curves with different concentrations of QDs. Solid tissue samples were solubilized and calibration curves were established for each tissue type as previously described by Robe et al. [40] with minor adaptions. Both organ distribution and blood kinetics were analyzed by relating the fluorescence intensity value measured in the respective sample to the corresponding calibration curve established earlier. PEGQDs had a considerably long circulating half-life of 513.4 ± 152.1 min upon systemic application. Many studies have shown that PEG exhibits a stealth effect as it shields the decorated material from opsonization. So, the typically observed rapid clearance of circulating nanoparticles via the mononuclear phagocytic system is circumvented and the blood half-life significantly prolonged [41]. Accordingly, a lower overall tissue deposition profile was found compared to carboxyl- and amine-QDs. Carboxyl-QDs had a very low resident time in the circulation, the blood half-life was 5.8 ± 0.4 min. In an early imaging study by Ballou et al., the circulating half-life of carboxyl-modified 655 nm emitting QDs (QD655) was determined to be 4.6 ± 1.0 min [42]. The QDs were purchased from the same commercial provider and therefore identical to the carboxylQDs used in our studies. Amine QDs in our study exhibited a mean residence time in the circulation of 29.0 ± 2.8

min. The semiquantitative measurements of QD bloodkinetics were comparable to the real-time decay of QDs fluorescence out of the cremasteric vascular system observed by *in vivo* fluorescence microscopy. The blood kinetics of QDs were determined by the analysis of consecutively obtained blood samples applying a fluorescence-based imaging system. Organ distribution of QDs was analyzed after perfusion with ice-cold ringer solution by inserting a catheter in the jugular vein to wash out the remaining blood in the organ vascular system. The remaining blood pool within an extracted organ adulterates the quantitative value of organ-specific accumulation expressed as percentage of the injected dose (% ID)/g tissue. This could lead to a substantial overestimation of the actual tissue-specific deposition [43]. On the other hand, Su and Sun have pointed out that rheological effects of systemic perfusion could also wash out QDs residing in the extravascular space or those being only loosely attached to cellular surfaces [44]. It suggests itself to exploit the QDs inherent fluorescence for quantification of their biokinetics. However, next to fluorescence-based quantification approaches, the biodistribution of QDs can be determined by coupling the particle with a radioactive tracing compound [45] or applying inductively coupled plasma-mass spectrometry (ICP-MS) for element analysis. Fluorescence-based quantification techniques work on the assumption that the fluorescence intensity values measured are a direct function of the QD concentration. It has been argued that the validity may be weakened by the variability of background fluorescence in biological samples [46], compartment-derived fluorescence intensity changes, and fluorescence decay in the course of structural degradation or aggregation [47, 48]. We therefore cannot positively rule out that our fluorescence-based measurements of QD-concentrations in biological samples might be affected by e.g. fluorescence quenching due to unspecific surface defects or as a result from intracellular vesicular compartmentalization [49]. However, for the time being, there is no overwhelming evidence for substantial chemical *in vivo* dissolution of the customized QDs we used reported in the literature [50].

2.3 Association of QDs with the capillary vascular endothelium

Within the time course similar to the calculated half-life, the clearance of circulating carboxyl-QDs in the cremasteric microcirculation revealed that the endothelial lining of the capillary network remained continuously and exclusively fluorescent. CarboxylQDs were also weakly and more irregularly associated with the endothelial layer of postcapillary venules but practically absent in precapillary vessel segments. The first order clearance-kinetics of nanoparticles in the circulation are generally attributed to

either the mononuclear phagocyte system (phago-/endocytosis due to opsonization with serum proteins [51]) or renal filtration (relevant for nanoparticles with hydrodynamic diameters > 5.5 nm [52]). Lee and colleagues were probably the first to demonstrate a possible link between coating-dependent differences in the biodistribution of QDs and the occurrence of interactions with the vascular system in a more complex *ex vivo* tissue model. Neutral QDs decorated with polyethylene glycol (QD-PEG) or negative QDs decorated with carboxyl-groups (QD-COOH) with a hydrodynamic size of approximately 40 nm were used [53]. Quantitative tissue deposition was assessed after intra-arterial infusion of QD-PEG or QD-COOH in media for 4 h at different concentrations (1.67, 3.33 and 6.67 nM, respectively) into isolated perfused porcine skin flaps harvested from Weanling Yorkshire pigs, followed by a 4-h wash-out phase (perfusion with media solely). QDs were quantified in arterial and venous media via fluorescence intensity as well as ICP-MS. Frozen skin flap sections were prepared for confocal microscopy and hematoxylin/eosin staining. The differences in arterial-venous fluorescence values for QD-COOH were significantly higher than those obtained for QD-PEG, indicating a stronger tissue deposition of QD-COOH. Confocal microscopy analysis of frozen tissue sections further showed that QD-COOH accumulated in the capillaries of the skin [54]. The occurrence of capillary endothelial cell-mediated clearance of carboxyl-QDs from the circulation in our experiments has also been verified in the myocardium and skeletal muscle tissue of the abdominal wall by *ex vivo* 2-photon microscopy.

2.4 *In vitro* uptake of QDs

Confocal microscopy and flow cytometry analysis of cultured human microvascular endothelial cells exposed to carboxyl-QDs show a high amount of endocytotic uptake and intracellular accumulation in terms of vesicular storage. The endothelial layer of the human cardiovascular system is estimated to cover a total luminal surface area of approximately 350 m^2 [55]. Although the entirety of endothelial cells builds up a coherent epithelial monolayer, this cellular population is not homogeneous but shows considerable adaptive differences by means of morphology and functional features. The anatomical location within the vascular tree determines dissimilar and eventually changing rheological parameters, the composition of subintimal tissues, exposure towards signaling factors, nutrients, and many more micro-environmental differences significantly influencing the endothelial cellular phenotype [56]. TEM confirmed that carboxyl-QDs were internalized into capillary endothelial cells by caveolae-mediated endocytosis. Caveolae are cellular invaginations which belong to the class of glycolipid raft membrane

domains defined by the co-localization with the protein caveolin-1 [57]. Endothelial cells of non-fenestrated continuous capillaries in lung, skeletal and heart muscle tissues show by far the highest density of caveolae [58]. Caveolae of continuous capillary endothelial cells are morphological and functional distinct microdomains implicated in a variety of endocytotic pathways. Caveolae-mediated receptor-dependent endocytosis of albumin [59], insulin [60], and α1-acidic glycoprotein [61] is a specific function of the continuous capillary network. Scavenger receptors (SRs) have been shown to concentrate within these specialized lipid-domains [62]. The human plasma proteome is presently reported to consist of 1929 different proteins [63] under which albumin is the most abundant protein. Since endothelial caveolae account for the specific receptor-mediated uptake and/or transcytosis of endogenous plasma proteins but also recognize intrinsic macromolecules with an altered structure, a possible relation between the pronounced adsorption of serum proteins to carboxyl-QDs or their intrinsic structural properties and their selective association with the capillary endothelium of skeletal and heart muscle tissue could exist. There is a limited amount of *in vitro* studies available which specifically provide mechanistic insights into principal modes of surface-related QDs cellular uptake. A number of limitations should be considered when the results obtained *in vitro* are transferred to an *in vivo* scenario. These include a great heterogeneity regarding QD synthesis, core structure, surface chemistry, dosage, cell lines, incubation time, and culture media. Zhang and Monteiro-Riviere specifically addressed the *in vitro* endocytosis of carboxyl-QDs (QD655-COOH) from the same commercial source and identical to those we used in our in experiments. QD655-COOH were rapidly internalized by cultured human epidermal keratinocytes within 5 min after application. The involvement of caevolin-1 and competitive binding with cholera toxin B indicated a lipid raft/caveolae-mediated mechanism of endocytosis. The surfacedependent specificity of binding and internalization led the authors hypothesize that QD655-COOH nanocrystals initialize a receptor-mediated endocytotic pathway [17]. The effects exerted by the inhibitors of SRs, polyinosinic acid and fuicodan, argue for their role in QD655-COOH-mediated endocytosis. Interestingly, both low-density lipoprotein (LDL) and acetylated low-density lipoprotein (AcLDL) dose-dependently competed with QD655-COOH-mediated endocytosis in coincubation experiments. Thus, the authors conclude a combined mechanism of clathrin-independent receptormediated endocytosis involving a LDL receptor/SRBI-pathway [17]. In a study by Fujivara et al., the endocytosis of anionic liposomes by cultured macrophages was investigated. The involvement of SRs was proofed in cross-experiments in which preincubation with poly(acrylic acid) (PAA)-

coated liposomes reduced the uptake of AcLDL, dextran sulfate as well as maleylated-bovine serum albumin. Also LDL, being no specific ligand of SRs, partially inhibited PAA-liposome uptake [65]. In an *in vitro* study by Xiao et al. the uptake mechanisms of the very same three QD-species used in our studies were assessed in two human epithelial cell lines. Solely QD655-COOH but neither amine-PEG nor PEG-QDs were internalized after a 12 h incubation period. As QDs were recovered in lysosomes, the authors hypothesize a clathrin-dependent mode of internalization [66]. Different results were reported by the group around Al-Hajaj N. et al. who investigated the endocytosis of different semiconductor QDs. The cationic QDs showed a generally higher rate of cellular internalization as assessed by spectrofluorometric analysis. Despite ligand- and cell-specific differences, lipid-raft mediated endocytosis was identified as the common mechanism of internalization [67]. In our own experiments, endocytosis of QDs by murine macrophages was analyzed 15 min after *in vitro* incubation. Confocal laser-scanning microscopy showed that carboxylQDs were highly endocytosed and found in cytoplasmatic vesicles. Mean fluorescence intensity (MFI)-values were approximately 50 times higher for macrophages challenged with carboxyl-QDs compared to those obtained for amine-QDs and PEG-QDs. Clift et al. also observed a principally more rapid internalization of carboxyl-modified QDs with a 565 nm (QD565) emission-spectrum in comparison to amine-modified QD565. However, co-localization of carboxyl-QDs with the early endosomal marker 1 was not noticed before 30 min of *in vitro* incubation [68]. This is comparatively slow when compared to our *in vitro* uptake rates but may be explained by strain differences and other culture conditions. Some SRs have been specifically localized to endothelial caveolae of microvascular networks. A high expression of both caveolin and CD36 in the murine lung, heart, and skeletal muscle-tissue is reported. The majority of caveolinrich domains containing CD36 is provided by the capillary endothelial lining due to the large surface area occupied; especially in heart and muscle tissue, whereas the lung epithelial tissue, mainly consisting of type I pneumocytes, accounts for probably 50% of the total amount of lung caveolae [62]. Other (micro)vascular SRs include lectin-type oxidized LDL receptor-1 [69], SR-BI [70], receptor for advanced glycation endproducts [71], collectin placenta 1 [72], SR expressed by endothelial cells-I [73], fasciclin EGF (endothelial growth factor)-like, laminin-type EGF-like, and link domain-containing SR-1 (FEEL-1) and FEEL-2 [74].

2.5 Clearance of carboxyl-QDs by capillary endothelial cells

In conclusion, our data can describe the capillary endothelial network of skeletal and heart muscle tissue as an arborescent nonphagocytic functional entity with the yet underestimated ability to reduce the systemic bioavailability and influence the tissue deposition of carboxyl-modified QDs in addition to the clearance via the mononuclear phagocyte system. The entirety of skeletal muscle tissue in mice and man averages approximately 45 % of the total body weight [75, 76]. In our study, we found that upon systemic injection of carboxyl-QDs, 2.4 ± 0.2 % ID/g tissue were recovered after 1 h in skeletal muscle tissue. At this point due to complete clearance, no more circulating carboxyl-QDs are detectable in the blood stream. An almost exclusive staining of the capillary endothelial network was detected. Ultrastructural analysis reveals a caveolaemediated endocytosis of carboxyl-QDs within the capillary networks of skeletal muscle. We therefore conclude that, next to the clearance by the mononuclear phagocytic system, the capillary endothelial lining of the murine skeletal muscle system has a significant impact on the biokinetics of carboxyl-QDs by means of active capillary retention of approximately 26 % of the applied dose.

2.6 Modulation of leukocyte rolling *in vivo* by PEG- and carboxyl-QDs

The leukocyte recruitment cascade is usually initiated by transient interactions between leukocyte and endothelial surfaces. Capture and subsequent rolling of leukocytes on the luminal surface of vascular endothelial cells are mediated by a family of three single chained carbohydrate-recognizing transmembrane glycoproteins, namely E-, platelet (P)-, and lymphocyte (L)-selectin [77]. Overlapping as well as distinct functions of these C-type lectins for leukocyte recruitment *in vivo* have been scrutinized over the last two decades. The expression of E-selectin is limited to endothelial cells and upregulated upon cytokine-induced endothelial activation [78]. P-selectin on the other hand is also expressed in resting endothelial cells where it is stored in Weibel-Palade bodies and rapidly translocated to the endothelial surface by fusion of P-selectin-containing storage vesicles with the cellular membrane after endothelial activation. In the mouse cremaster model, tissue exteriorization-induced early leukocyte rolling in postcapillary venules via P-selectin is a direct consequence of this process [79]. L-selectin is constitutively expressed on many leukocyte subsets, contributes to leukocyte recruitment during inflammation, and is critically involved in lymphocyte binding to high endothelial venules [80]. Leukocyte rolling flux fraction after dosing with carboxyl- or amine-QDs did not differ from vehicle-treated control animals but was significantly increased upon

application of PEG-QDs. *In vivo* fluorescence microscopy showed a discontinuous staining of postcapillary venules suggesting local clustering of PEG-QDs. Electron microscopy analysis revealed that PEG-QDs associate with amorphous, probably lipid containing structures adjacent to the luminal side of or in between microvascular endothelial cells. Next to reducing unspecific protein binding, this polymer also acts as a fusogen of biological membranes [81]. Given the rapid onset of the PEG-QD-elicited increase in leukocyte rolling flux fraction, it can be speculated that clusters of PEG-QDs may lead to distortions of the endothelial membrane structure, eventually promoting the fusion of intracellular vesicles and possibly Weibel-Palade bodies in close proximity to the luminal surface with the outer membrane, thereby increasing the amount of Pselectin on the endothelial surface. PEG-QDs do not further influence leukocyte adhesion and transmigration. It could also be the case that the extracellular PEGQD/lipid-clusters facilitate leukocyte rolling but impede the formation of firm molecular contacts between leukocytes and the actual endothelial surface. Although no changes in the number of rolling leukocytes in postcapillary venules were detected, a significant reduction of leukocyte rolling velocity was observed at 45 and 60 min after application of carboxyl-QDs. Hence, intensified bidirectional signaling events can occur, thereby promoting further steps of leukocyte recruitment [82]. The involvement of E-selectin is mandatory for cytokine-induced slow leukocyte rolling in postcapillary venules *in vivo* [83].

2.7 Engagement of E-selectin in modulation of leukocyte recruitment by carboxyl-QDs *in vivo*

E-selectin exerts its functions via three glycoprotein-ligands expressed on neutrophils: P-selectin glycoprotein-ligand 1, E-selectin ligand 1 and CD44 [84]. E-selectinmediated leukocyte-endothelial interactions functionally activate lymphocyte functionassociated antigen 1 (LFA-1), a ß2-integrin expressed on leukocytes, by converting the molecular structure towards an intermediate-affinity state facilitating binding to endothelial ICAM-1. Thus, slow leukocyte rolling also involves LFA-1/ICAM-1 interactions. Interestingly, leukocyte rolling velocities on P-selectin in autoperfused flow chambers are comparable to those observed on E-selectin when ICAM-1 is added to P-selectin [85]. Also macrophage receptor-1 has been described to contribute to slow rolling by interacting with endothelial ICAM-1 [86]. E-selectin-promoted slow leukocyte rolling is typically characterized by rolling velocities ~5 µm/s [83] whereas P-selectin-dependent leukocyte rolling velocities are in the range of ~35 µm/s [87].

However, rolling velocities ≤5 µm/s in the mouse cremaster assay are usually observed within at least two hours following the intrascrotal injection of proinflammatory cytokines

[83] since the expression of E-selectin is regulated on the transcriptional level requiring *de novo* synthesis. Therefore, the full amount of E-selectin engagement within the 60 min observation window in our studies is unlikely to be registered since the peak expression of E-selectin following endothelial activation has been shown to occur after ~6h [88, 89]. Nevertheless, the observed reduction in leukocyte rolling velocity as early as 45 min after injection of carboxyl-QDs seems to reflect an increasing availability of E-selectin on the postcapillary endothelial surface as a consequence of enhanced expression of E-selectin. This was confirmed by confocal immunofluorescence microscopy of E-selectin in postcapillary venules 60 min after application of carboxylQDs. The expression of E-selectin is controlled by proinflammatory cytokines. Wellinvestigated cytokines which have been shown to exercise control on the endothelial expression of E-Selectin in a direct and/or intermediate fashion include tumor necrosis factor-alpha (TNF-α), interleukin-1 beta (IL-1ß), lipopolysaccharide (LPS) [90], interleukin (IL)-6, interferon gamma [91], and macrophage inflammatory protein-2 (MIP-2) [92]. As the functional consequence, i.e. significant reduction in leukocyte rolling velocity upon systemic application of carboxyl-QDs was paralleled by a considerably fast upregulated expression of E-Selectin in postcapillary venules, it is likely to assume that a very rapid chemokine-driven mode of postcapillary endothelial activation precedes this event. Although proinflammatory cytokines themselves underlie transcriptional regulation, rapid endothelial activation can be achieved by the release of pre-synthesized cytokines which enables immediate transcellular communication.

2.8 Preparation-induced activation of perivascular macrophages is necessary for the uptake of carboxyl-QDs and further events leading to a modulation of leukocyte recruitment *in vivo*

Given the temporary dynamics observed, the immunomodulatory properties following the acute challenge of carboxyl-QDs in the microcirculation of the surgically exposed cremaster muscle most likely reflects a secondary endothelial activation in succession of the local liberation of pre-synthesized chemokines. The fact that no significant changes in leukocyte recruitment were noted when carboxyl-QDs were injected 60 min *prior* to surgical preparation of the cremaster muscle gives some important hints regarding the hypothetical pathways carboxyl-QDs might influence the leukocyte recruitment cascade. To begin with, the presence of carboxyl-QDs in the systemic circulation apparently does not seem to provoke an acute systemic inflammatory response at the dosage tested. This assumption is supported by the lack of quantitative alterations in leukocyte recruitment in

the cremaster muscle when surgical exposure was done at 60 min after systemic administration. No changes in white blood cell counts and no apparent signs of discomfort or illness were observed. Interestingly, dose- and chargedependent acute toxicity and prothrombotic effects of Catskill green, carboxyl- or amine-modified QDs (Type I EviTags) were observed in a study conducted by Geys et al. A dose-dependent potency to induce fibrin-rich thrombi in the pulmonary circulation was noted for both QD types, but more pronounced in the case of carboxyl-QDs [31]. In our experiments no obvious prothrombotic events were noticed, however, we did not assess this systematically. Moreover, no carboxyl-QDs were found in perivascular cells of the native cremaster muscle. Thus, the merely contact of circulating carboxyl-QDs with the postcapillary endothelium of the cremaster muscle does not seem to directly activate endothelial cells in the absence of preparation-induced tissue injury. A mild sterile inflammatory response to microsurgical tissue manipulation and exteriorization of the cremaster muscle is a well-known model-inherent phenomenon. Sterile alterations of tissue integrity in the absence of pathogens or toxins etc. still lead to inflammatory reactions as a result from the endogenous release of different signals from cells experiencing stress, lesions, or necrosis [93]. Normally hidden endogenous molecules, which are liberated when the structural integrity of a tissue is destroyed and subsequently activate innate immunological responses, are termed "damage-associated molecular patterns" (DAMPs). The recognition of these normally sequestered DAMPs by corresponding receptors on innate immune cells leads to their activation and initiation of further inflammatory reactions [94]. In macrophages, the nucleotidebinding oligomerization domain (NOD)-like receptor family, pyrin domain containing 3
(NLRP3) inflammasome reacts on a broad variety of "pathogen-associated molecular patterns" (PAMPS) and DAMPs and exerts important functions, also in sterile inflammation upon tissue injury. The full activation of the NLRP3 inflammasome obviously requires initial priming via pattern recognition receptor-signaling which seems to be a necessary step preceding the induction of complete activation [95]. Wellestablished DAMPs include extracellular nucleotides, extracellular heat shock proteins, extracellular high-mobility group protein B1, uric acid crystals, oxidative stress, laminin, S100 proteins, and hyaluronan [96]. With regard to immune effects of engineered nanoparticles, it has been observed that protein adsorption to nanoparticles can lead to conformational changes and subsequent exposure of cryptic epitopes. The hypothesis that the activation of pattern recognition receptors by DAMPs on tissueresident cells with

innate immunity function is required for activating perivascular macrophages to take up carboxyl-QDs is supported by the following: Intrascrotal application of LPS 2 h prior to systemic application of carboxyl-QDs caused a strong accumulation of carboxyl-QDs in perivascular cells independent of the surgical preparation. Vehicle-treated controls did not show an accumulation of carboxyl-QDs in perivascular cells (Praetner and Rehberg, unpublished observations).

2.9 Endocytosis of carboxyl-QDs by perivascular macrophages *in vivo*

I*n vivo*, MFI-values of regions of interest over perivascular macrophages visibly increased already 180 sec after systemic application of carboxyl-QDs in our study [29]. When antigen-presenting cells are stimulated *in vitro* towards an active state, this usually includes a more efficient endocytosis and might go along with a different morphology. For instance, Zhang et al. reported an increased uptake of QD655-COOH by dendritic cells after treatment with LPS. *In vitro* activated dendritic cells (derived from porcine monocytes matured in the presence of granulocyte-macrophage colonystimulating factor and IL-4 preferentially ingested carboxyl-QDs by rapid clathrindependent scavenger-mediated endocytosis involving F-actin as well as phospholipase C [33]. Interestingly, Bateman et al. made a similar observation in an *in vivo* study where a model of endotoxemia increased the clearance of methoxy-PEGylated 5000MW QDs [97]. Liver sinusoidal fenestrated endothelium provides Kupffer cells and hepatocytes excellent opportunities to come into contact with circulating QDs. Also splenic macrophages, which are situated in an open circuit environment, are in a different activation state compared to macrophage populations in tissues which are normally shielded from the external surrounding [98]. In the case of skeletal muscle perivascular macrophages in our model, preparation-induced activation by DAMPs seems to be a prerequisite for the induction of a highly active endocytotic phenotype. *In vitro* activated dendritic cells preferentially ingest carboxyl-QDs by rapid clathrindependent scavenger-mediated endocytosis [33]. Vessel-lining macrophages have been reported to extend cytoplasmatic protrusion through endothelial and epithelial tissues [99]. Recently, perivascular CX3C chemokine receptor 1^{+}-cells were shown to sample the luminal content of adjunct microvessels via a dendritic extension *in vivo* [100]. The basement membrane of the postcapillary endothelial cell lining is surrounded by a heterogeneous population of perivascular cells of the myeloid lineage, including cells which mediate innate immunity responses [101]. Particle uptake in our model probably leads to secretion of cytokines and parallel activation of mast cells and endothelial cells.

2.10 Nanoparticle-induced release of proinflammatory cytokines *in vitro* – insights from the literature

Ryman-Rasmussen et al. analyzed the cellular uptake of commercially available QD 565 and QD655 semiconductor nanocrystals with the identical three different surface functionalizations utilized in our studies. All types of QDs investigated were found inside primary human neonatal epidermal keratinocytes (HEK) 24 h after incubation. Carboxylic-acid-coated QDs of both sizes showed the highest degree of stained HEKs. TEM revealed that all QD-types were either found agglomerated within vesicular structures or free in the cytoplasm. The most pronounced cytotoxicity was found upon challenge with carboxylic-acid coated QDs. Carboxyl-acid coated QDs of both sizes also showed a significant release of IL-1ß. The IL-6 release was significantly higher for carboxylic-acid coated QD565 particles. A significant release of IL-8 was detected for carboxylic-acid coated QD565 particles. PEG-amine QDs of both sizes induced cytotoxicity 48 h after incubation (20 nM). Also, PEG-amine-QDs induced a significant increase in the release of IL-6 after incubation with 20 nM after 48 h. No change in the release of proinflammatory cytokines was detected in the case of PEG-QDs [25]. Adachi et al. showed that 20-nm but not 1000-nm particles induced a IL-1ß response which involved the adenosine triphosphate-binding P2X purinoceptor 7 [102]. In a study by Fischer et al, octadecylamine-modified poly(acrylic acid)-coated QDs caused an increase in TNFα levels, but not high enough to reach statistical significance [103]. Zhang Y. et al. observed that exposure to PAA-coated QDs in a macrophage cell line led to high concentrations of TNFα and IL-1ß after 24 h and activation of the nuclear factor kappa-light-chain-enhancer of activated B cells-pathway [32]. Adherence, as the next step in the leukocyte recruitment cascade, is characterized by firm adhesion at the postcapillary endothelium, mediated by the interaction of leukocyte integrins and an endothelial receptor of the immunoglobulin superfamily [104]. ICAM-1 is a member of the immunoglobulin superfamily and constitutively expressed on postcapillary endothelial cells under physiologic conditions [105].

2.11 ICAM-1 plays a functional role for carboxyl-QD-elicited modulation of leukocyte recruitment *in vivo*

To further understand the mechanisms of carboxyl-QD elicited modulation of leukocyte recruitment, we used a specific anti-ICAM-1 monoclonal antibody (YN-1) in additional experiments. A significant reduction of adherent as well as transmigrated leukocytes in the YN-1-treated group was noted. These results suggest that ICAM-1 is a central

adhesion molecule for the carboxyl-QD evoked amplification of leukocyte recruitment in the cremaster muscle. Interestingly, Foy and Ley demonstrated a central role of ICAM-1 for chemoattractant-induced acute leukocyte adhesion following perivenular microinjection to the unstimulated postcapillary endothelium [106]. It was shown that MIP-2-induced neutrophil recruitment is mediated by TNF-α from resident mast cells. Contrasting to TNF-α, the expression of E-selectin upon challenge with MIP-2 was increased in wild type mice but not in mast cell-deficient animals [92]. In a study by Kneilling et al., it was found that local tissue inflammation in a mouse model of T-cellinduced and TNF-dependent delayed-type hypersensitivity reaction strictly requires a direct crosstalk between mast cell-derived TNF and TNF-receptor-expressing endothelial cells, subsequently leading to upregulation of adhesion molecules necessary for leukocyte recruitment such as E- and P-selectin, ICAM-1, and vascular cell adhesion molecule 1 [107].

2.12 Mast cells contribute to the carboxyl-QD-induced modulation of leukocyte recruitment *in vivo*

Mast cells origin from a hematopoietic lineage and are characterized by the large number of densely packed cytoplasmatic granules containing a variety of preformed inflammatory mediators which are rapidly released upon activation. Mast cells are found in most tissues, often in close vicinity to epithelial or vascular structures. Mast cells are being increasingly recognized as central effectors and regulators of macrophage, dendritic, and endothelial cell function during inflammatory responses [108]. Apparently, mast cells distinguish themselves from other innate immunity cells in the way that they appear to be the main source of preformed TNF-α, which can therefore be immediately released upon corresponding activation [109]. Also, a rapid release of eicosanoid mediators adds to the fast acting mode of mast cells [110]. The anatomical distance between mast cells and venular basement membrane probably averages 10 μm as estimated by *in vivo* microscopy of the mouse cremaster muscle [111]. To investigate whether mast cells are involved in carboxyl-QD-evoked modulation of leukocyte recruitment, the effect of cromolyn-pretreatment was assessed in an additional set of experiments. Cromolyn is a member of mast cell-stabilizing agents which are thought to prevent mast cell degranulation. However, the specificity of cromolyn to act solely on mast cells has recently been questioned [112]. Species-, tissue-, and model-inherent differences might influence the specificity of mast cellstabilizers.

3. Author contributions

The author of this thesis contributed to the original, peer-reviewed publication "**The contribution of the capillary endothelium to blood clearance and tissue deposition of anionic quantum dots in vivo." (*Biomaterials. 2010 Sep;31(26):6692-700)*** by i) participating in conceiving of the study and its design ii), writing the manuscript, iii) performing the majority of animal experiments and iv) participating in data analysis and statistics.

The author of this thesis contributed to the original, peer-reviewed publication **"Quantum dots modulate leukocyte adhesion and transmigration depending on their surface modification." *(Nano Lett. 2010 Sep 8;10(9):3656-64.)*** by i) participating in conceiving and designing the study, ii) performing the majority of animal experiments, iii) participating in data analysis and statistics and iv) writing parts of the manuscript.

II. CUMULATIVE THESIS

1. The contribution of the capillary endothelium to blood clearance and tissue deposition of anionic quantum dots in vivo:

Biomaterials 31 (2010) 6692–6700

Contents lists available at ScienceDirect

Biomaterials

journal homepage: www.elsevier.com/locate/biomaterials

The contribution of the capillary endothelium to blood clearance and tissue deposition of anionic quantum dots *in vivo*

Marc Praetner [a], Markus Rehberg [a], Peter Bihari [a], Max Lerchenberger [a], Bernd Uhl [a], Martin Holzer [a], Martin E. Eichhorn [a,b], Robert Fürst [d], Tamara Perisic [a], Christoph A. Reichel [a], Ulrich Welsch [c], Fritz Krombach [a,*]

[a] *Walter Brendel Centre of Experimental Medicine, Ludwig-Maximilians-Universität München, Munich 81377, Germany*
[b] *Department of Surgery, Klinikum der Universität München, Munich, Germany*
[c] *Department of Anatomy, Ludwig-Maximilians-Universität München, Munich, Germany*
[d] *Munich Center for System-Based Drug Research, Department of Pharmacy, Pharmaceutical Biology, Ludwig-Maximilians-Universität München, Munich, Germany*

ARTICLE INFO

Article history:
Received 22 April 2010
Accepted 20 May 2010
Available online 17 June 2010

Keywords:
Quantum dots
Nanoparticles
Surface modifications
Blood kinetics
In vivo microscopy
Microcirculation

ABSTRACT

The increasing interest in biomedical applications of semiconductor quantum dots (QDs) is closely linked to the use of surface modifications to target specific sites of the body. The immense surface area of vascular endothelium is a possible interaction platform with systemically administered QDs. Therefore, the aim of this study was to investigate the microvascular distribution of neutral, cationic, and anionic QDs *in vivo*. QDs with carboxyl-, amine- and polyethylene glycol surface coatings were injected into the blood circulation of mice. *In vivo* microscopy of the cremaster muscle, two-photon microscopy of skeletal and heart muscle, as well as quantitative fluorescence measurements of blood, excreta, and tissue samples were performed. Transmission electron microscopy was used to detect QDs at the cellular level. The *in vitro* association of QDs with cultured endothelial cells was investigated by flow cytometry and confocal microscopy. Anionic QDs exhibited a very low residence time in the blood stream, preferably accumulated in organs with a prominent mononuclear phagocytic component, but were also found in other tissues with low phagocytic properties where they were predominantly associated with capillary endothelium. This deposition behavior was identified as a new, phagocyte-independent principle contributing to the rapid clearance of anionic QDs from the circulation.

1. Introduction

Over the last few decades, efforts to directly manipulate matters at an ultrastructural level culminated in the multidisciplinary fields of nanotechnologies. Due to numerous unique physicochemical features [1], a high potential for the clinical utilization of nanomaterials is discussed [2]. Among other nanomaterials, a subset of engineered nanocrystals known as semiconductor quantum dots (QDs) seem to be promising candidates for clinical purposes [3]. Nanomaterial formulations with quantum dots carry convincing attributes for new or advanced uses in several medical applications including photodynamic therapy [4,5], drug delivery [6,7], and versatile imaging purposes [8–12]. Based on their outstanding tunable optophysical properties, they have attracted the attention of biomedical researchers and clinicians interested in new tools for diagnostics and targeting of specific sites in the body.

Lessons learned from earlier studies on the *in vivo* performance of liposomes, microbubbles, and various nanoformulations [13–15] provided the foundation for a deeper understanding of the *in vivo* behavior of QDs. Recent studies have confirmed previous observations that organs with a prominent mononuclear phagocyte system such as liver and spleen are chiefly responsible for the clearance of QDs after administration into the blood stream [16,17]. Moreover, the conjugation of polyethylene glycol (PEG) derivates to the QD-surface has been verified to significantly prolong the circulation half-life resulting in an expanded imaging window for *in vivo* applications [18–20].

Since the visualization of the vasculature *in vivo* is both important for clinicians and biomedical researchers, most works involving QDs focus on their use as angiographic probes [21,22] and do not assess possible interactions with the endothelial surface itself. With respect to the fact that most *in vivo* approaches require a systemic

* Corresponding author.
E-mail address: krombach@med.uni-muenchen.de (F. Krombach).

0142-9612/$ – see front matter © 2010 Elsevier Ltd. All rights reserved.
doi:10.1016/j.biomaterials.2010.05.051

application of QDs, surprisingly little is known about the binding kinetics of surface-modified QDs to the vascular endothelium [23]. Particularly, the microvascular branch of the vascular system offers an enormous surface area for interactions with nanoparticles. The capillary networks as well as pre- and postcapillary vessels form an interrelated complex entity which plays a fundamental role in numerous regulatory, metabolic, and immunologic functions.

Especially with regard to recent improvements in microvascular imaging for pathophysiological research and bedside applications as well as progress towards clinical applications of QDs [24], an evaluation of possible interactions with the microcirculation is clearly indicated [25–27]. Up to now, the binding kinetics of differently charged QDs to microvascular endothelium *in vivo* has not been systematically analyzed. Here, we assessed the impact of carboxyl-, amine-, and PEG-surface modifications on i) plasma kinetics, ii) microvascular distribution, iii) tissue deposition, and iv) excretion of QDs in a whole animal study.

2. Materials and methods

2.1. Particles

Qdot® ITK™ carboxyl, Qdot® ITK™ amine (PEG), and Qdot® ITK™ non-targeted (PEG)quantum dots (655 nm fluorescence peak emission) were purchased from Invitrogen Cooperation, Karlsruhe, Germany. Carboxyl – (8 μM), amine – (8 μM) and PEG-QDs (2 μM) are provided in a 50 μM borate buffer. These QDs consist of a semiconductor CdSe core encapsulated with a ZnS shell and an additional layer of either polyethylene glycol only (PEG-QDs), polyethylene glycol with an amine coating (amine-QDs), or carboxyl functions solely (carboxyl-QDs). The PEG coating itself consists of short oligomers with a molecular weight of 1–3 kDa. Batches were stored at 4 °C and consumed within 4 weeks.

2.2. Physical characterization of QDs

Carboxyl-, amine- and PEG-QDs were prepared at a concentration of 16 nM in distilled water, saline (0.9% NaCl), or saline with 3% mouse serum (Janvier). Size, polydispersity, and zeta potential of QDs in different solutions were analyzed with dynamic light scattering (DLS) with a Zetasizer-Nano ZS instrument (Malvern, Malvern Hills, United Kingdom). Each assigned size and corresponding polydispersity index (PDI) was the mean of 10 sub-runs. All measurements were carried out in triplicate with a temperature equilibration time of 1 min at 25 °C. For the dispersant, a refractive index (R_i) of 1.330 and a viscosity of 0.8872 cP were chosen. The data processing mode was set to high multi-modal resolution. The optical model for the zeta potential measurements was interpreted by the method of Smoluchowski.

2.3. Animals

Male C57BL/6 mice (23–25 g; purchased from Charles River; Sulzfeld, Germany) were held under standard laboratory conditions with free access to animal chow and water *ad libitum*. The experiments were performed according to German legislation for the protection of animals.

2.4. Blood kinetics

Mice ($n = 5$ per experimental group) were anesthetized with a ketamine/xylazine mixture (100 mg/kg ketamine and 10 mg/kg xylazine) by i.p. injection and afterwards fixed on a heating plate to ensure constant body temperature. The left femoral artery was cannulated in a retrograde manner using a polyethylene catheter. Mice were injected 80 pmol of carboxyl-, amine-, or PEG-QDs in 100 μl of saline (0.9% NaCl). For the evaluation of plasma kinetics, a polyethylene catheter was inserted into the left carotid artery for consecutive blood sampling over time. Blood samples (50 μl) were collected in heparin-containing Eppendorf tubes prior to intra-arterial administration of QDs (blank value) and at 1, 3, 5, 15, 30, 45, and 60 min after QD injection as well as after 4 and 24 h in separate experiments. Blood samples were stored at 4 °C until further analysis. For measurement of QD blood concentrations, a quantitative fluorescence imaging system was used. Blood samples were filled into rectangular capillary tubes (Vitrotubes, CMS, Charlestown, UK) and fluorescence was excited for 1 s at specific wave lengths (510–560 nm) using a modified fluorescence microscope fitted with a 10× objective (Axiotech vario, Zeiss, Oberkochen, Germany). The fluorescence signal (LP 590 nm) was quantitatively detected using a photomultiplier tube (P30A-11; Electron Tubes, Middx, UK) and averaged by a digital storage oscilloscope (Tektronix TDS1012; Tektronix Inc., Berkshire, UK). To calculate QD blood concentration from fluorescence intensities, different concentrations of QD were diluted in mouse blood samples to establish calibration curves. Plasma half-life ($t_{1/2}$) values were obtained by fitting measurement data points to an exponential function curve ($f = ae^{-bt}$) with Sigma Plot 11.0 Software (Systat Software Inc, Chicago, USA) and calculating the $t_{1/2}$ values from the $t_{1/2} = \ln 2/b$ equation.

2.5. Hematologic parameters

Blood samples were collected from animals used for the evaluation of blood kinetics as described above by cardiac puncture after 1, 4 and 24 h. For the determination of systemic leukocyte, platelet, and erythrocyte counts, hematocrit, hemoglobin concentration, mean corpuscular volume, mean corpuscular hemoglobin, and mean corpuscular hemoglobin concentration of erythrocytes, a Coulter AcT counter (Coulter Corp., Miami, FL) was used.

2.6. In vivo microscopy of QD distribution in the cremasteric microvasculature

Mice ($n = 3$) were anesthetized and prepared as described above. The cremaster preparation was carried out as originally described by Baez [28] with minor modifications. The right cremaster muscle was exposed through a ventral incision of the scrotum. Then, the muscle was opened ventrally in a relatively avascular zone using careful electrocautery to stop any bleeding and spread over the transparent pedestal of a custom-made microscopic stage. Epididymis and testicle were detached from the cremaster muscle and replaced into the abdominal cavity. Throughout the procedure as well as after surgical preparation during *in vivo* microscopy, the muscle was superfused with warm (35 °C) buffered saline.

The setup for *in vivo* microscopy was centered around an AxioTech-Vario 100 Microscope (Zeiss MicroImaging GmbH, Göttingen, Germany), equipped with a Colibiri LED light source (Zeiss MicroImaging GmbH) for fluorescence epi-illumination microscopy. For QD excitation and reflected oblique light illumination [29], 470 nm and 625 nm were used, respectively. Light was directed onto the specimen via filter set 62 HE (Zeiss MicroImaging GmbH) fitted with dichroic and emission filters [TFT 495 + 610 (HE); TBP 527 + LP615 (HE)]. Microscopic images were obtained with an AxioCam Hsm digital camera using a 20× water immersion lens (0.5 NA, Zeiss MicoImaging Gmbh). The images were analyzed with AxioVision 4.6 software (Zeiss MicroImaging GmbH). Further image processing and analysis was done using ImageJ software (National Institutes of Health, Bethesda, MD). Off-line fluorescence analysis of pixel brightness values served as a semiquantitative method to assess the association patterns of QDs with the microvasculature. Arterioles were identified by high blood flow velocity and the absence of rolling or adherent leukocytes, capillaries by their small diameter, and venules by the presence of rolling or adhering leukocytes.

2.7. Two-photon microscopy of QD distribution in skeletal and heart muscle tissue

Mice ($n = 2$) were anesthetized and prepared as described above. A polyethylene catheter was inserted in the left jugular vein and carboxyl-, amine-, or PEG-QDs (80 pmol in 100 μl 0.9% NaCl) were injected through the femoral artery catheter. One hour after application of QDs, a midline laparotomy was performed, the inferior caval vein opened, and the animal perfused with ice-cold 0.9% NaCl solution via the jugular vein for 20 min with physiological pressure. After perfusion, a part of the abdominal wall (contralateral to the femoral artery catheter) and the left ventricle of the heart were excided. Tissue samples were placed on a Petri dish, plainly fixed with canulae and superfused with 0.9% NaCl solution.

Two-photon microscopy on excised tissue obtained as described above was performed on a TriMScope (LaVision Biotec, Bielefeld, Germany) built around an Olympus BX 51 microscope (Olympus, Hamburg, Germany) and equipped with a tunable Ultra II Titan:Sapphire Laser (Coherent, Dieburg, Germany). An Olympus XLUMPlanFI 20×/0.95W water immersion objective was used. Excitation wavelength was 860 nm. QD emission was detected at 635–695 nm using a Hamamatsu H6780-20 photomultiplier tube and a 700 nm short pass filter. Optical sections were recorded at 10 μm distances using the same settings for all samples analyzed. Z-stacks covering 100 μm were projected and further processed using ImageJ software (National Institutes of Health, Bethesda, MD, USA).

2.8. Interaction of QDs with human vascular endothelial cells in vitro

Human microvascular endothelial cells (HMECs) were provided by the Centers for Disease Control and Prevention (Atlanta, GA, USA) and cultured in EC growth medium (Promocell, Heidelberg, Germany). HMECs cell culture, incubation with QDs, and imaging were performed on μ-slide 8 well ibiTreat microscopy chambers (ibidi, Martinsried, Germany). QDs were prepared at 0.8 μM in PBS and added to the medium to a final concentration of 16 nM, thus preventing aggregation of QDs and achieving a homogenous distribution. For confocal microscopy, medium was removed after incubation with QDs for 15 min at 37 °C, cells were briefly washed with PBS, fixed with buffered 4% paraformaldehyde, and embedded in PermaFluor (Beckman Coulter, Fullerton, CA). Images were acquired with a Leica SP5 confocal laser-scanning microscope (Leica Microsystems, Wetzlar, Germany) with a 40× oil immersion objective (NA 1.25). Excitation wavelength was 488 nm and QDs emission was detected at 630–700 nm. Optical sections were recorded at 0.5 μm distances using the same settings for all samples. Z-stacks covering complete cells were projected using ImageJ software (National Institutes of Health, Bethesda, MD). For FACS analysis, cells were harvested after incubation, transferred into round

bottom polypropylene tubes, washed in PBS and resuspended in 200 µl PBS. Cellular QD fluorescence intensity was measured in a flow cytometer (BD FACSCalibur) using an excitation wavelength of 488 nm and detected at 661 nm (channel FL-3). The recorded results were analyzed using CellQuest™ software (Becton Dickinson). At least 8000 cells were measured for each independent experiment.

2.9. Tissue deposition and excretion of QDs

Mice ($n = 4–5$) were anesthetized and prepared as described above. A catheter was inserted into the jugular vein. At the end of each experiment, a midline laparotomy was performed, the inferior caval vein opened, and the animal perfused with ice-cold 0.9% NaCl solution via the jugular vein for 10 min with physiological pressure. Then, organ and excretion samples of interest were removed, such as brain, heart, lung, right liver lobe, spleen, right kidney, thoracic aorta, muscle tissue from the right *M. quadriceps femoris*, thymus, lymph nodes (inguinal, axillary, and superficial cervical), bile, intestinal content, feces from the colon, and urine from the urinary bladder. Casually attached blood clots were carefully washed away. Samples were immediately stored at −80 °C until further processing. Quantitative determination of QDs was done according to previous protocols [30] with minor modifications. Briefly, samples were weighed and solubilized in Solvable® (Perkin–Elmer, Waltham, USA) at 50 °C for 2 h. QD fluorescence of the samples was analyzed by a spectrofluorometer (Spectrafluor plus; Tecan, Crailsheim, Germany). For excitation, a BP 390 nm filter was used and QD emission was detected using a BP 635 nm filter. Calibration curves were generated for each class of tissue and QD type by measuring dissolved control tissue samples after addition of different concentrations of QDs. QD concentrations were calculated from the measured fluorescence intensities using the matching calibration curves.

2.10. Transmission electron microscopy

Mice ($n = 2$) were anesthetized and prepared as described above. Amine-, carboxyl- or PEG-QDs (80 pmol) were injected through the femoral artery. 24 h after QD application, anesthetized mice were perfused with glutaraldehyde (3.5% in 0.1 M cacodylate buffer) and then heart and spleen were removed. Organs were diced into 0.5- to 1-mm^3 pieces and immersed into glutaraldehyde (3.5% in 0.1 M cacodylate buffer) until further preparation for electron microscopy. The organs were rinsed in 0.1 M cacodylate buffer, post-fixed in 1% OsO_4 containing 1.5% $C_6FeK_4N_8$ in 0.1 M cacodylate buffer for 1 h, dehydrated in a graded series of ethanol and embedded in Araldite (Serva). Sections were cut with a diamond knife, using a Leica Ultracut UCT ultramicrotome. Ultrathin (50–70 nm) sections were slightly stained with a saturated aqueous uranyl acetate solution for 10 min. Stained and unstained ultrathin sections were examined in a Zeiss EM 900 transmission electron microscope.

2.11. Statistics

Data analysis was performed with a statistical software package (SigmaStat for Windows, Jandel Scientific Erkrath, Germany). The ANOVA on ranks test followed by the Student-Newman-Keuls test was used for the estimation of stochastic probability in intergroup comparisons. When unequal group numbers were compared, the ANOVA on ranks test was followed by the Dunn's test. Mean values and SEM are given. P values <0.05 were considered significant.

3. Results

3.1. Physical characterization of QDs

The size, polydispersity, and zeta potential of QDs in different vehicles were measured by DLS (Table 1). QDs used had hydrodynamic diameters in the range of 21–34 nm in PBS which generally increased in the presence of mouse serum proteins in comparison to their hydrodynamic diameters in PBS solely. Interestingly, quantitative differences in the increase in hydrodynamic diameter were noted, depending on the surface modification present (carboxyl-QDs +230%, amine-QDs +150%, and PEG-QDs +130% of initial diameter, respectively). All QDs used had low polydispersity indices (PdI) in distilled water, NaCl, and PBS. However, PdI-values strongly increased when QDs were dispersed in PBS with mouse serum. QDs had a negative zeta potential in all vehicles tested. However, carboxyl-QDs had the lowest zeta potential values.

3.2. Blood kinetics

First, we analyzed the blood kinetics of carboxyl-, amine-, and PEG-QDs after intra-arterial dosing (Fig. 1). Immediately after bolus injection of PEG-QDs, high fluorescence intensities were measured in whole blood (31.9 ± 3.4% ID/ml blood) which were found to be not significantly changed at 4 h after dosing (35.0 ± 2.4% ID/ml blood). 24 h after dosing, low concentrations of PEG-QDs (1.0 ± 0.06% ID/ml blood) were still traceable in the blood (half-life time 513.4 ± 152.1 min). In contrast, the fluorescence values of whole blood samples from amine- or carboxyl-QD-treated animals were rapidly decreasing after application. Whole blood fluorescence of carboxyl-QDs (half-life time 5.8 ± 0.4 min) decreased more rapidly than that of amine-QDs (half-life time 29.0 ± 2.8 min). After 1h, carboxyl-QDs were no longer detectable in the blood stream, whereas amine-QDs were still present (4.7 ± 1.2% ID/ml blood).

Table 1
Physical characterization of QDs.

Particle	Diameter (nm)	PdI	Zeta potential (mV)
Carboxyl-QDs			
H_2O	22.2 ± 0.8	0.113 ± 0.111	−42.5 ± 0.6
NaCl	21.2 ± 0.9	0.123 ± 0.103	−28.8 ± 5.2
PBS	18.1 ± 0.2	0.025 ± 0.029	−22.5 ± 4.3
PBS + serum	41.9 ± 0.3	0.448 ± 0.039	−14.8 ± 0.3
Amine-QDs			
H_2O	22.7 ± 0.3	0.037 ± 0.026	−29.2 ± 4.2
NaCl	25.8 ± 0.2	0.016 ± 0.013	−8.5 ± 5.0
PBS	25.2 ± 0.6	0.054 ± 0.030	−5.2 ± 1.8
PBS + serum	36.5 ± 0.4	0.405 ± 0.007	−5.9 ± 0.2
PEG-QDs			
H_2O	37.5 ± 1.0	0.053 ± 0.025	−32.2 ± 5.4
NaCl	34.4 ± 0.4	0.094 ± 0.010	−7.2 ± 2.1
PBS	36.1 ± 0.7	0.078 ± 0.042	−1.1 ± 1.4
PBS + serum	46.6 ± 0.8	0.578 ± 0.008	−7.2 ± 0.8

QDs were prepared in distilled water at a concentration of 16 nM (H_2O), 0.9% NaCl, phosphate–buffered saline (PBS), or PBS and mouse serum (PBS + serum). The measurements were carried out in triplicate. The mean value and the standard deviation of the measurements are shown.

3.3. Hematologic parameters

Intra-arterial application of the different QD species did not cause any significant differences in platelet, leukocyte, or erythrocyte counts, hematocrit, hemoglobin concentration, mean corpuscular volume, mean corpuscular hemoglobin, and mean corpuscular hemoglobin concentration of erythrocytes among groups treated with QDs (data not shown).

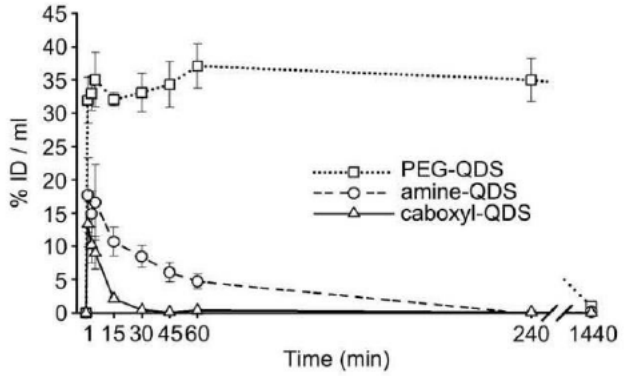

Fig. 1. Blood kinetics of QDs upon intra-arterial injection. Mice received a bolus injection of either carboxyl-, amine-, or PEG-QDs [3 pmol/g body weight] via a femoral artery catheter. Blood was sampled through a carotid artery catheter before and 1, 3, 5, 15, 30, 45 and 60 min after injection as well as after 4 and 24 h. QD content in whole blood probes was calculated by fitting fluorescence intensity values obtained for each time point with calibration curves for each QD-surface modification. QD content is expressed as percent of injected dose per ml blood (% ID/ml blood). Data points represent the mean values of 5 experiments ± SEM.

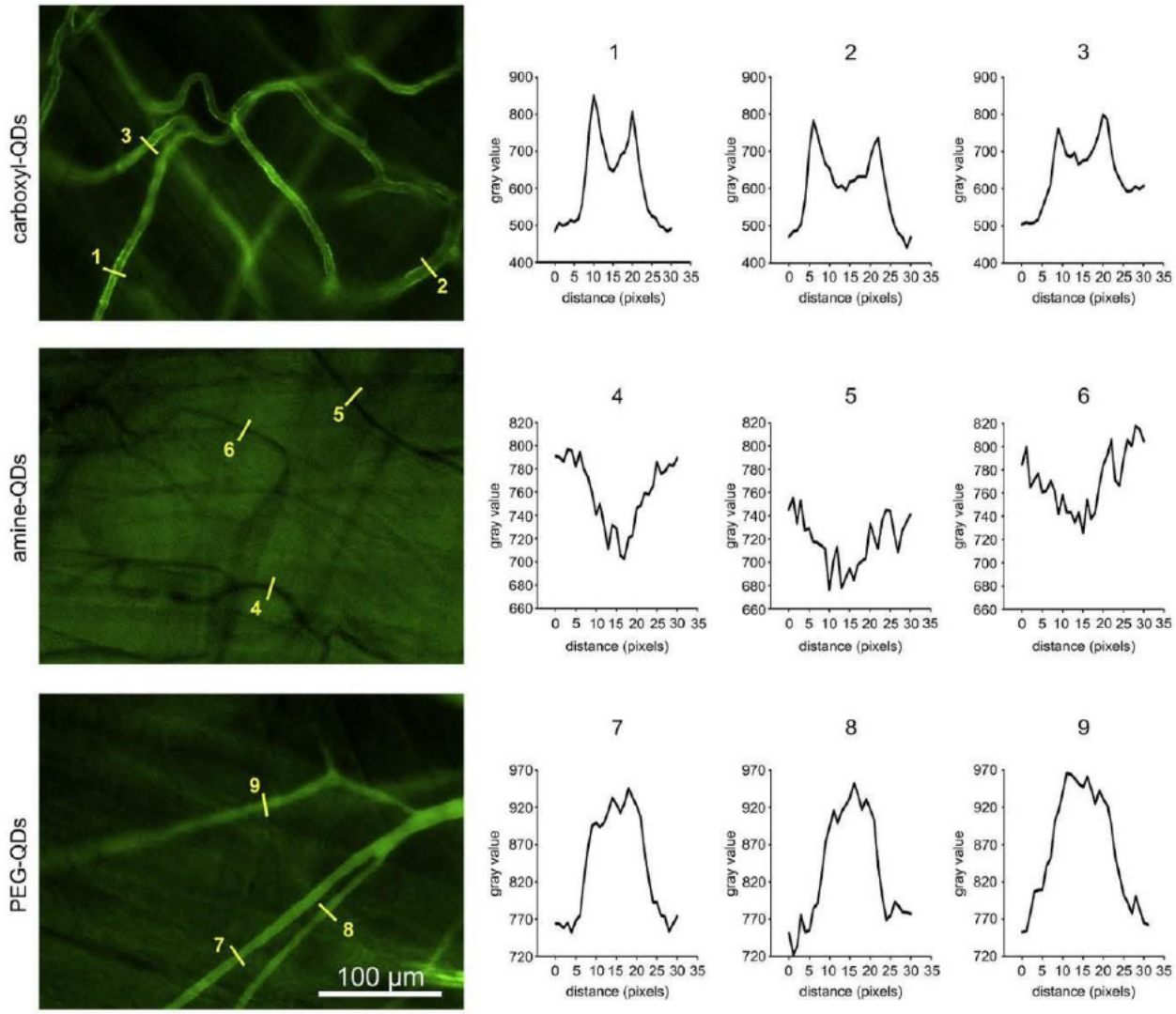

Fig. 2. *In vivo* association of QDs with capillaries in skeletal muscle. A) Mice received a bolus injection of carboxyl-, amine-, or PEG-QDs [3 pmol/g body weight] via a femoral artery catheter. Representative *in vivo* microscopic fluorescence images (original objective magnification 20×) of cremasteric capillaries obtained at 1 h after dosing are shown. Experiments were carried out in triplicate. Scale bars indicate 100 µm. B) Graphs depict representative tracings of fluorescence intensity values along a 15 µm line across capillaries as indicated in the microscopic images.

3.4. *In vivo microscopy of QD distribution in the cremasteric microvasculature*

A rapid intraluminal fluorescence signal peak was observed in the microcirculation in the first few seconds after application of QDs by means of *in vivo* fluorescence microscopy. Thereafter, homogeneous fluorescence signals were detected in the vessel lumina of carboxyl- or amine-QD-treated mice, whereas small, sub-micrometer-sized agglomerates were detected floating in the blood stream in PEG-QD-treated mice. PEG-QD fluorescence was visible in the blood stream for the whole experimental duration of 1 h, whereas carboxyl- and amine-QD fluorescence decreased continuously and eventually disappeared. For carboxyl-QDs, it was a constant observation that their fluorescence was co-localized with the capillary endothelial lining (Fig. 2 and Supplementary data, movie file 1) and abruptly diminished at the point where capillaries passed into postcapillary venules. Pixel brightness graphs for capillaries associated with carboxyl-QDs depict two positions of fluorescence intensity maxima which co-localize with vessel wall borders. Fluorescence intensity values for capillaries after dosing with amine-QDs however were below background values. Pixel brightness graphs of capillaries after application of PEG-QDs were parabolic with single maxima between the vessel walls (Fig. 2).

In contrast, heterogeneous interactions with the endothelium of some postcapillary venules were observed for carboxyl-QDs and to a lesser extent for amine- and PEG-QDs, whereas no binding to arterioles was confirmed for any QDs investigated (data not shown). Occasionally, we observed some few leukocytes rolling in postcapillary venules being heavily filled with QDs. Although a rare event, this was only the case in animals treated with amine-QDs.

3.5. *Two-photon microscopy of QD distribution in skeletal and heart muscle tissue*

One hour after application, the association of carboxyl-, amine-, or PEG-QDs with capillary endothelium in heart and skeletal muscle (abdominal wall) was visualized by two-photon microscopy (Fig. 3). At 1h after systemic application, two-photon imaging of

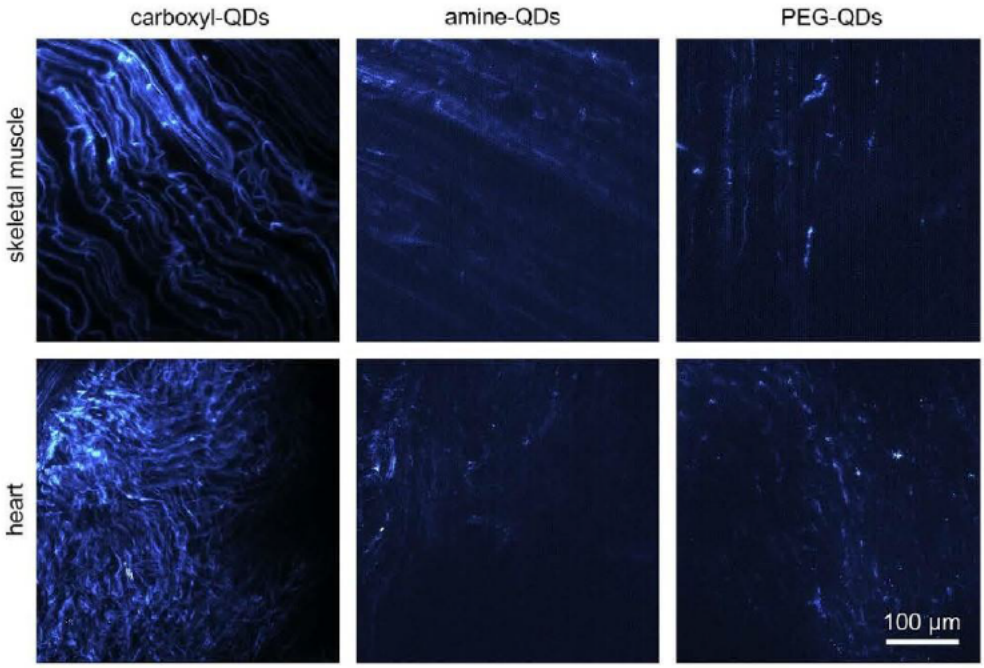

Fig. 3. *Ex vivo* two-photon microscopy of QDs in the heart and skeletal muscle. Mice received a bolus injection of carboxyl-, amine-, or PEG-QDs [3 pmol/g body weight] via a femoral artery catheter. 1 h after application, animals were perfused with NaCl for complete exsanguination. Representative *ex vivo* two-photon-microscopic fluorescence images (original objective magnification 20×) of heart and skeletal muscle tissue obtained 1 h after dosing are shown. Experiments were carried out in triplicate. Scale bars indicate 100 µm.

carboxyl-QDs in skeletal and heart muscle tissue showed a high signal to background ratio and clear co-localization with the capillary network in those tissues. In contrast, the fluorescence of both amine- and PEG-QDs in the skeletal and heart muscle microvasculature could not clearly be associated with the capillary network. Instead, low signal to background ratios and only diffuse fluorescence patterns were visible.

3.6. Interaction of QDs with microvascular endothelial cells in vitro

HMECs were chosen as *in vitro* approach to investigate the cellular uptake of QDs. First, FACS analysis of liberated HMECs after incubation with QDs was done (Fig. 4). Carboxyl-QDs had the highest rate of association to HMECs (95.4 ± 1.6% gated cells) whereas considerably lower associations were observed using amine- (4.5 ± 2.1% gated cells) or PEG-QDs (1.2 ± 0.4% gated cells). Confocal microscopy, performed to visualize the association of QDs with HMECs, showed preferential uptake and localization of carboxyl-QDs in vesicular structures (Fig. 4). According to the FACS analysis, amine and PEG-QDs exhibited a week association with HMECs.

3.7. Tissue deposition and excretion of QDs

Quantitative fluorescence analysis revealed a deposition hierarchy of QDs depending on the surface modification present (Fig. 5; Table 2 in Supplementary data). In heart, lung, liver, spleen, skeletal muscle, thoracic aorta, and brain, carboxyl-QDs were detected in significantly higher amounts than amine- or PEG-QDs. Amine-QDs on the other hand were deposited in increasing amounts in lymph nodes and, like carboxyl-QDs, in significantly higher amounts in the thymus gland than PEG-QDs. Solely in the kidney, carboxyl-, amine-, and PEG-QDs accumulated in similar quantities. Interestingly, in skeletal muscle and brain tissue, just carboxyl-QDs were deposited whereas amine- or PEG-QDs were not detectable in these tissues at any time point.

We further addressed the issues of hepatic and renal excretion from the body (Fig. 6, Table 2 in Supplementary data). All QDs were detected in gallbladder content. PEG-QDs were found in bile in a very constant manner over 1, 4, and 24 h whereas carboxyl-QD-excretion into bile decreased at 24 h. In contrast, amine-QDs were detected in bile at 24 h in significantly higher amounts than carboxyl-QDs. Moreover, all QDs were present in the small intestinal content. However, their concentration did not significantly differ between QD subtypes. In feces, carboxyl- and PEG-QDs were found in significantly higher amounts at 1 and 24 h compared to amine-QDs. In urine samples, amine-QDs were detected at 24 h after dosing but not after 1 and 4 h. On the other hand, carboxyl- and PEG-QDs were detectable at 4 h and 24 h after dosing.

3.8. Electron microscopy

In the spleen, all QD species were found to be localized predominantly in phagocytic cells residing in the red pulp. In contrast to amine- and PEG-QDs, carboxyl-QDs were also found to be stored in endocytotic vesicles of splenic capillary endothelium and within cytoplasmatic vesicles in endothelial cells of heart muscle capillaries (Fig. 7). Carboxyl-QDs but neither amine- nor PEG-QDs were also occasionally detected in the endocardium. In heart muscle cells, no carboxyl-QDs but minor amounts of amine- and no PEG-QDs were found (data not shown).

4. Discussion

This study aimed to investigate the microvascular distribution of neutral, cationic, and anionic QDs *in vivo* and to assess the effects of surface modifications (charge) on their biokinetics and distribution in a whole animal study.

Recent basic research studies investigating the pharmacokinetics and toxic effects of QDs for biomedical applications mainly utilized simple surface modifications of QDs including PEG, dihydrolipoic acid (DHLA), cysteamine as well as amine- or carboxyl-

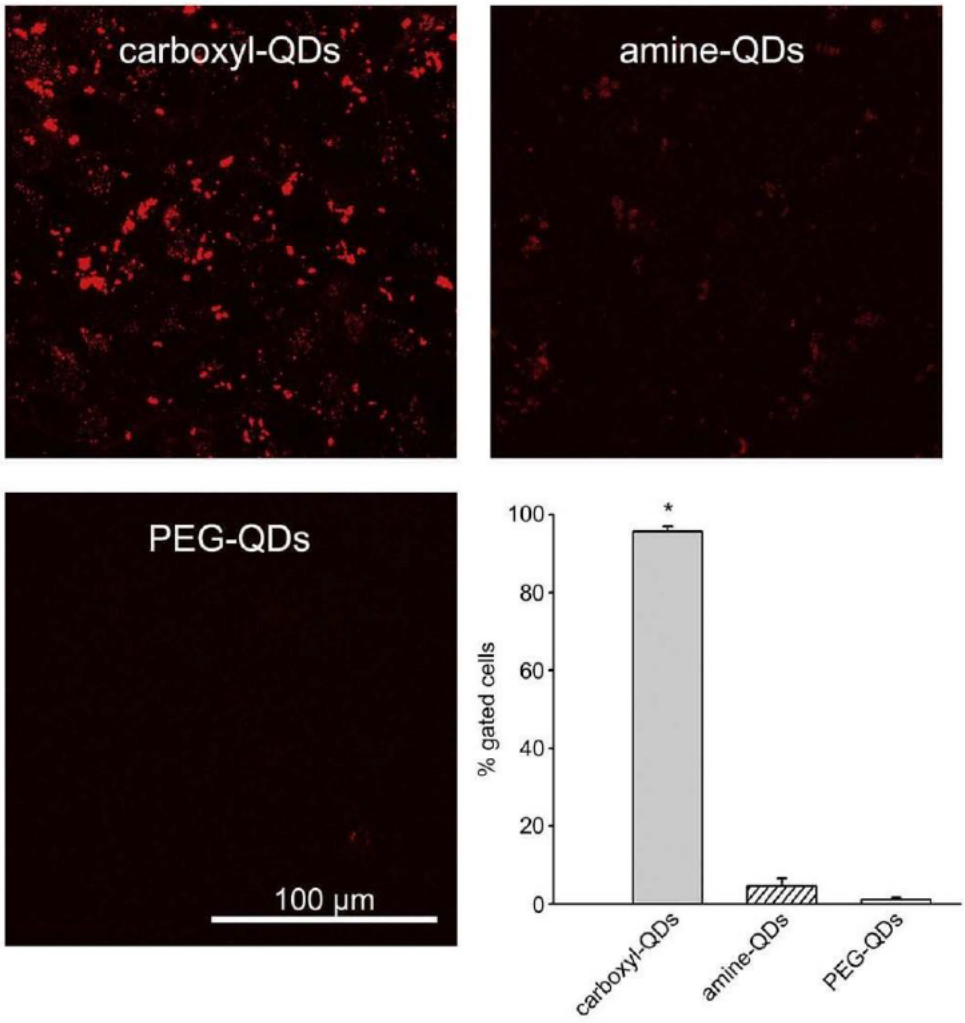

Fig. 4. QD uptake by endothelial cells *in vitro*. Confocal images (original objective magnification 40×) of HMECs in cell culture 15 min after incubation with either carboxyl-, amine-, or PEG-QDs [16 nmol]. Scale bar indicates 100 µm. After 15 min of incubation, FACS analysis of HMECs was performed. The association between cell counts and fluorescence signals was measured and is expressed as % gated cells. Data points represent the mean values of 3 independent measurements ± SEM (*$p < 0.05$).

functions [19,20,31–33]. Cationic amine-, anionic carboxyl-, and neutral PEG-QDs used in our study had similar average hydrodynamic diameters of 21–34 nm in NaCl (0.9%) and considerably low PdI-values of 0.016–0.123 therefore excluding the possibility of preexisting agglomerates which may influence the data obtained. The results of our size measurements are in very good accordance with those obtained elsewhere [34]. Carboxyl-QDs always had a more negative zeta potential in all media tested than amine- or PEG-QDs. The hydrodynamic parameters measured after incubation with mouse serum (Table 1) indicate that all QDs tested, once they come in contact with blood plasma, are covered with serum proteins, with the largest increase in hydrodynamic diameter seen for carboxyl-QDs.

To determine critical time points of organ accumulation, we analyzed the impact of amine-, carboxyl- and PEG-surface modifications on blood kinetics. The longest plasma half-life times were observed for PEG-QDs. It is well known that PEGylation of liposomes and solid nanoparticles (including QDs) heavily increases their circulating lifetime by reducing protein binding [35,36]. In contrast, amine- and carboxyl-QDs used in our study are significantly faster cleared from plasma, most likely due to opsonization and accelerated uptake by phagocytic cells [37]. An intriguing observation, however, is that carboxyl-QDs were still significantly faster cleared from the circulation than amine-QDs. Comparing the half-life data obtained by quantitative fluorescence measurements with the *in vivo* microscopic observations, it is noticeable that the capillary network of skeletal muscle became rapidly (at least within few minutes) associated with carboxyl-QDs. This finding is suggestive to contribute to the short half-life time of 5.8 ± 0.4 min of carboxyl-QDs in the blood stream.

Data on the interaction of QDs with the vascular system *in vivo* are generally scarce. However, arterial extraction of anionic QDs after infusion into isolated-perfused skin was reported previously [38]. In this *ex vivo* study, the model of the isolated-perfused porcine skin flap (IPPSF) was used to investigate the pharmacokinetics of QDs with either carboxyl- or PEG-surface coating and it was observed, that carboxylated QDs had greater tissue deposition than PEGylated QDs. Although the mechanisms responsible for this observation remain to be elucidated, the authors suggest that the observed differences in tissue deposition may be due to interactions of carboxylated QDs with the vascular endothelium.

Our own *in vivo* data suggest a stable interaction of anionic carboxyl-QDs with capillary endothelial cells of skeletal muscle tissue for at least 1 h. Electron microscopy of the myocardium and

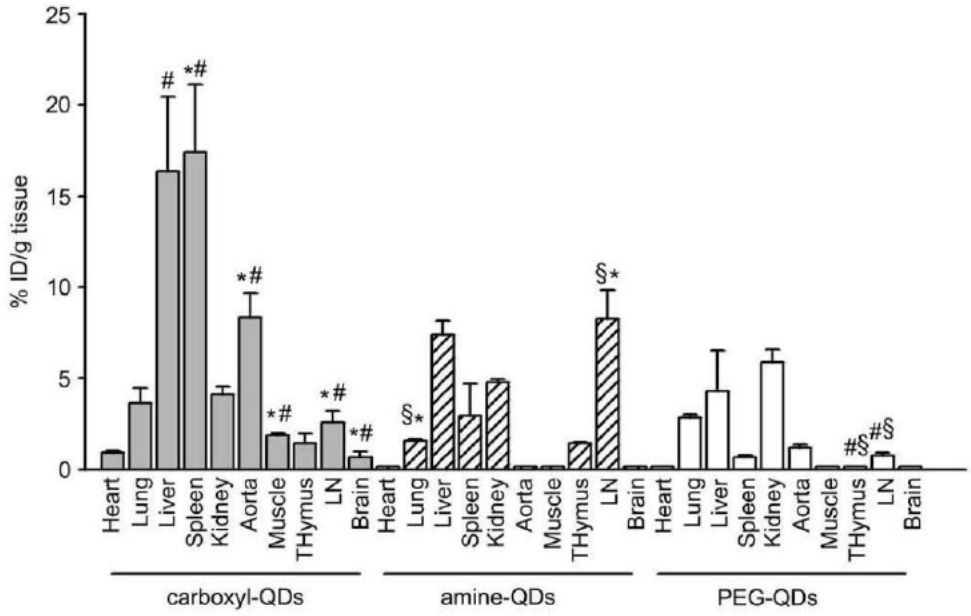

Fig. 5. Tissue distribution of QDs [3 pmol/g body weight] 24 h after intra-arterial injection determined by quantitative spectrofluorometry. Bars represent the mean values of 4–5 experiments ± SEM ($^{*}p < 0.05$ [carboxyl-QDs vs PEG-QDs], $^{*}p < 0.05$ [carboxyl-QDs vs amine-QDs], $^{\S}p < 0.05$ [amine-QDs vs PEG-QDs]). Data is given as percent of injected dose per g tissue weight [% ID/g tissue].

the spleen revealed that carboxyl-QDs were occasionally localized in endocytotic vesicles of capillary endothelial cells even 24 h after dosing.

In vivo microscopy as well as *ex vivo* two-photon microscopy confirmed a distinct staining of the capillary network both in skeletal and heart muscle tissue. Therefore it is presumable that the selective interaction of anionic carboxyl-QDs with capillary endothelial cells is chiefly responsible for the deposition of carboxyl-QDs in skeletal and heart muscle tissue *in vivo*. This observation is further supported by quantitative fluorescence analysis of skeletal and heart muscle tissue. Carboxyl-QDs are found in traceable amounts in both tissues after 1, 4 and 24 h, amine-QDs are only detectable in the heart muscle after 1 h and PEG-QDs were not detectable in both tissues at any time point investigated. We ascertained the detection limit of quantitative fluorescence analysis to be 0.5% ID/g tissue. Due to the high sensitivity of two-photon microscopy, even lower quantities can be visualized although the quantitative deposition may be far less than 0.5% ID/g tissue.

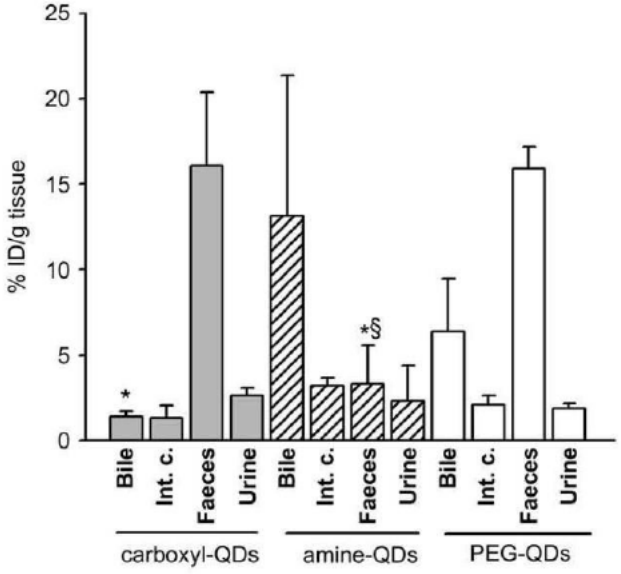

Fig. 6. Excretion of QDs [3 pmol/g body weight] 24 h after intra-arterial injection determined by quantitative spectrofluorometry. Bars represent the mean values of 4–5 experiments ± SEM ($^{*}p < 0.05$). Data is given as percent of injected dose per g sample weight (% ID/g sample).

Amine-QDs were also cleared from the circulation with a relatively low half-life time of 29.0 ± 2.8 min and, like carboxyl-QDs, sequestered in phagocytic cells in spleen and liver. But unlike carboxyl-QDs, they do not bind to capillary endothelium and, therefore, it is likely that the blood kinetics of amine-QDs reflects the clearance kinetics of a nanoscale agent undergoing predominantly phagocytic clearance. In any case, carboxyl-QDs were found in organs with a prominent phagocytic system in significantly higher amounts than amine- or PEG-QDs. It is anticipated in the literature that anionic carboxyl-QDs may also undergo pronounced phagocytic uptake. But these effects may also be augmented by rapid capillary binding. It is possible that binding of anionic QDs to capillary endothelium is not a muscle tissue-specific phenomenon but a general event in the body including different tissue types.

There are few studies dealing with the effect of surface charge of injectable particulate drug formulations on the healthy microvascular system. However, a former study investigated the influence of the surface charge of microbubbles, micrometer-sized liposomal agents used for advanced applications in ultrasound imaging, on capillary transit and myocardial contrast enhancement. In this study, size-independent capillary retention of microbubbles, occurring for a few seconds to 10 min, was frequently observed with anionic, but rarely with neutral microbubbles [39]. However, the hydrodynamic diameter of QDs (30 nm) is two orders of magnitude lower than that of most microbubbles (2–4 μm). This means that mechanisms responsible for the behavior of large, micrometer-sized particles can not necessarily be assigned to small, nano-sized particles even if they carry a comparable surface charge.

In vitro studies [40,41] revealed that anionic nanoparticles are preferably taken up by cultured cells. In this study, we also asked if

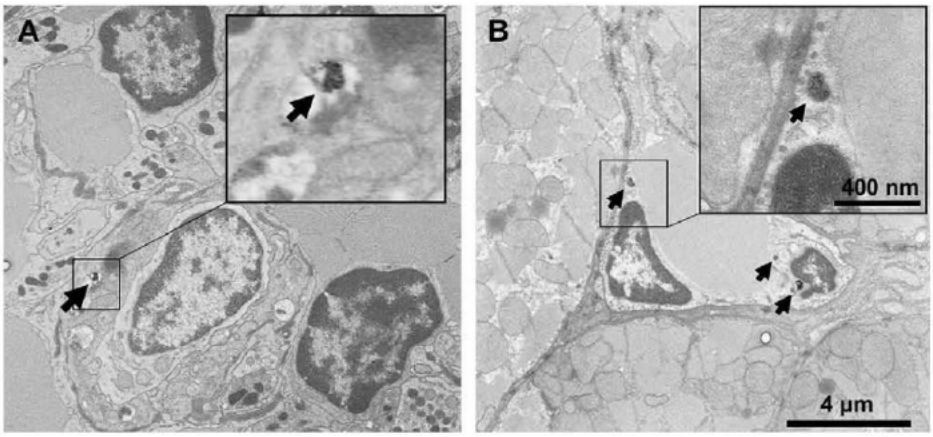

Fig. 7. Transmission electron micrographs showing uptake of carboxyl-QDs into capillary endothelial cells [3 pmol/g body weight] 24h after intra-arterial injection and perfusion-assisted exsanguination. A) Spleen. 4000× magnification. B) Heart. 4500× magnification.

a similar charge-dependent uptake of QDs occurs in cultured HMECs. HMECs were chosen since this cell line is known to retain endothelial phenotypic and functional characteristics [42]. Both FACS analysis and confocal microscopy of HMECs confirmed a preferable uptake of anionic carboxyl-QDs. Still, whether this observation depicts the *in vivo* situation is questionable because also non-endothelial cells such as human epidermal keratinocytes show a high and selective uptake of QDs with a carboxylic acid surface coating [34].

Nanoparticles in biological environments immediately become covered by an evolving corona of biomolecules which gives a biological identity to the nanoparticle [43]. It is anticipated in the literature that the protein corona is essentially responsible for the uptake of nanoparticles by tissue cells *in vivo*. Since we followed an *in vivo* approach to investigate the fate of QDs within the microcirculation, we determined the hydrodynamic diameter of QDs dispersed in mouse serum using dynamic light scattering. As discussed above, carboxyl-QDs showed the highest increase in hydrodynamic diameter in mouse serum as a correlate to binding of serum proteins to the particle surface. In a recent work, the endocytotic uptake of anionic carboxylic acid-coated QDs was found to be primarily regulated by the G-protein-coupled receptor-associated pathway and low density lipoprotein receptor/scavenger receptor [34]. This in turn raises the question if the same mechanisms occur *in vivo* and if yes, what is the explanation for the selective interactions of carboxyl-QDs with capillary endothelium.

The identities of the serum proteins attached to the surface of anionic carboxyl-QDs remain to be elucidated but we hypothesize that the adsorbed protein corona of carboxyl-QDs can facilitate a pronounced binding to capillaries of the microcirculation which might significantly contribute to the bioaccumulation of carboxyl-QDs in the body.

5. Conclusions

In this *in vivo* study, we investigated the microvascular distribution of three differently charged QD species by *in vivo* microscopy of the cremasteric microvasculature and by deep tissue imaging using two-photon microscopy of heart and skeletal muscle. Anionic carboxyl-QDs were not only found in higher amounts in various tissues, but were also associated with the capillary network. This unique pattern of interaction with capillary endothelial cells visualized by *in vivo* microscopy is probably linked to an accelerated clearance of carboxyl-QDs from the circulation. This phenomenon may also contribute to the pronounced deposition of carboxyl-QDs in the body as determined by quantitative fluorescence measurements, especially important for the deposition in tissue types with a poor mononuclear phagocyte system such as skeletal and heart muscle tissue.

Acknowledgements

We greatly appreciate the technical assistance of Beate Aschauer, Sabine Tost, Siiri Lüdemann, and Gerhard Adams. We are also much obliged to Dr. Jürgen Peters for his always constructive advices. Additionally, we want to thank Dr. Rolf Nitzsche as well as Dr. Stephan Schultes and Prof. Gerhard Winter for their uncomplicated and professional help with dynamic light scattering. The data presented in this study are part of the doctoral thesis of Marc Praetner. This work was supported by European Commission grant NMPT-CT-2006-032777 (NANOSH).

Appendix. Supplementary data

Supplementary data associated with this article can be found in the on-line version, at doi:10.1016/j.biomaterials.2010.05.051.

Appendix

Figures with essential color discrimination. Figs. 2–4 in this article are difficult to interpret in black and white. The full color images can be found in the on-line version, at doi:10.1016/j.biomaterials.2010.05.051.

References

[1] Biju V, Itoh T, Anas A, Sujith A, Ishikawa M. Semiconductor quantum dots and metal nanoparticles: syntheses, optical properties, and biological applications. Anal Bioanal Chem 2008;391:2469–95.
[2] Cao YC. Nanomaterials for biomedical applications. Nanomed 2008;3:467–9.
[3] Medintz IL, Mattoussi H, Clapp AR. Potential clinical applications of quantum dots. Int J Nanomedicine 2008;3:151–67.
[4] Hsieh JM, Ho ML, Wu PW, Chou PT, Tsai TT, Chi Y. Iridium-complex modified CdSe/ZnS quantum dots; a conceptual design for bi-functionality toward imaging and photosensitization. Chem Commun (Camb); 2006:615–7.
[5] Yaghini E, Seifalian AM, MacRobert AJ. Quantum dots and their potential biomedical applications in photosensitization for photodynamic therapy. Nanomed 2009;4:353–63.
[6] Orndorff RL, Rosenthal SJ. Neurotoxin quantum dot conjugates detect endogenous targets expressed in live cancer cells. Nano Lett 2009;9:2589–99.
[7] Wei Y, Jana NR, Tan SJ, Ying JY. Surface coating directed cellular delivery of TAT-functionalized quantum dots. Bioconjug Chem 2009;20:1752–8.

[8] Allen PM, Liu W, Chauhan VP, Lee J, Ting AY, Fukumura D, et al. In As(ZnCdS) quantum dots optimized for biological imaging in the near-infrared. J Am Chem Soc 2010;132:470–1.
[9] Kim S, Lim YT, Soltesz EG, De Grand AM, Lee J, Nakayama A, et al. Near-infrared fluorescent type II quantum dots for sentinel lymph node mapping. Nat Biotechnol 2004;22:93–7.
[10] Kobayashi H, Ogawa M, Kosaka N, Choyke PL, Urano Y. Multicolor imaging of lymphatic function with two nanomaterials: quantum dot-labeled cancer cells and dendrimer-based optical agents. Nanomed 2009;4:411–9.
[11] Lee PW, Hsu SH, Tsai JS, Chen FR, Huang PJ, Ke CJ, et al. Multifunctional core–shell polymeric nanoparticles for transdermal DNA delivery and epidermal Langerhans cells tracking. Biomaterials 2010;31:2425–34.
[12] Rhyner MN, Smith AM, Gao X, Mao H, Yang L, Nie S. Quantum dots and multifunctional nanoparticles: new contrast agents for tumor imaging. Nanomed 2006;1:209–17.
[13] Alexis F, Pridgen E, Molnar LK, Farokhzad OC. Factors affecting the clearance and biodistribution of polymeric nanoparticles. Mol Pharmacol 2008;5:505–15.
[14] Semmler-Behnke M, Kreyling WG, Lipka J, Fertsch S, Wenk A, Takenaka S, et al. Biodistribution of 1.4- and 18-nm gold particles in rats. Small 2008;4:2108–11.
[15] Tartis MS, Kruse DE, Zheng H, Zhang H, Kheirolomoom A, Marik J, et al. Dynamic microPET imaging of ultrasound contrast agents and lipid delivery. J Control Release 2008;131:160–6.
[16] Fischer HC, Liu L, Pang KS, Chan WCW. Pharmacokinetics of nanoscale quantum dots: in vivo distribution, sequestration, and clearance in the rat. Adv Funct Mat 2006;16:1299–305.
[17] Kennel SJ, Woodward JD, Rondinone AJ, Wall J, Huang Y, Mirzadeh S. The fate of MAb-targeted Cd(125m)Te/ZnS nanoparticles in vivo. Nucl Med Biol 2008;35:501–14.
[18] Ballou B, Lagerholm BC, Ernst LA, Bruchez MP, Waggoner AS. Noninvasive imaging of quantum dots in mice. Bioconjug Chem 2004;15:79–86.
[19] Choi HS, Ipe BI, Misra P, Lee JH, Bawendi MG, Frangioni JV. Tissue- and organ-selective biodistribution of NIR fluorescent quantum dots. Nano Lett 2009;9:2354–9.
[20] Daou TJ, Li L, Reiss P, Josserand V, Texier I. Effect of poly(ethylene glycol) length on the in vivo behavior of coated quantum dots. Langmuir 2009;25:3040–4.
[21] Ballou B, Ernst LA, Andreko S, Fitzpatrick JA, Lagerholm BC, Waggoner AS, et al. Imaging vasculature and lymphatic flow in mice using quantum dots. Methods Mol Biol 2009;574:63–74.
[22] Larson DR, Zipfel WR, Williams RM, Clark SW, Bruchez MP, Wise FW, et al. Water-soluble quantum dots for multiphoton fluorescence imaging in vivo. Science 2003;300:1434–6.
[23] Pelley JL, Daar AS, Saner MA. State of academic knowledge on toxicity and biological fate of quantum dots. Toxicol Sci 2009;112:276–96.
[24] Stroh M, Zimmer JP, Duda DG, Levchenko TS, Cohen KS, Brown EB, et al. Quantum dots spectrally distinguish multiple species within the tumor milieu in vivo. Nat Med 2005;11:678–82.
[25] Bihari P, Holzer M, Praetner M, Fent J, Lerchenberger M, Reichel CA, et al. Single-walled carbon nanotubes activate platelets and accelerate thrombus formation in the microcirculation. Toxicology 2010;269:148–54.
[26] Gentile F, Curcio A, Indolfi C, Ferrari M, Decuzzi P. The margination propensity of spherical particles for vascular targeting in the microcirculation. J Nanobiotechnology 2008;6:9.
[27] Lee SY, Ferrari M, Decuzzi P. Design of bio-mimetic particles with enhanced vascular interaction. J Biomech 2009;42:1885–90.
[28] Baez S. An open cremaster muscle preparation for the study of blood vessels by in vivo microscopy. Microvasc Res 1973;5:384–94.
[29] Mempel TR, Moser C, Hutter J, Kuebler WM, Krombach F. Visualization of leukocyte transendothelial and interstitial migration using reflected light oblique transillumination in intravital video microscopy. J Vasc Res 2003;40:435–41.
[30] Robe A, Pic E, Lassalle HP, Bezdetnaya L, Guillemin F, Marchal F. Quantum dots in axillary lymph node mapping: biodistribution study in healthy mice. BMC Cancer 2008;8:111.
[31] Bateman RM, Hodgson KC, Kohli K, Knight D, Walley KR. Endotoxemia increases the clearance of mPEGylated 5000-MW quantum dots as revealed by multiphoton microvascular imaging. J Biomed Opt 2007;12:064005.
[32] Choi HS, Liu W, Misra P, Tanaka E, Zimmer JP, Itty Ipe B, et al. Renal clearance of quantum dots. Nat Biotechnol 2007;25:1165–70.
[33] Geys J, Nemmar A, Verbeken E, Smolders E, Ratoi M, Hoylaerts MF, et al. Acute toxicity and prothrombotic effects of quantum dots: impact of surface charge. Environ Health Perspect 2008;116:1607–13.
[34] Zhang LW, Monteiro-Riviere NA. Mechanisms of quantum dot nanoparticle cellular uptake. Toxicol Sci 2009;110:138–55.
[35] Schipper ML, Iyer G, Koh AL, Cheng Z, Ebenstein Y, Aharoni A, et al. Particle size, surface coating, and PEGylation influence the biodistribution of quantum dots in living mice. Small 2009;5:126–34.
[36] Peracchia MT, Harnisch S, Pinto-Alphandary H, Gulik A, Dedieu JC, Desmaele D, et al. Visualization of in vitro protein-rejecting properties of PEGylated stealth polycyanoacrylate nanoparticles. Biomaterials 1999;20:1269–75.
[37] Owens 3rd DE, Peppas NA. Opsonization, biodistribution, and pharmacokinetics of polymeric nanoparticles. Int J Pharm 2006;307:93–102.
[38] Lee HA, Imran M, Monteiro-Riviere NA, Colvin VL, Yu WW, Riviere JE. Biodistribution of quantum dot nanoparticles in perfused skin: evidence of coating dependency and periodicity in arterial extraction. Nano Lett 2007;7:2865–70.
[39] Fisher NG, Christiansen JP, Klibanov A, Taylor RP, Kaul S, Lindner JR. Influence of microbubble surface charge on capillary transit and myocardial contrast enhancement. J Am Coll Cardiol 2002;40:811–9.
[40] Ryman-Rasmussen JP, Riviere JE, Monteiro-Riviere NA. Variables influencing interactions of untargeted quantum dot nanoparticles with skin cells and identification of biochemical modulators. Nano Lett 2007;7:1344–8.
[41] Ryman-Rasmussen JP, Riviere JE, Monteiro-Riviere NA. Surface coatings determine cytotoxicity and irritation potential of quantum dot nanoparticles in epidermal keratinocytes. J Invest Dermatol 2007;127:143–53.
[42] Ades EW, Candal FJ, Swerlick RA, George VG, Summers S, Bosse DC, et al. HMEC-1: establishment of an immortalized human microvascular endothelial cell line. J Invest Dermatol 1992;99:683–90.
[43] Hellstrand E, Lynch I, Andersson A, Drakenberg T, Dahlback B, Dawson KA, et al. Complete high-density lipoproteins in nanoparticle corona. FEBS J 2009;276:3372–81.

Table 2
Tissue deposition and excretion of QDs

Organ	Time	carboxyl-QDs	amine-QDs	PEG-QDs
Heart	1 h	1.7 ± 0.1	0.9 ± 0..5	0
	4 h	1.5 ± 0.2 # *	0	0
	24 h	0.9 ± 0.1 # *	0	0
Lung	1 h	6.7± 0.4 # *	1.9 ± 0.1	4.8 ± 0.5
	4 h	6.2 ± 0.9 *	2.3 ± 0.1 §	3.9 ± 0.3
	24 h	3.6 ± 0.9 *	1-6 ± 0.1 §	2.8 ± 0.2
Liver	1 h	19.0 ± 10.6	5.1 ± 1.4	5.5 ± 1.5
	4 h	4.8 ± 2.3	8.4 ± 1.7	2.4 ± 0.5
	24 h	16.4 ± 4.1 # *	7.4 ± 0.8	4.3 ± 2.2
Spleen	1 h	18.0 ± 1.3 # *	1.8 ± 0.4 §	0.8 ± 0.2
	4 h	16.2 ± 1.0 # *	3.6 ± 1.9	2.5 ± 0.6
	24 h	17.4 ± 3.7 # *	2.9 ± 1.8	0.7 ± 0.1
Kidney	1 h	8.5 ± 1.5	4.9 ± 0.2	10.6 ± 2.1
	4 h	7.7 ± 2.4	5.6 ± 0.4	10.5 ± 1.5
	24 h	4.1 ± 0.4	4.8 ± 0.2	5.9 ± 0.7
Thoracic aorta	1 h	10.3 ± 2.6 # *	0.6 ± 0.8	1.6 ± 0.1
	4 h	8.2 ± 0.5 # *	0..5 ± 0.8	2.3 ± 1.2
	24 h	8.3 ± 1.3 # *	0 §	1.2 ± 0.2
Skeletal muscle	1 h	2.4 ± 0.4	0	0
	4 h	2.4 ± 0.2 # *	0	0
	24 h	1.9 ± 0.2 # *	0	0
Thymus gland	1 h	2.2 ± 1.5	2.8 ± 1.1	0
	4 h	2.0 ± 0.3 *	1.7 ± 0.1 §	0
	24 h	1.4 ± 0.5 *	1.4 ± 0.1 §	0
Lymph nodes	1 h	3.1 ± 0.9	2.7 ± 0.9	0.7 ± 0.1
	4 h	3.6 ± 0.9 *	5.4 ± 1.0 §	1.2 ± 0.2
	24 h	2.6 ± 0.6 # *	8.3 ± 1.5 §	0.8 ± 0.2
Brain	1 h	1.0 ± 0.1 # *	0	0
	4 h	0.7 ± 0.2 # *	0	0
	24 h	0.7 ± 0.3 # *	0	0

Excreta				
Bile	1 h	15.7 ± 9.0	19.0 ± 7.8	6.1 ± 2.6
	4 h	18.5 ± 10.4	13.0 ± 2.7	6.2 ± 1.1
	24 h	1.4 ± 0.3 # *	13.1 ± 8.2	6.4 ± 3.1
Duodenal Content	1 h	2.3 ± 0.6	3.2 ± 1.8	7.9 ± 3.5
	4 h	5.0 ± 2.0	2.7 ± 1.0	3.1 ± 0.9
	24 h	1.3 ± 0.7	3.2 ± 0.5	2.1 ± 0.5
Faeces	1 h	11.2 ± 2.4 *	2.5 ± 0.9 §	13.7 ± 3.1
	4 h	7.6 ± 4.1	3.8 ± 1.4	10.4 ± 2.7
	24 h	16.1 ± 4.3 *	3.3 ± 2.3 §	15.9 ± 1.3
Urine	1h	0	0	0
	4h	1.0 ± 0.2	0	1,0 ± 1.2
	24h	2.6 ± 0.4	2.3 ± 2.1	1.9 ± 0.3

QDs were given intra-arterially (3 pmol/g body weight) into anesthetized male C57BL/6 mice (n = 5 per group; control mice received vehicle). To assess blood and tissue kinetics, fluorescence was quantitatively measured in blood and tissue samples at subsequent time points. Mean values of 4-5 experiments ± SEM are given (#, $p<0.05$ [carboxyl-QDs vs PEG-QDs], *, $p<0.05$ [carboxyl-QDs vs amine-QDs], §, $p<0.05$ [amine-QDs vs PEG-QDs]). Zero (0) denotes values below detection limit (< 0.5 % ID/g tissue).

Supplementary movie file:

http://www.sciencedirect.com/science/article/pii/S0142961210006885

2. Quantum dots modify leukocyte recruitment depending on their surface modification:

NANO LETTERS

pubs.acs.org/NanoLett

Quantum Dots Modulate Leukocyte Adhesion and Transmigration Depending on Their Surface Modification

M. Rehberg,*,† M. Praetner,† C. F. Leite,†,‡ C. A. Reichel,† P. Bihari,† K. Mildner,§ S. Duhr,|| D. Zeuschner,§ and F. Krombach†

†Walter Brendel Centre of Experimental Medicine, Ludwig-Maximilians-Universität München, Munich, Germany, ‡Department of Thoracic Surgery, Faculty of Medical Sciences, State University of Campinas, Campinas, Brazil, §MPI of Molecular Biomedicine, Münster, Germany, and ||NanoTemper Technologies GmbH, Munich, Germany

ABSTRACT Although different nanosized materials, including quantum dots (QDs), are intended to be used for biomedical applications, their interactions with microvessels and their inflammatory potential are largely unknown. In this in vivo study we report that leukocyte recruitment is modulated in the presence of quantum dots. We found that the surface chemistry of QDs strongly affects their localization in postcapillary venules, their uptake by perivascular macrophages, and their potential to modify steps of leukocyte recruitment.

KEYWORDS Quantum dots, nanoparticles, surface modifications, inflammation, in vivo microscopy, microcirculation

Nanotechnology is a fast developing new area of research and industry. Various nanomaterials including quantum dots (QDs) are developed for biomedical applications,[1] e.g., as drug carriers and new tools for molecular diagnosis and treatment.[2,3] QDs exhibit unique fluorescent properties such as high emission intensity, photostability, and narrow emission spectra which makes them ideally suited for novel imaging approaches.[4] QDs emitting in the far-red region are especially promising for biomedical imaging in living tissues, for example, in tumor imaging and therapy.[5]

The expansion in production and use of nanomaterials raises the need to study potential impacts of the interactions between nanomaterials and biological systems.[6,7] It is well-established that nanosized particles can penetrate the biobarrier in the lungs and transfer into the bloodstream.[8,9] Nanosized ambient particles can trigger cardiovascular disorders including myocardial infarction.[10] Furthermore, they have the capability to augment ischemia−reperfusion injury,[11] to alter vascular reactivity,[12] and to induce inflammation at the systemic microvascular level.[13,14] Beyond that, intentionally administered nanomaterials, e.g., for diagnostic or therapeutic purposes, may also translocate into the circulation or directly reach the bloodstream via injection and thus induce systemic microvascular dysfunction.[15−17] In vitro studies showed that nanoparticles can induce expression of endothelial cell adhesion molecules[18] as well as production of inflammatory mediators in monocytes[19] and macrophages.[20]

Recently, it was demonstrated that the surface properties of nanomaterials determine the interaction with biological fluids and this in turn facilitates the biological activity of nanomaterials.[21,22] Interestingly, different surface chemistry of nanosized polystyrene particles led to altered affinity toward or uptake by cultured endothelial cells.[23] Moreover, the endocytic uptake of QDs by human epidermal keratinocytes was determined by their surface properties.[24] Uptake of nanoparticles by phagocytic cells can result in inflammatory cytokine production, as it happens after ingestion of microbial pathogens.[21,25]

In vivo, leukocyte recruitment from the microvasculature into inflamed tissue is a key event in both innate and adaptive immune response. The acute inflammatory response is associated with the release of soluble proinflammatory mediators, e.g., by tissue macrophages or mast cells, resulting in the activation of the endothelium. This includes the expression of endothelial adhesion molecules (selectins) that facilitate capture and rolling of leukocytes along the vessel wall. Rolling leukocytes are subsequently activated by the interaction with chemokines presented or secreted by endothelial cells. This leads to slow rolling and arrest followed by firm adhesion of leukocytes mediated by the action of integrins and intercellular adhesion molecules such as ICAM-1. Subsequently, leukocytes emigrate through the vascular wall into the interstitial tissue.[26]

The potential of nanoparticles to affect this process is still unknown. Therefore, we designed this study to investigate the impact of nanoparticles on leukocyte recruitment in an in vivo setting. We used QDs of the same size but with different surface modifications (carboxyl-, amine-, and PEG-QDs) to assess their effects on leukocyte recruitment in the mouse cremaster muscle preparation.

* To whom correspondence should be addressed, markus.rehberg@lrz.uni-muenchen.de.

Received for review: 06/15/2010
Published on Web: 08/09/2010

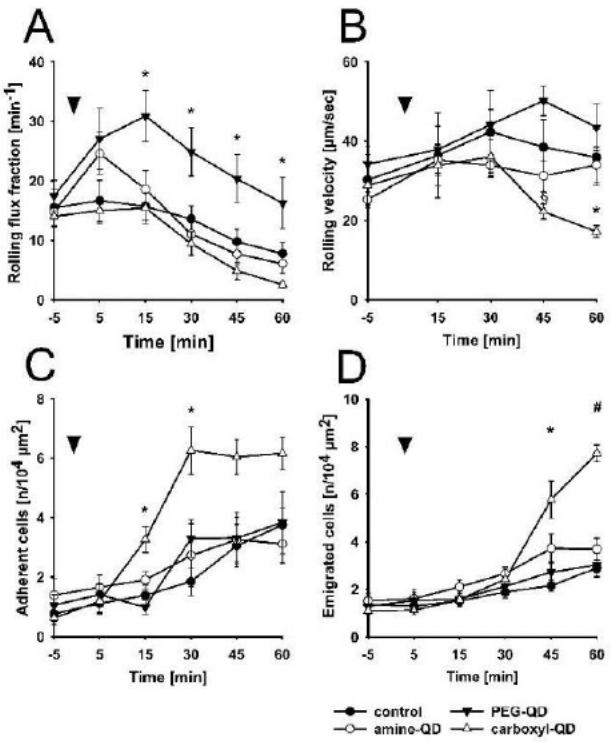

FIGURE 1. Quantitative analysis of parameters of leukocyte-endothelial cell interactions and leukocyte emigration after QD application. Leukocyte rolling (A), leukocyte rolling velocity (B), firm adherence (C), and transmigration (D) were quantified in postcapillary venules in the cremaster muscle using in vivo transillumination microscopy at baseline conditions and upon intra-arterial injection (arrow) of either carboxyl-QDs, amine-QDs, PEG-QDs, or vehicle at 3 pmol/g BW. Mean ± standard error of the mean for $n = 6$ per group: # $P < 0.001$ and * $P < 0.05$, vs all groups; § $P < 0.05$, carboxyl-QDs vs vehicle-control and PEG-QDs).

No statistically significant differences in microhemodynamic parameters and systemic leukocyte counts were detected among experimental groups receiving carboxyl-QDs, amine-QDs, PEG-QDs, or vehicle control, via intra-arterial injection, respectively (Table S1 in Supporting Information).

Effect of Carboxyl-QDs, Amine-QDs, and PEG-QDs on Leukocyte Recruitment. Using in vivo microscopy on the mouse cremaster muscle, steps of leukocyte recruitment were investigated. Due to the mechanical trauma of the surgical preparation, a certain degree of an inflammatory response was present in the cremasteric tissue under baseline conditions. This effect is well-defined[27,28] and responsible for leukocyte rolling (Figure 1A) and adhesion (Figure 1C) at the endothelium of postcapillary venules observed in the control group. Under control conditions, the number of rolling leukocytes decreased from 15.5 ± 3.1 min^{-1} at baseline to 7.8 ± 2.0 min^{-1} at 60 min, while the numbers of adherent and extravasated cells slightly increased (Figure 1A,C,D). Administration of PEG-QDs caused a 2-fold increase in leukocyte rolling (30.9 ± 4.3 min^{-1}) as compared to control (15.7 ± 2.3 min^{-1}) at 15 min after application which persisted over time (Figure 1A). In contrast, rolling leukocyte numbers did not differ from control after application of carboxyl- or amine-QDs (Figure 1A).

Mean leukocyte rolling velocities along the vessel wall of postcapillary venules (Figure 1B) after PEG- and amine-QDs injection matched those of control conditions (35.9 ± 7.1 μm/s at 60 min). The rolling velocity in control mice was in accordance to previously reported values.[27,29] In contrast, a significant decrease in leukocyte rolling velocity was observed at 45 min (22.2 ± 1.8 μm/s) and 60 min (17.2 ± 1.5 μm/s) after application of carboxyl-QDs (Figure 1B).

As shown in Figure 1C, administration of amine- or PEG-QDs did not affect leukocyte recruitment, whereas a significant increase (about 3-fold) in numbers of firmly adherent leukocytes (3.3 ± 0.4/10^4 μm^2) was found already at 15 min after application of carboxyl-QDs as compared to control (1.4 ± 0.4/10^4 μm^2). Consistent with the results obtained for leukocyte firm adherence, the number of transmigrated leukocytes detected within the perivascular tissue was elevated about 3-fold (5.8 ± 0.8/10^4 μm^2) as compared to control (2.2 ± 0.2/10^4 μm^2) at 45 min after application of carboxyl-QDs, but not after treatment with amine- and PEG-QDs (Figure 1D). Taken together, these data indicate that carboxyl-QDs but neither amine-QDs nor PEG-QDs increase leukocyte recruitment in the cremaster muscle preparation.

To investigate whether the basal inflammatory response caused by the surgical preparation was a prerequisite for the carboxyl-QD-evoked leukocyte recruitment, we performed cremaster preparation and subsequent in vivo microscopy 60 min *after* intra-arterial injection of carboxyl-QDs. Under these experimental conditions, leukocyte adhesion (3.9 ± 1.1/10^4 μm^2) and transmigration (1.8 ± 0.1/10^4 μm^2) were not elevated in animals treated with carboxyl-QDs as compared to animals receiving vehicle control (2.8 ± 0.9/10^4 μm^2 and 1.6 ± 0.1/10^4 μm^2, respectively).

To identify the phenotype of transmigrated leukocytes, immunostaining for CD45 (common leukocyte antigen), Gr-1 (neutrophils/monocytes), and F4/80 (monocytes/macrophages) of cremasteric tissue samples was performed: 75.0 ± 13.1 % of the transmigrated leukocytes were positive for Gr-1 and 22.2 ± 6.8 % of transmigrated leukocytes were positive for F4/80, respectively.

Carboxyl-QD-Evoked Leukocyte Recruitment Is ICAM-1 Dependent. To investigate whether carboxyl-QD-evoked adhesion and transmigration are mediated by endothelial adhesion molecules, we blocked ICAM-1 by intra-arterial injection of an anti-ICAM-1 mAb (YN-1) (Figure 2). Leukocyte adherence (3.4 ± 0.9/10^4 μm^2) as well as transmigration (1.5 ± 0.3/10^4 μm^2) were significantly diminished in YN-1 pretreated animals 30 min after administration of carboxyl-QDs as compared to control mice pretreated with an isotype-matched control mAb (7.2 ± 0.5/10^4 μm^2; 7.1 ± 1.4/10^4 μm^2). Furthermore, E-selectin expression was investigated in cremasteric postcapillary venules by means of confocal immunofluorescence microscopy. Prominent E-selectin ex-

DOI: 10.1021/nl102100m | Nano Lett. 2010, 10, 3656–3664

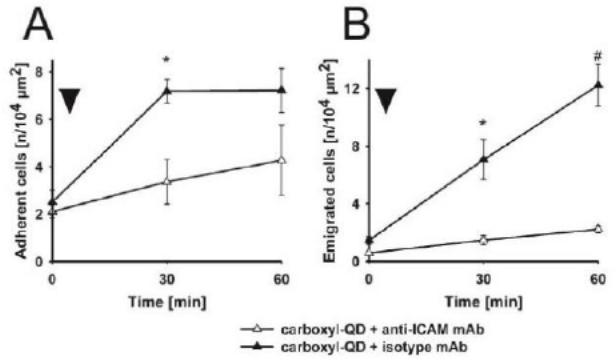

FIGURE 2. Carboxyl-QD-evoked leukocyte firm adhesion and transmigration is mediated by ICAM-1. Quantification of leukocyte firm adherence (A) and leukocyte transmigration (B) in postcapillary venules of mice pretreated with either a blocking anti ICAM-1 mAb or an isotype control mAb upon i.a. injection of carboxyl-QDs (arrow). (mean ± standard error of the mean for $n = 6$ per group; # $P < 0.001$ and * $P < 0.05$, vs all groups.)

pression was detected in postcapillary venules 60 min upon application of carboxyl-QDs (Figure 3A and 3B) in contrast to weak E-selectin staining observed under control conditions (parts C and D of Figure 3).

Carboxyl-QD-Evoked Leukocyte Recruitment Is Mast Cell Mediated. Mast cells are known to account for leukocyte recruitment by the release of inflammatory mediators, resulting in an upregulation or activation of endothelial cell adhesion molecules.[30,31] Mast cells are present in the cremasteric tissue (Figure 4A), predominantly located in close proximity to vessels as we have reported previously.[32] Therefore, the effect of an inhibitor of mast cell degranulation, cromolyn, on carboxyl-QDs elicited leukocyte responses was evaluated.

In cromolyn-pretreated animals, carboxyl-QD-evoked leukocyte adherence was found to be significantly reduced

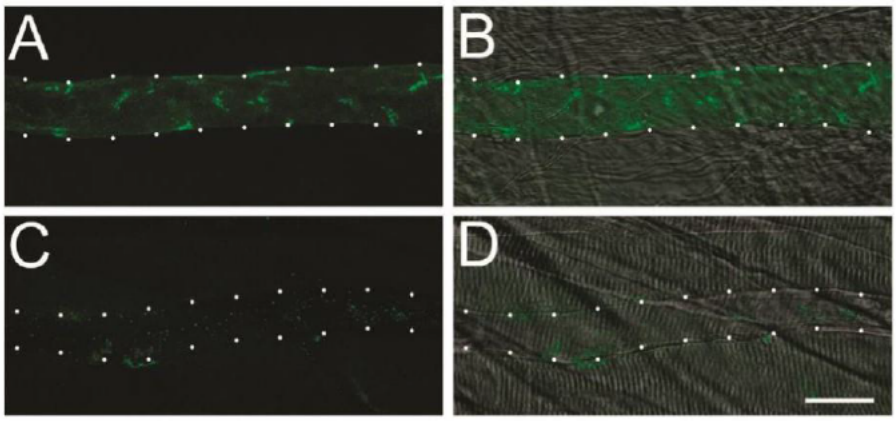

FIGURE 3. E-selectin expression is enhanced in postcapillary venules upon carboxyl-QD application. Representative images of E-selectin expression (green) in cremasteric postcapillary venules, obtained by confocal immunofluorescence microscopy 60 min upon application of carboxyl-QDs (A, B) or vehicle (C, D). Projections of z-planes covering whole vessels (projection of 30 z-planes; z-spacing 1 μm) are shown in (A) and (C) merged with the corresponding transmitted light images (single z-plane) of the cremasteric tissue in (B) and (D). The outline of the vessel wall is indicated by white dots. Scale bar: 30 μm.

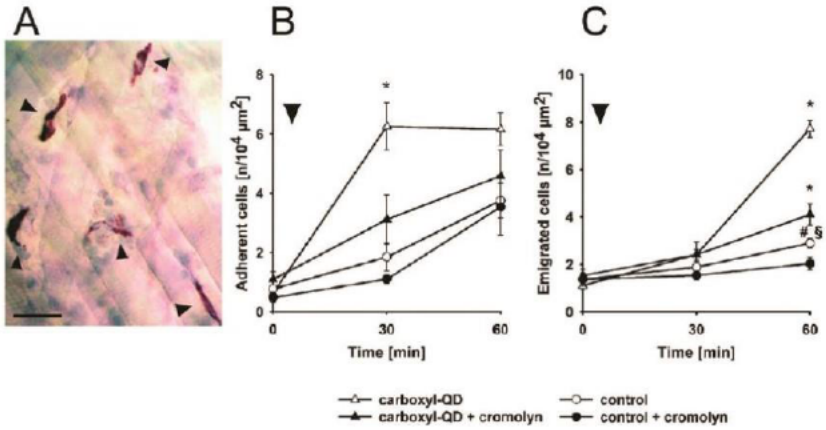

FIGURE 4. Mast cell inhibition reduces carboxyl-QD-evoked leukocyte adherence and transmigration. (A) Toluidine blue-stained mast cells (arrowheads) in the cremasteric tissue. Leukocyte firm adherence (B) and transmigration (C) was quantified in postcapillary venules of mice receiving cromolyn, an inhibitor of mast cell degranulation, or saline prior to injection of carboxyl-QDs or vehicle-control. Scale bar: 50 μm (mean ± standard error of the mean for $n = 6$ per group; * $p < 0.001$ vs all groups; # $p < 0.001$ vs carboxyl-QDs; § $p < 0.05$ vs carboxyl-QDs + cromolyn).

DOI: 10.1021/nl102100m | Nano Lett. 2010, 10, 3656–3664

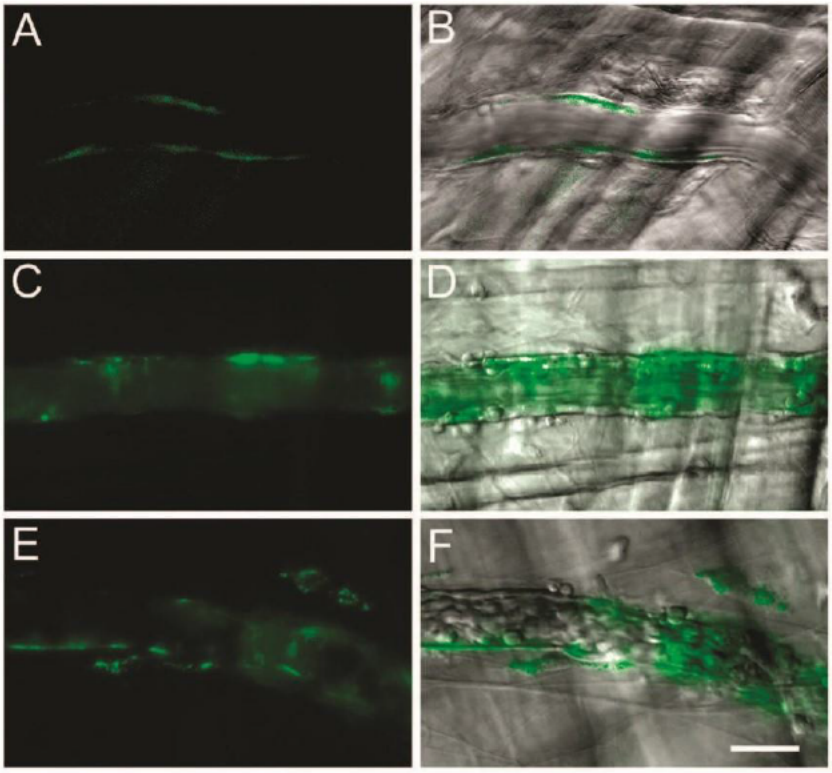

FIGURE 5. QD localization in postcapillary venules. In vivo fluorescence microscopy revealed localization of amine-QDs (panels A and B and movie S1 in the Supporting Information), PEG-QDs (panels C and D and movie S2 in the Supporting Information), and carboxyl-QDs (panels E and F and movie S3 in the Supporting Information) in postcapillary venules. Images displayed are taken from movies available in the Supporting Information section and show representative localization patterns 30 min after QD application (3 pmol/g of BW). QD fluorescence is depicted in (A), (C), and (E) and merged with the corresponding bright field images of the cremasteric tissue in (B), (D), and (F). Due to the low fluorescence, in the case of amine-QDs image contrast was enhanced; therefore fluorescence intensities are not directly comparable. Scale bar represents 30 μm.

at 30 min ($3.1 \pm 0.8/10^4$ μm^2) as compared to animals receiving vehicle instead of cromolyn ($6.3 \pm 0.8/10^4$ μm^2) (Figure 4B). Cromolyn treatment in animals receiving vehicle ($1.1 \pm 0.1/10^4$ μm^2) did not alter the number of firmly adherent leukocytes as compared to animals receiving vehicle only at 30 min ($1.9 \pm 0.5/10^4$ μm^2) (Figure 4B).

Cromolyn pretreatment also caused a significant decrease in carboxyl-QD-elicited leukocyte transmigration ($4.1 \pm 0.5/10^4$ vs μm^2) as compared to animals receiving carboxyl-QDs only at 60 min ($7.7 \pm 0.4/10^4$ μm^2) (Figure 3C). Leukocyte numbers detected in the perivascular tissue of cromolyn- and carboxyl-QD-treated animals were still significantly higher than those found in animals receiving vehicle only ($2.9 \pm 0.2/10^4$ μm^2).

Carboxyl-QDs Are Preferentially Taken up by Perivascular Macrophages. Next we analyzed QD localization in postcapillary venules. All types of QDs were detectable in the bloodstream within seconds after application by in vivo fluorescence microscopy in postcapillary venules and found to be associated with the vessel wall within minutes after injection. Amine-QDs exhibited a weak association (panels A and B of Figure 5 and movie S1 in the Supporting Information) with the vessel wall, whereas PEG-QDs (panels C and D of Figure 4 and movie S2 in the Supporting Information) as well as carboxyl-QDs showed a stable but discontinuous distribution along the vessel wall (panels E and F in Figure 5 and movie S3 in the Supporting Information). Moreover, carboxyl-QDs but not amine- and PEG-QDs, appeared to be localized in vesicles of perivascular cells (panels E and F in Figure 5 and movie S3 in the Supporting Information).

Real-time observation of carboxyl-QD dynamics in postcapillary venules revealed a rapid uptake of carboxyl-QDs by perivascular cells (Figure 6 and movie S4 in the Supporting Information). Already at 3 min after injection, QDs first appeared in these cells (Figure 6A and movie S4 in the Supporting Information). Fluorescence intensity measurements in individual cells showed an accumulation of carboxyl-QDs over time (Figure 6B). A stretch of carboxyl-QD fluorescence at the vessel wall was visible already 60 s after application and stable for the whole observation time of 30 min. Carboxyl-QD fluorescence in the vessel lumen was swiftly declining over time, indicating QD clearance from the bloodstream.

Interestingly, carboxyl-QDs were not detectable in perivascular cells of cremasteric tissue, when the intra-arterial QD

DOI: 10.1021/nl102100m | Nano Lett. 2010, 10, 3656–3664

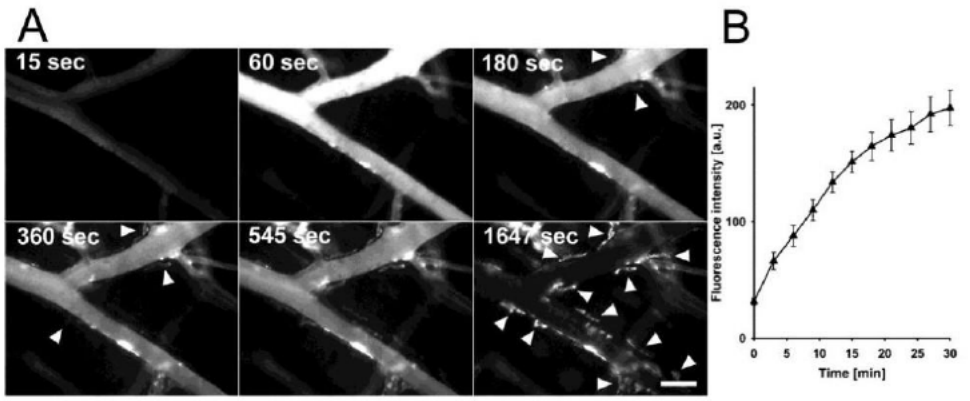

FIGURE 6. In vivo fluorescence microscopy of carboxyl-QD dynamics in postcapillary venules (panel A and movie S4 in the Supporting Information). Live observation of carboxyl-QD dynamics in postcapillary venules revealed rapid uptake of carboxyl-QDs by perivascular cells (arrows). In this example, QD fluorescence is visible 180 s after intra-arterial injection of carboxyl-QDs (6 pmol/g of BW). Images shown are selected from a movie acquired using 2 × 2 binning, a time delay of 5 s between frames, and an exposure of 300 ms/frame; scale bar: 100 μm. (B) QD fluorescence intensity was determined in individual cells over time. Analyzed cells are indicated by arrows. (mean ± standard error of the mean for $n = 11$; scale bar, 50 μm).

application was performed 60 min prior to the surgical preparation.

We further asked whether carboxyl-QDs were present in mast cells. Therefore, we analyzed toluidine blue-stained cremasteric tissue. Carboxyl-QD fluorescence was not detected in toluidine blue-stained mast cells.

Preferential uptake and vesicular localization (Figure S1 in the Supporting Information) of carboxyl-QDs was also observed in vitro using the RAW264.7 murine macrophage cell line. Macrophage cellular QD-fluorescence was analyzed after 15 min of incubation with QDs by confocal microscopy. Carboxyl-QD cellular fluorescence intensities were 40- to 60-fold higher as compared to amine- and PEG-QDs (carboxyl-QDs 100 ± 13.4; amine-QDs 2.7 ± 0.6; PEG-QDs 1.8 ± 0.1 relative fluorescence intensities).

Electron microscopy was employed to further investigate the localization of QDs in the cremasteric tissue. Elliptical-shaped QDs were only unambiguously identified after omitting the standard counterstain (uranyl acetate and lead). The image contrast is caused predominantly by membrane lipids. As depicted, carboxyl-QDs were detected in perivascular cells in close vicinity to blood vessels in the perivascular tissue (Figure S2A and S2B in the Supporting Information). On the basis of their morphology and their ability to ingest carboxyl-QDs, these cells were identified as perivascular macrophages. Carboxyl-QDs were found in the cytoplasm and enriched in the endosomal-lysosomal compartment (Figure 7B) of perivascular macrophages, thus confirming localization patterns obtained by in vivo fluorescence microscopy (Figures 5 and 6). On the ultrastructural level, the secretory pathway (ER and Golgi) was found to be negative for carboxyl-QDs, as was the nucleus and mitochondria. Endothelial cells also contained carboxyl-QDs—here most of the QDs were found in caveolae (Figure 7A) indicating caveolae-mediated endocytosis.

Amine-QDs were rarely seen in the endothelial cell layer (Figure 7C) of postcapillary venules, and only some perivascular cells exhibited cytoplasmic staining (Figure 7D) and little labeling of vesicles with characteristics of early endosomes. In contrast to carboxyl- and amine-QDs, PEG-QDs were mainly found outside endothelial cells (Figure 7E), attached to amorphous lipid containing material which was deposited at the vessel wall. Only few perivascular cells showed a cytoplasmic label for PEG-QDs (Figure 7F).

Carboxyl-QD Associate with Serum Protein. Since nanoparticles present in the circulation encounter serum proteins and it is generally accepted that protein−surface interactions determine the biological activity of nanomaterials or mediate their uptake by macrophages,[21,33] we analyzed the diameter of QD particles as a measure of QD−protein interaction at 15 min after incubation with serum. PEG-QDs incubated in serum exhibited no increase in size compared to PBS (serum 32.2 ± 0.6 nm vs PBS 32.2 ± 0.4 nm), in accordance with the well-documented fact that PEGylation extensively prevents protein binding.[34,35] In contrast, amine-QDs showed a moderate increase in diameter (serum 29.7 ± 1.1 nm vs PBS 23.6 ± 1.6 nm), whereas the diameter of carboxyl-QDs was highly enhanced (serum 38.9 ± 3.7 nm vs PBS 19.8 ± 2.2 nm), indicating a strong QD−protein interaction.

QDs and other nanosized structures are expected to have a greater inflammatory potential compared to larger particles owing to a large surface area to volume ratio.[9] Recent research shows that nanoparticles can stimulate and/or suppress immune responses and that their compatibility with the immune system is largely determined by their surface chemistry.[33] Experiments by Nurkiewicz et al. have indicated that exposure to particulate matter leads to enhanced leukocyte rolling and adhesion in venules of the spinotrapezius muscle.[13,14] Moreover, our group recently reported that the capillary endothelium contributes to blood

DOI: 10.1021/nl102100m | Nano Lett. 2010, 10, 3656–3664

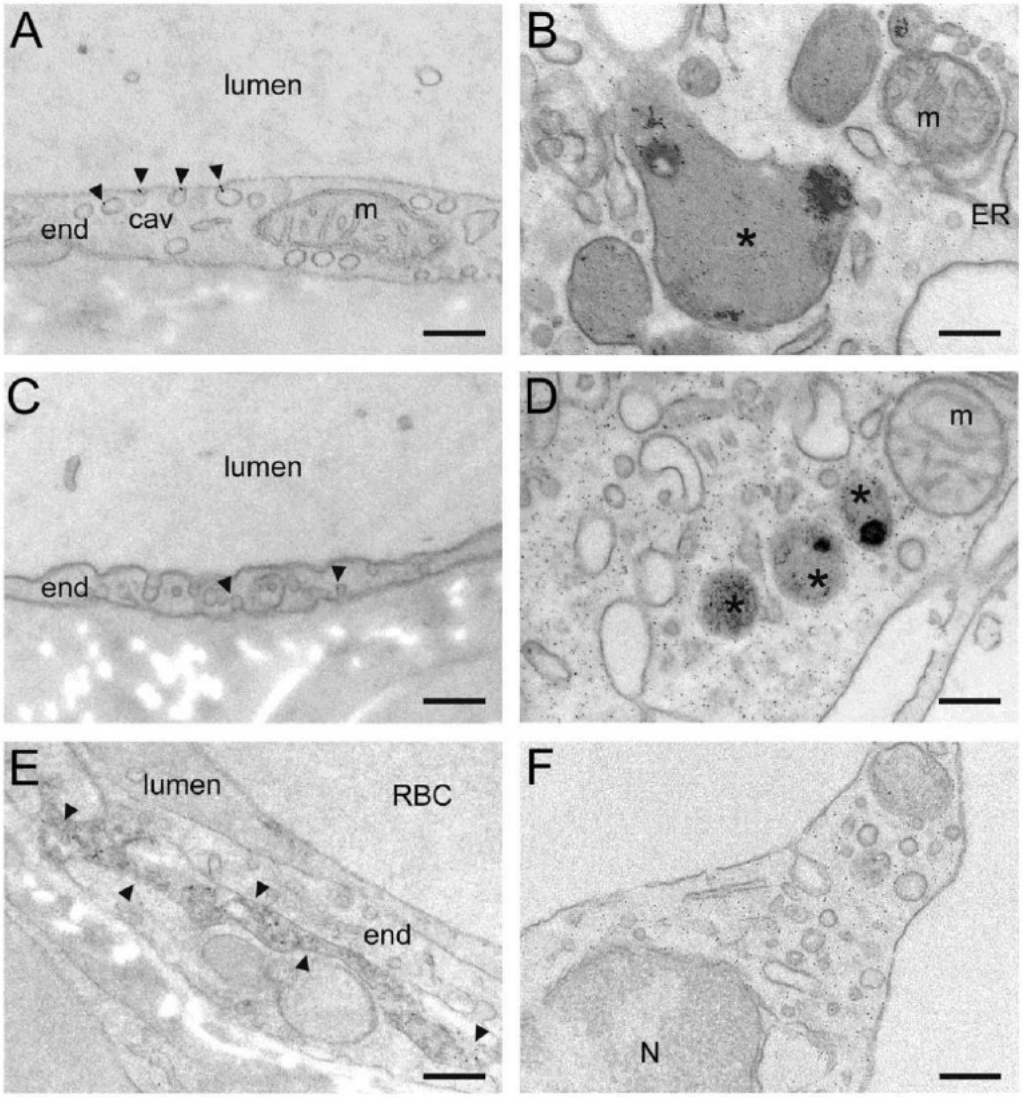

FIGURE 7. Electron microscopic examination of QD localization in postcapillary venules. Transmission electron microscopy was performed on ultrathin cross sections of cremasteric tissue 60 min upon application of QDs. Contrast of the tissue results from postfixation of lipids with OsO_4 only, representative images are shown. (A) High magnification of an endothelial cell layer shows single carboxyl-QDs (arrowhead) during uptake in caveolae (cav). (B) Carboxyl-QDs in perivascular macrophages localize predominantly to the endosomal-lysosomal compartment (asterisk). In the cytoplasm, carboxyl-QDs are more randomly distributed; note their absence in mitochondria (m). (C) Amine-QDs were found in endothelial cells (arrowhead) and also in the cytoplasm of perivascular macrophages (D), there to some extent also in early endosomes (asterisk). These organelles, as they mature to late endosomes and lysosomes, also contain dark stained membrane sheets that can be seen as fuzzy material to which some regular shaped QDs are associated. (E) PEG-QDs were found clustered in between endothelial cells (arrowheads), where they seem to be associated with amorphous lipid-containing material. (F) Some PEG-QDs reached also perivascular macrophages. Abbreviations: cav, caveolae; end, endothelial cell; ER, endoplasmic reticulum; N, nucleus; m, mitochondria; RBC, red blood cell. Scale bar represents 200 nm.

clearance and tissue deposition of anionic quantum dots in vivo.[46] Although nanomaterials, including QDs, are intended to be used for biomedical applications and therefore injected into the blood circulation, the interaction of different surface modified QDs with postcapillary venules and their potential to influence leukocyte recruitment had not yet been explored in vivo.

To our knowledge, our in vivo study is the first to demonstrate that leukocyte recruitment is modulated in the presence of nanoparticles. We found that the surface chemistry of nanomaterials strongly affects their localization in postcapillary venules, their uptake by perivascular macrophages, and their potential to modify steps of leukocyte recruitment. We speculate that the observed differences in localization are causal for the impact on leukocyte recruitment.

We have chosen to apply commercially available QDs which are intended to be used for in vivo imaging ap-

DOI: 10.1021/nl102100m | Nano Lett. 2010, 10, 3656–3664

plications including vascular imaging. In addition, these QDs have been already extensively utilized to investigate surface-coating-dependent cytotoxicity and cellular uptake mechanisms.[24,36−38]

The cremaster muscle preparation is a well-defined and widely used model system which allows for high-quality in vivo microscopy to investigate mode and mechanisms of leukocyte recruitment.[26,28,39] Model-inherent properties include P-selectin-dependent leukocyte rolling, followed by slight leukocyte adhesion and transmigration due to the surgical preparation. This basal inflammatory response is very mild compared to inflammation obtained after application of inflammatory mediators such as PAF and MIP-1-alpha or after ischemia-reperfusion.[28,32,40] Mast cells do not contribute to preparation-induced leukocyte recruitment indicating that the surgical preparation of the cremaster muscle does not evoke mast cell activation.[41] The extent of leukocyte recruitment upon carboxyl-QD injection was considerable, although only approximately half the cell numbers were recruited to the perivascular tissue compared to extravasation after ischemia−reperfusion or upon superfusion with PAF.[28,40]

Coating of nanoparticles, once in contact with biological fluids, with proteins and other biomolecules[42,43] mediates nanoparticle biological identity and activity, thus determining nanoparticle interactions, clearance, and biodistribution.[35,44,45] Various opsonizing proteins mark nanoparticles for uptake by the mononuclear phagocytic system. However, PEGylation of nanoparticles largely prevents protein binding and thus renders them invisible for macrophages.[34] Accordingly, we found in our size-measurements that PEG-QD exhibited no increased hydrodynamic diameter in serum whereas the carboxyl-QD size in serum indicated strong protein interaction. The QD size distributions measured in PBS were in accordance with previously reported values obtained by dynamic light scattering[24,46] as well as by the method used here, Microscale Thermophoresis, a novel sensitive method to analyze biomolecule and nanoparticle−protein interactions.[47,48]

Interestingly, PEGylation of QDs did not prevent interactions with the vessel wall. On the contrary, we observed PEG-QD clustered with lipidous structures at the vessel wall. Recently, a pronounced interaction of PEG-QDs with intracellular lipid droplets has been reported after in vitro exposure of human epidermal keratinocytes.[37] Since PEG is able to induce fusion of pure lipids as well as fusion between liposomes,[49] PEG-coated QDs might induce local lipid clustering in the microvasculature. The localization of carboxyl-QD in caveolae of endothelial cells and in the endosomal-lysosomal system of perivascular macrophages together with the rapid onset of QD accumulation argues for an active and specific uptake via the endocytic pathway.[50] Endocytic uptake of nanoparticles has been described frequently in the literature and, in the case of carboxyl-QD, is discussed to be mediated by G-protein-coupled receptor-associated pathways and low density lipoprotein receptor/scavenger receptors in vitro.[9,24]

Vessel-lining macrophages associated with endothelia can be found throughout the body.[51] The existence of macrophages spreading longitudinally along microvessel walls in the cremaster muscle and probably probing the blood vessels was reported previously.[52] Most interestingly, the uptake of carboxyl-QD in our in vivo situation was strictly dependent on tissue preparation, suggesting that tissue trauma leads to activation of endothelial cells and perivascular macrophages. This observation is in accordance with previous findings that tissue resident macrophages are biased toward phagocytosis upon tissue injury and in sterile wounds.[51] Thus, resident phagocytic cells in muscle tissue might contribute to nanoparticle clearance under pathophysiological conditions. Further studies defining more precisely the mode and mechanisms of carboxyl-QD uptake by perivascular macrophages in vivo are on their way.

It has been previously shown that the uptake of nanoparticles by macrophages stimulates the generation of inflammatory mediators.[21,25] Moreover phagocytosis of nanoparticles seems to be crucial for triggering cytokine production and release.[53] Therefore, it is intriguing to speculate that carboxyl-QD-containing macrophages might stimulate mast cells which are likewise located in close vicinity to the vascular endothelium.

Mast cells are known to account for leukocyte recruitment by the release of inflammatory mediators, resulting in an upregulation or activation of endothelial cell adhesion molecules.[30,31] Activated mast cells degranulate and thus distribute potent inflammatory mediators such as histamine, platelet activating factor, or TNF-alpha leading to subsequent endothelial activation.[30] Indeed, mast cells express several receptors which make them capable of responding to macrophage-released chemokines.[31] Furthermore, several studies pointed out that mast-cell-regulated neutrophil recruitment is essential for mounting efficient innate immunity.[31] In this context, we demonstrate that blocking mast cell degranulation almost completely prevents carboxyl-QD-evoked leukocyte recruitment. Involvement of mast cells could also explain the rapid increase in leukocyte adherence already at 15 min after carboxyl-QD application, since it has been shown that mast cell activation rapidly (within 10 min) increases leukocyte adhesion.[54] In addition to an intermediate role of mast cells after stimulation through macrophage-derived inflammatory mediators,[55] we cannot rule out direct activation of mast cells by carboxyl-QDs, e.g., due to cross-linking of IgE receptors or via activated complement proteins.[56]

Endothelial activation by inflammatory mediators such as TNF-alpha results in strong upregulation of the constitutively expressed immunoglobulin superfamily member ICAM-1 as well as expression of E-selectin on endothelial cells. Subsequently, ICAM-1 actively mediates leukocyte firm adhesion as well as transendothelial migration in a complex

DOI: 10.1021/nl102100m | Nano Lett. 2010, 10, 3656–3664

interplay with several other molecules.[26] Interestingly, it has been shown that ICAM-1 is essential for fast leukocyte adhesion after local application of the chemoattractants fMLP and MIP-2 close to postcapillary venules in the cremaster muscle.[57] The ICAM-1 dependency of carboxyl-QD-enhanced leukocyte recruitment might, as discussed above, reflect a chemokine-induced inflammatory response and indicates activation of the endothelial cell layer. The retarded leukocyte rolling velocity after application of carboxyl-QD additionally further strengthens this point, since slow rolling mediated via endothelial expressed E-selectin is a hallmark of the leukocyte recruitment cascade.[26,29] Furthermore, we could clearly demonstrate that E-selectin was highly expressed in cremasteric postcapillary venules 60 min upon application of carboxyl-QDs. Endothelial activation might, at least to a little extent, be a direct consequence of carboxyl-QD uptake by endothelial cells. The fact that PEG-QDs amplify leukocyte rolling cannot be easily explained. This effect might be facilitated by PEG-induced unspecific lipid interactions between leukocyte and endothelium or due to enhanced receptor availability or modulated receptor/ligand affinity. Interactions of PEG-QDs with receptor molecules, e.g., P-selectin, could result in receptor clustering or promote the formation and strengthening of catch bonds.[26] Further work addressing this effect is clearly necessary. However, the enhanced rolling did not initiate leukocyte recruitment to the surrounding tissue.

Taken together, these findings demonstrate that the surface chemistry of quantum dots strongly affects their fate in vivo, i.e., their cellular and noncellular interactions in murine microvessels as well as their potential to modify inflammatory processes in a mouse model. Thus, this study strongly corroborates the view that the surface chemistry of nanomaterials is a crucial parameter to be considered with regard to biomedical applications.

Acknowledgment. This work was supported by the Bio-Imaging Network of Ludwig-Maximilians-Universität München and by grants of the Friedrich-Baur-Stiftung (to M.R.) and the European Union (STREP "NANOSH" to F.K.). The authors thank A. Schropp for technical assistance and Dr. Jürgen Peters for statistical review of the data. Data presented in this study are part of the doctoral thesis of M.P.

Supporting Information Available. Information regarding animals, experimental protocols, immunohistochemistry, electron microscopy, and statistics are provided in the SI Material and Methods, and surgical procedure, in vivo microscopy, and quantification of leukocyte kinetics and microhemodynamic parameters as well as QD size measurements were performed as described previously[48,58] and are detailed in SI Materials and Methods. This material is available free of charge via the Internet at http://pubs.acs.org.

REFERENCES AND NOTES

(1) Xia, Y. *Nat. Mater.* **2008**, *7* (10), 758–760.
(2) Gao, X.; Cui, Y.; Levenson, R. M.; Chung, L. W.; Nie, S. *Nat. Biotechnol.* **2004**, *22* (8), 969–976.
(3) Zintchenko, A.; Susha, A. S.; Concia, M.; Feldmann, J.; Wagner, E.; Rogach, A. L.; Ogris, M. *Mol. Ther.* **2009**, *17* (11), 1849–1856.
(4) Medintz, I. L.; Uyeda, H. T.; Goldman, E. R.; Mattoussi, H. *Nat. Mater.* **2005**, *4* (6), 435–446.
(5) Kim, S.; Lim, Y. T.; Soltesz, E. G.; De Grand, A. M.; Lee, J.; Nakayama, A.; Parker, J. A.; Mihaljevic, T.; Laurence, R. G.; Dor, D. M.; Cohn, L. H.; Bawendi, M. G.; Frangioni, J. V. *Nat. Biotechnol.* **2004**, *22* (1), 93–97.
(6) Borm, P. J.; Robbins, D.; Haubold, S.; Kuhlbusch, T.; Fissan, H.; Donaldson, K.; Schins, R.; Stone, V.; Kreyling, W.; Lademann, J.; Krutmann, J.; Warheit, D.; Oberdorster, E. *Part. Fibre Toxicol.* **2006**, *3*, 11.
(7) Maynard, A. D.; Aitken, R. J.; Butz, T.; Colvin, V.; Donaldson, K.; Oberdorster, G.; Philbert, M. A.; Ryan, J.; Seaton, A.; Stone, V.; Tinkle, S. S.; Tran, L.; Walker, N. J.; Warheit, D. B. *Nature* **2006**, *444* (7117), 267–269.
(8) Nemmar, A.; Hoet, P. H.; Vanquickenborne, B.; Dinsdale, D.; Thomeer, M.; Hoylaerts, M. F.; Vanbilloen, H.; Mortelmans, L.; Nemery, B. *Circulation* **2002**, *105* (4), 411–414.
(9) Oberdorster, G.; Oberdorster, E.; Oberdorster, J. *Environ. Health Perspect.* **2005**, *113* (7), 823–839.
(10) Peters, A.; Dockery, D. W.; Muller, J. E.; Mittleman, M. A. *Circulation* **2001**, *103* (23), 2810–2815.
(11) Cozzi, E.; Hazarika, S.; Stallings, H. W., 3rd; Cascio, W. E.; Devlin, R. B.; Lust, R. M.; Wingard, C. J.; Van Scott, M. R. *Am. J. Physiol. Heart Circ. Physiol.* **2006**, *291* (2), H894–903.
(12) O'Neill, M. S.; Veves, A.; Zanobetti, A.; Sarnat, J. A.; Gold, D. R.; Economides, P. A.; Horton, E. S.; Schwartz, J. *Circulation* **2005**, *111* (22), 2913–2920.
(13) Nurkiewicz, T. R.; Porter, D. W.; Barger, M.; Castranova, V.; Boegehold, M. A. *Environ. Health Perspect.* **2004**, *112* (13), 1299–1306.
(14) Nurkiewicz, T. R.; Porter, D. W.; Barger, M.; Millecchia, L.; Rao, K. M.; Marvar, P. J.; Hubbs, A. F.; Castranova, V.; Boegehold, M. A. *Environ. Health Perspect.* **2006**, *114* (3), 412–419.
(15) Bihari, P.; Holzer, M.; Praetner, M.; Fent, J.; Lerchenberger, M.; Reichel, C. A.; Rehberg, M.; Lakatos, S.; Krombach, F. *Toxicology* **2010**, *269*, 148–154.
(16) Geys, J.; Nemmar, A.; Verbeken, E.; Smolders, E.; Ratoi, M.; Hoylaerts, M. F.; Nemery, B.; Hoet, P. H. *Environ. Health Perspect.* **2008**, *116* (12), 1607–1613.
(17) Nurkiewicz, T. R.; Porter, D. W.; Hubbs, A. F.; Cumpston, J. L.; Chen, B. T.; Frazer, D. G.; Castranova, V. *Part. Fibre Toxicol.* **2008**, *5*, 1.
(18) Oesterling, E.; Chopra, N.; Gavalas, V.; Arzuaga, X.; Lim, E. J.; Sultana, R.; Butterfield, D. A.; Bachas, L.; Hennig, B. *Toxicol. Lett.* **2008**, *178* (3), 160–166.
(19) Lee, H. M.; Shin, D. M.; Song, H. M.; Yuk, J. M.; Lee, Z. W.; Lee, S. H.; Hwang, S. M.; Kim, J. M.; Lee, C. S.; Jo, E. K. *Toxicol. Appl. Pharmacol.* **2009**, *238* (2), 160–169.
(20) Kang, C. M.; Jang, A. S.; Ahn, M. H.; Shin, J. A.; Kim, J. H.; Choi, Y. S.; Rhim, T. Y.; Park, C. S. *Am. J. Respir. Cell Mol. Biol.* **2005**, *33* (3), 290–296.
(21) Dobrovolskaia, M. A.; McNeil, S. E. *Nat. Nanotechnol.* **2007**, *2* (8), 469–478.
(22) Lundqvist, M.; Stigler, J.; Elia, G.; Lynch, I.; Cedervall, T.; Dawson, K. A. *Proc. Natl. Acad. Sci. U.S.A.* **2008**, *105* (38), 14265–14270.
(23) Ehrenberg, M. S.; Friedman, A. E.; Finkelstein, J. N.; Oberdorster, G.; McGrath, J. L. *Biomaterials* **2009**, *30* (4), 603–610.
(24) Zhang, L. W.; Monteiro-Riviere, N. A. *Toxicol. Sci.* **2009**, *110* (1), 138–55.
(25) Cui, Z.; Mumper, R. J. *Int. J. Pharm.* **2002**, *238* (1–2), 229–239.
(26) Ley, K.; Laudanna, C.; Cybulsky, M. I.; Nourshargh, S. *Nat. Rev. Immunol.* **2007**, *7* (9), 678–689.
(27) Kunkel, E. J.; Jung, U.; Bullard, D. C.; Norman, K. E.; Wolitzky, B. A.; Vestweber, D.; Beaudet, A. L.; Ley, K. *J. Exp. Med.* **1996**, *183* (1), 57–65.
(28) Mempel, T. R.; Moser, C.; Hutter, J.; Kuebler, W. M.; Krombach, F. *J. Vasc. Res.* **2003**, *40* (5), 435–441.
(29) Kunkel, E. J.; Ley, K. *Circ. Res.* **1996**, *79* (6), 1196–1204.
(30) Kneilling, M.; Mailhammer, R.; Hultner, L.; Schonberger, T.; Fuchs, K.; Schaller, M.; Bukala, D.; Massberg, S.; Sander, C. A.; Braumuller, H.; Eichner, M.; Maier, K. L.; Hallmann, R.; Pichler,

DOI: 10.1021/nl102100m | *Nano Lett.* **2010**, *10*, 3656–3664

B. J.; Haubner, R.; Gawaz, M.; Pfeffer, K.; Biedermann, T.; Rocken, M. *Blood* **2009**, *114* (8), 1696–1706.
(31) Schramm, R.; Thorlacius, H. *Inflammation Res.* **2004**, *53* (12), 644–652.
(32) Reichel, C. A.; Rehberg, M.; Lerchenberger, M.; Berberich, N.; Bihari, P.; Khandoga, A. G.; Zahler, S.; Krombach, F. *Arterioscler., Thromb., Vasc. Biol.* **2009**, *29*, 1787–1793.
(33) Dobrovolskaia, M. A.; Germolec, D. R.; Weaver, J. L. *Nat. Nanotechnol.* **2009**, *4* (7), 411–414.
(34) Gref, R.; Minamitake, Y.; Peracchia, M. T.; Trubetskoy, V.; Torchilin, V.; Langer, R. *Science* **1994**, *263* (5153), 1600–1603.
(35) Owens, D. E., 3rd; Peppas, N. A. *Int. J. Pharm.* **2006**, *307* (1), 93–102.
(36) Ryman-Rasmussen, J. P.; Riviere, J. E.; Monteiro-Riviere, N. A. *Toxicol. Sci.* **2006**, *91* (1), 159–165.
(37) Ryman-Rasmussen, J. P.; Riviere, J. E.; Monteiro-Riviere, N. A. *J. Invest. Dermatol.* **2007**, *127* (1), 143–153.
(38) Zhang, L. W.; Yu, W. W.; Colvin, V. L.; Monteiro-Riviere, N. A. *Toxicol. Appl. Pharmacol.* **2008**, *228* (2), 200–211.
(39) Baez, S. *Microvasc. Res.* **1973**, *5* (3), 384–394.
(40) Reichel, C. A.; Khandoga, A.; Anders, H. J.; Schlondorff, D.; Luckow, B.; Krombach, F. *J. Leukocyte Biol.* **2006**, *79* (1), 114–122.
(41) Guo, Y.; Lindbom, L.; Hedqvist, P. *Inflammation Res.* **2000**, *49* (7), 325–329.
(42) Hellstrand, E.; Lynch, I.; Andersson, A.; Drakenberg, T.; Dahlback, B.; Dawson, K. A.; Linse, S.; Cedervall, T. *FEBS J.* **2009**, *276* (12), 3372–3381.
(43) Rocker, C.; Potzl, M.; Zhang, F.; Parak, W. J.; Nienhaus, G. U. *Nat. Nanotechnol.* **2009**, *4* (9), 577–580.
(44) Aggarwal, P.; Hall, J. B.; McLeland, C. B.; Dobrovolskaia, M. A.; McNeil, S. E. *Adv. Drug Delivery Rev.* **2009**, *61* (6), 428–437.
(45) Schipper, M. L.; Iyer, G.; Koh, A. L.; Cheng, Z.; Ebenstein, Y.; Aharoni, A.; Keren, S.; Bentolila, L. A.; Li, J.; Rao, J.; Chen, X.; Banin, U.; Wu, A. M.; Sinclair, R.; Weiss, S.; Gambhir, S. S. *Small* **2009**, *5* (1), 126–134.
(46) Praetner, M.; Rehberg, M.; Bihari, P.; Lerchenberger, M.; Uhl, B.; Holzer, B.; Eichhorn, M. E.; Fürstv, R.; Perisic, T.; Reichel, C. A.; Welsch, U.; Krombach, F. *Biomaterials* **2010**, *31*, 6692–6700.
(47) Duhr, S.; Braun, D. *Proc. Natl. Acad. Sci. U.S.A.* **2006**, *103* (52), 19678–19682.
(48) Sperling, R. A.; Liedl, T.; Duhr, S.; Kudera, S.; Zanella, M.; Lin, C.-A. J.; Chang, W. H.; Braun, D.; Parak, W. J. *J. Phys. Chem. C* **2007**, *111*, 11552–11559.
(49) Boni, L. T.; Stewart, T. P.; Alderfer, J. L.; Hui, S. W. *J. Membr. Biol.* **1981**, *62* (1−2), 65–70.
(50) Riezman, H.; Woodman, P. G.; van Meer, G.; Marsh, M. *Cell* **1997**, *91* (6), 731–738.
(51) Hume, D. A. *J Immunol.* **2008**, *181* (9), 5829–5835.
(52) Sasmono, R. T.; Ehrnsperger, A.; Cronau, S. L.; Ravasi, T.; Kandane, R.; Hickey, M. J.; Cook, A. D.; Himes, S. R.; Hamilton, J. A.; Hume, D. A. *J. Leukocyte Biol.* **2007**, *82* (1), 111–123.
(53) Haberzettl, P.; Duffin, R.; Kramer, U.; Hohr, D.; Schins, R. P.; Borm, P. J.; Albrecht, C. *Arch. Toxicol.* **2007**, *81* (7), 459–470.
(54) Thorlacius, H.; Raud, J.; Rosengren-Beezley, S.; Forrest, M. J.; Hedqvist, P.; Lindbom, L. *Biochem. Biophys. Res. Commun.* **1994**, *203* (2), 1043–1049.
(55) Wan, M. X.; Wang, Y.; Liu, Q.; Schramm, R.; Thorlacius, H. *Br. J. Pharmacol.* **2003**, *138* (4), 698–706.
(56) Prussin, C.; Metcalfe, D. D. *J. Allergy Clin. Immunol.* **2003**, *111* (2 Suppl), S486–S494.
(57) Foy, D. S.; Ley, K. *Microvasc. Res.* **2000**, *60* (3), 249–260.
(58) Khandoga, A. G.; Khandoga, A.; Reichel, C. A.; Bihari, P.; Rehberg, M.; Krombach, F. *PLoS One* **2009**, *4* (3), No. e4693.

DOI: 10.1021/nl102100m | *Nano Lett.* **2010**, *10*, 3656–3664

SI Materials and Methods

Quantum dots

Qdot® ITK™ carboxyl, Qdot® ITK™ amine (PEG), and Qdot® ITK™ non-targeted (PEG) quantum dots (655 nm fluorescence peak emission) were purchased from Invitrogen Corporation (Karlsruhe, Germany). These QDs consist of a semiconductor CdSe core encapsulated with a ZnS shell and an additional layer of either polyethylene glycol only (PEG-QDs), polyethylene glycol with an amine coating (amine-QDs), or carboxyl functions solely (carboxyl-QDs). The PEG coating itself consists of short oligomers with a molecular weight of 1-3 kDa. Prior to use, QDs were resuspended to a final volume of 100 µl in sterile 0.9% NaCl at a concentration of 0.8 µM, thoroughly vortexed, and injected intra-arterially.

Animals

Male C57BL/6 mice at the age of 10 – 12 weeks were purchased from Charles River (Sulzfeld, Germany). Animals were housed under conventional conditions with free access to food and water. All experiments were performed according to German legislation for the protection of animals.

Surgical procedure

The surgical preparation was performed as described by Baez with minor modifications (39). Briefly, mice were anesthetized using a ketamine/xylazine mixture (100 mg/kg ketamine and 10 mg/kg xylazine), administrated by i.p. injection. The left femoral artery was cannulated in a retrograde manner for administration of QDs, microspheres, and drugs. The right cremaster muscle was exposed through a ventral incision of the scrotum. The muscle was opened ventrally in a relatively avascular zone, using careful electrocautery to stop any bleeding, and spread over the pedestal of a custom-made microscopy stage. Epididymis and testicle were

detached from the cremaster muscle and placed into the abdominal cavity. Throughout the procedure as well as after surgical preparation during *in vivo* microscopy, the muscle was superfused with warm buffered saline.

In vivo microscopy

The setup for *in vivo* microscopy was centered around an AxioTech-Vario 100 Microscope (Zeiss MicroImaging GmbH, Göttingen, Germany), equipped with LED excitation light (Zeiss Colibri) for fluorescence epi-illumination. For QD excitation and transillumination, the LED module 470 nm (exposure time 150 ms) and the LED module 625 nm (exposure time 10 ms) were used in a fast switching mode, respectively. Light was directed onto the specimen via filter set 62 HE (Zeiss MicroImaging GmbH) fitted with dichroic and emission filters [TFT 495 + 610 (HE); TBP 527 + LP615 (HE)]. Microscopic images were obtained with a water dipping objective (20x, NA 0.5) and acquired with an AxioCam Hsm camera and Axiovision 4.6 software. Oblique illumination was obtained by positioning a mirroring surface (reflector) directly below the specimen and tilting its angle relative to the horizontal plane. The reflector consisted of a round cover glass (thickness, 0.19–0.22 mm; diameter, 11.8 mm), which was coated with aluminum vapor (Freichel, Kaufbeuren, Germany) and brought into direct contact with the overlying specimen as described previously (27). For measurement of centerline blood flow velocity, green fluorescent microspheres (2 µm diameter, Invitrogen) were injected via the femoral artery catheter, and their passage through the vessels of interest was recorded (filter set 62 HE, LED 470 nm).

Quantification of leukocyte kinetics and microhemodynamic parameters

For off-line analysis of parameters describing the sequential steps of leukocyte extravasation, we used Axiovision 4.6 software. Rolling leukocytes were defined as those moving slower than the associated blood flow and quantified during 30 s. Leukocyte rolling flux fraction was

determined from time-lapse recordings by counting all visible cells passing through a plane perpendicular to the vessel axis and dividing this number by the total leukocyte flux through the vessel, which was calculated as the product of the systemic leukocyte count, mean blood flow velocity, and vessel cross-sectional area. Leukocyte rolling velocity was determined by measuring their distance in consecutive movie frames for five individual leukocytes per analyzed vessel. Firmly adherent cells were determined as those resting in the associated blood flow for more than 30 s and related to the luminal surface per 100 µm vessel length. Transmigrated cells were counted in regions of interest (ROI), covering 75 µm on both sides of a vessel over 100 µm vessel length and are presented per 10^4 mm^2 tissue area. From consecutive movie frames of single fluorescent beads, centerline blood flow velocity was determined. From measured vessel diameters and centerline blood flow velocity, apparent wall shear stress was calculated, assuming a parabolic flow velocity profile over the vessel cross-section as described previously (58).

Experimental groups

In a first set of experiments, mice (n = 6 each group) received vehicle, carboxyl-QDs, amine-QDs, or PEG-QDs (3 pmol/g BW) as a bolus by intra-arterial injection 15 min after the preparation of the cremaster muscle. Additional experiments were performed in mice (n=6 each group) receiving cromolyn (0.2 mg kg^{-1}), an inhibitor of mast cell degranulation, as a bolus via intra-arterial injection 30 minutes before cremaster preparation and subsequent application of vehicle or carboxyl-QDs. In separate groups (n = 6 each), QD-treated animals received an anti-CD54/ICAM-1 antibody (clone YN-1/1.7.4, BD Biosciences Pharmingen, San Diego, CA, United States) or an isotype-matched control mAb (BD Biosciences Pharmingen) at 3 mg/kg BW as a bolus intra-arterial injection prior to the preparation of the cremaster muscle. In further experiments, the QD application protocol was altered. Mice (n =

5 each) received vehicle or carboxyl-QDs, 60 min prior to cremaster muscle preparation and subsequent *in vivo* microscopy.

Experimental protocols

Five postcapillary vessel segments in a central area of the spread-out cremaster muscle were randomly chosen among those that were at least 150 µm away from neighboring postcapillary venules and did not branch over a distance of at least 150 µm. After having obtained baseline recordings of leukocyte rolling, firm adhesion, and transmigration in all five vessel segments, QDs or vehicle were injected.

Image acquisition, which took about 5 min, was repeated at 15, 30, 45, and 60 min after injection as well as at 30 and 60 min for the cromolyn and anti-ICAM1 experiments. After having obtained recordings of leukocyte recruitment parameters, blood flow velocity was determined as described previously (57). After *in vivo* microscopy, tissue samples of the cremaster muscle were prepared for immunohistochemistry and electron microscopy. Blood samples were collected by cardiac puncture for the determination of systemic leukocyte counts using a Coulter ACT Counter (Coulter Corp., Miami, FL, USA). Anaesthetized animals were then euthanized by an intra-arterial pentobarbital overdose (Narcoren; Merial, Hallbergmoos, Germany).

Immunohistochemistry/ toluidine blue staining

To determine the phenotype of transmigrated leukocytes, immunostaining of paraffin-embedded serial tissue sections of the cremaster muscle was performed. Sections were incubated with primary rat anti-mouse Gr-1, anti-CD45 (BD Biosciences, San Jose, CA, USA), or anti-F4/80 (Serotec, Oxford, UK) IgG antibodies. The paraffin sections were stained with commercially available immunohistochemistry kits (Gr-1, CD45, Super Sensitive Link-

Label IHC detection system, BioGenex, San Ramon, CA, USA; F4/80, Vectastain ABC kit, Vector Laboratories, Burlingame, CA, USA), obtaining an easily detectable reddish or brownish end product, respectively. Counterstaining was performed with Mayer's hemalaun. The number of extravascularly localized Gr-1-, CD45- or F4/80-positive cells was quantified by light microscopy (objective magnification 40x) on two sections (10 observation fields per section) from six animals in a blinded manner, respectively. The number of transmigrated Gr-1-positive cells (neutrophils/monocytes) and F4/80-positive cells (monocytes/macrophages) is expressed as the percentage of total CD45-positive leukocytes.

Toluidine blue whole mount staining was performed on excised cremasteric tissue that was fixed for 10 min with buffered 4% paraformaldehyde (Microcos, Garching, Germany). Then the tissue was briefly stained with 0.1% toluidine blue O (Merck, Darmstadt, Germany) aqueous solution and rinsed thoroughly in H_2O. Tissue was mounted in PermaFluor (Beckman Coulter, Fullerton, CA) on glass slides and inspected using an oil-immersion objective (Leica Microsystems, Wetzlar, Germany; 63x NA 1.40). Toluidine blue staining was viewed using transmitted light. QDs were illuminated using a mercury light source and a longpass emission FITC-filter (Leica Microsystems).

For the analysis of E-selection expression in postcapillary venules, excised cremaster muscles were fixed in 2% paraformaldehyde. Tissues were then blocked and permeabilized in PBS, supplemented with 10% goat serum (Sigma) and 0.5% Triton X-100 (Sigma). After incubation at 4°C for 12 hours with a rat anti-mouse CD62E antibody (Abcam, Cambridge, UK), tissues were incubated for 3 hours at room temperature with an Alexa Fluor 488-linked goat anti-rabbit antibody (Invitrogen). Immunostained tissues were mounted in PermaFluor (Beckman Coulter, Fullerton, CA) on glass slides and observed using a Leica SP5 confocal laser-scanning microscope (Leica Microsystems, Wetzlar, Germany) with an oil-immersion lens (Leica; 63x; NA 1.40). Further image processing was done using ImageJ (National

Institutes of Health, Bethesda, MD) and Adobe Photoshop 7.0.1(Adobe Systems, San Jose, CA) software.

Electron Microscopy

The cremaster muscle was initially fixed in-situ in 1 % PFA, 0.1 M cacodylate buffer, pH 7.4 and after dissection, finally fixed in 2 % PFA, 2 % glutaraldehyde in 0.1 M cacodylate buffer, pH 7.4 for 2-3 hours at room temperature. The specimen were post-fixed in 1% OsO_4, containing 1.5 % potassium cyanoferrate and embedded after dehydration in Epon. 70-nm. Ultrathin sections of the sample were cut in serial sections (Leica- UC6 ultramicrotome, Vienna, Austria). Several sections were counterstained with uranyl acetate and lead, some of the sections were not counterstained. The samples were analyzed at 80 kV on a FEI-Tecnai 12 electron microscope (FEI, Eindhoven, Netherlands). The QDs could only be seen unambiguously in the unstained sections. The consecutive stained section was only viewed to identify the cellular organelle. Images were aquired using a CCD-camera (Megaview, Olympus-SIS, Muenster) or imaging plates (Ditabis, Pforzheim, Germany).

Quantification of QD uptake in RAW264.7 macrophages

Murine RAW264.7 macrophage cell culture, QD incubation, and imaging were performed on 1µ-slide 8 well ibiTreat microscopy chambers (ibidi, Martinsried, Germany). RAW264.7 cell culture was done according to standard lab protocols in DMEM (Invitrogen) containing 10% FCS (Invitrogen). QDs were prepared at 0.8 µM in PBS and added to the medium to a final concentration of 8 nM, thus preventing aggregation of QDs and achieving a homogenous distribution. After incubation for 15 min at 37°C, medium was removed and cells were fixed with buffered 4% paraformaldehyde (Microcos) and embedded in PermaFluor (Beckman Coulter, Fullerton, CA). Images were acquired with a Leica SP5 confocal laser-scanning microscope (Leica Microsystems) with a 40x oil immersion objective (NA 1.25). Excitation

wavelength was 488 nm and QDs emission was detected at 630-700 nm. Optical sections were recorded at 0.5 µm distances using the same settings for all samples. Z-stacks covering complete cells were projected and QDs fluorescence was determined as mean fluorescence per cell area using ImageJ software (National Institutes of Health, Bethesda, MD). Three independent experiments were performed and 120 cells were analyzed per group.

Quantum Dot size measurement

MicroscaleThermophoresis (MST) can be used to analyze biomolecule affinities and the hydrodynamic radius of molecules. The analysis is based on the free solution mobility of molecules in infra-red laser (IR-laser) generated temperature gradients. IR radiation is absorbed by water and a temperature increase of 5K is achieved instantaneously on a lengthscale of approx. 50 µm. The QDs show a directed motion to lower temperature. Thus, the observed concentration (i.e. QD fluorescence) in the heated region decreases. The amplitude of the concentration change allows analyzing changes in the molecules size, charge and hydration shell (46). In this work we analyzed the protein adsorption to the surface of the nanoparticle by measuring the back diffusion (i.e. Diffusion coefficient) of QDs after the heating laser was turned off (47). Therefore we diluted the QDs to 500 nM in PBS or goat serum and filled the sample in a microfluidic chamber with a height 100 µm. The fluorescence was excited at 400-500nm. The QD fluorescence was recorded with a CCD-Camera (Sensicam, PCO) at >560nm. The IR-laser heating was used for up to 20 seconds to obtain strong molecule depletion within the heated region. Following the heating step, the IR laser was turned off and the relaxation of the concentration profile was measured for up to 30 seconds. These data were used to determine the diffusion coefficient of the QDs. Three independent experiments were performed. The diffusion coefficient is related to the hydrodynamic radius by the following equation: D= kT/(6*pi*eta*r), where k is Boltzmann constant, T is the ambient temperature, eta is the viscosity of the solution and r is the

hydrodynamic radius. To obtain the hydrodynamic radius, the diffusion coefficients measured in serum are corrected by the viscosity, which is typically higher by factor of 1.5 in serum compared to water.

Statistics

Data analysis was performed with a statistical software package (SigmaStat for Windows, SPSS Inc. Chicago, USA).

The ANOVA on ranks test, which includes tests for normality and equal variance of the data, was performed. When p values < 0.05 were detected by ANOVA, then the appropriate post-hoc test (Student-Newman-Keuls) for all pairwise multiple comparisons was used to estimate the stochastic probability in intergroup comparisons. P values < 0.05 were considered significant.

Table S1. Systemic leukocyte counts and microhemodynamic parameters

Experimental group	Inner vessel diameter [µm]	Blood flow velocity [mm/s]	Wall shear rate [s-1]	Systemic leukocyte counts [x 10^3 $µl^{-1}$]
Vehicle	25.4 ± 0.4	1.5 ± 0.1	1613.9 ± 221.2	4.6 ± 0.7
Carboxyl-QDs	24.5 ± 0.6	1.5 ± 0.2	1696.2 ± 218.9	5.4 ± 0.7
Amine-QDs	26.2 ± 0.9	1.6 ± 0.1	1630.7 ± 172.3	4.1 ± 0.4
PEG-QDs	24.4 ± 0.5	1.3 ± 0.1	1493.1 ± 128.5	4.2 ± 0.5
Cromolyn + vehicle	26.1 ± 1.0	1.3 ± 0.1	1375.3 ± 140.1	4.5 ± 0.6
Cromolyn + carboxyl-QDs	26.2 ± 0.9	1.4 ± 0.2	1475.0 ± 217.6	4.3 ± 0.7
Anti-ICAM-1 + carboxyl-QDs	23.7 ± 1.1	1.6 ± 0.1	1688.0 ± 185.4	5.8 ± 1.2
Isotype mAb + carboxyl-QDs	26.1 ± 0.6	1.4 ± 0.2	1348.2 ± 212.7	3.55 ± 0.74

Systemic leukocyte counts as well as microhemodynamic parameters, including inner vessel diameter, blood flow velocity, and wall shear rate, were obtained as detailed in *Materials and Methods* (mean ± SEM for $n = 6$ per group).

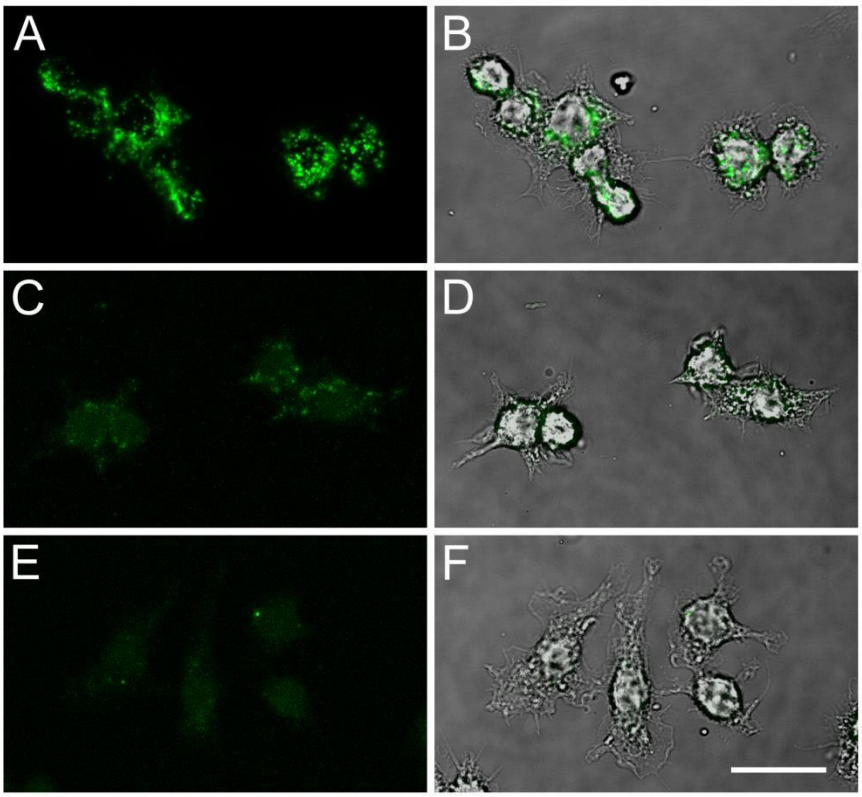

Figure S1. QD localization in RAW264.7 murine macrophage cells
Confocal fluorescence microscopy revealed localization of carboxyl-QDs (A, B), amineQDs (C, D), and PEG-QDs (E, F) in RAW264.7 macrophages 15 min after incubation with 8 nM QDs. Z-stacks covering complete cells were projected. QD fluorescence is depicted in (A), (C), and (E) and merged with the corresponding bright field images in (B), (D) and (F). Fluorescence intensities are not directly comparable since PMT gain was reduced during image acquisition to avoid pixel oversaturation in case of carboxyl-QD. Scale bar: 30 µm

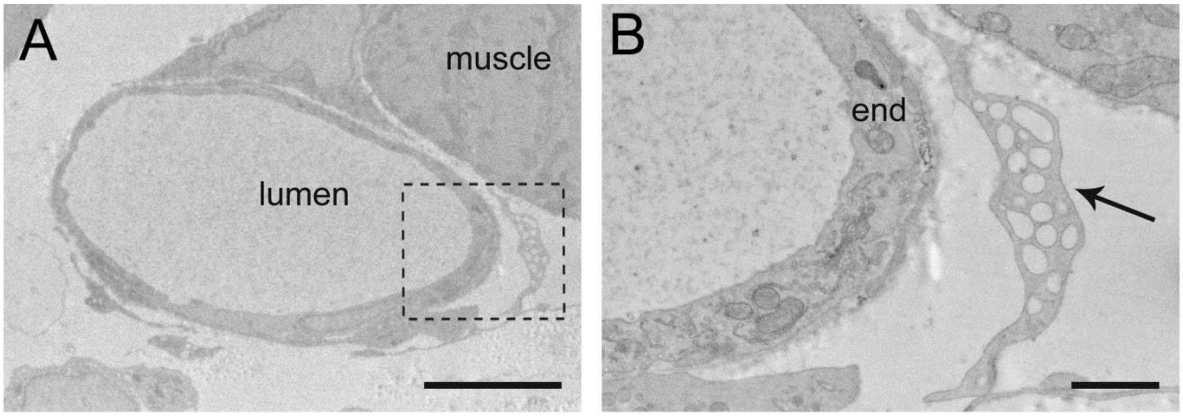

Figure S2. Electron microscopic examination of QD localization in postcapillary venules
Transmission electron microscopy was performed on ultrathin cross sections of cremasteric tissue 60 minutes upon application of QDs. Contrast of the tissue results from post-fixation of lipids with OsO_4 only, representative images are shown. (A) Carboxyl-QDs were detected in perivascular macrophages (outlined in B, marked by arrow) in close vicinity to a blood

vessel embedded between muscle fibres. QDs are not visible at this magnification. Scale bar: A = 5 μm, B = 1 μm Supplemental movie files:

http://pubs.acs.org/doi/suppl/10.1021/nl102100m/suppl_file/nl102100m_si_005.avi

http://pubs.acs.org/doi/suppl/10.1021/nl102100m/suppl_file/nl102100m_si_006.avi

http://pubs.acs.org/doi/suppl/10.1021/nl102100m/suppl_file/nl102100m_si_007.avi

http://pubs.acs.org/doi/suppl/10.1021/nl102100m/suppl_file/nl102100m_si_008.avi

III. PUBLICATIONS

Abstracts

1. Bernd Uhl, **Marc Praetner**, Gabriele Zuchtriegel, Max Lerchenberger, Paul J. Declerck, Sandip Kanse, Fritz Krombach, Christoph A. Reichel.
Complex formation of urokinase-type plasminogen activator with plasminogen activator inhibitor-1 enhances its potential to promote extravasation of neutrophils and inflammatory monocytes.
International Vascular Biology Meeting, June 3-5 2012, Wiesbaden, Germany

2. C.A. Reichel, **M. Praetner**, B. Uhl, M. Lerchenberger, F. Krombach. Plasminogen Activator Inhibitor-1 (PAI-1) reguliert Leukozytenakkumulation und mikrovaskuläre Dysfunktion im postischämischen Gewebe über low density lipoprotein receptor-related protein-1 (LRP-1). 83. Jahresversammlung der deutschen Gesellschaft für Hals-Nasen-Ohren-Heilkunde, Kopf- und Halschirurgie e.V., 16.-20. Mai 2012, Bonn.

3. M. Lerchenberger, B. Uhl, **M. Praetner**, A. Khandoga, F. Krombach, C.A. Reichel.
Matrix metalloproteinases promote interstitial migration of leukocytes.
Joint Meeting of the European Society for Microcirculation (ESM) and the German Society of Microcirculation and Vascular Biology (GfMVB). J Vasc Res 2011;48(Suppl.1):249

4. **M. Praetner**, M. Lerchenberger, B. Uhl, F. Krombach, C.A. Reichel.
Plasminogen activator inhibitor-1 promotes extravasation of neutrophils to postischemic tissue via low-density lipoprotein receptor-related protein-1.
Joint Meeting of the European Society for Microcirculation (ESM) and the German Society of Microcirculation and Vascular Biology (GfMVB). J Vasc Res 2011;48(Suppl.1):301

5. B. Uhl, **M. Praetner**, M. Lerchenberger, P.J. Declerck, S. Kanse, F. Krombach, C.A. Reichel.
Complex formation of urokinase-type plasminogen activator with plasminogen activator inhibitor-1 enhances its potential to promote extravasation of monocytes.
Joint Meeting of the European Society for Microcirculation (ESM) and the German Society of Microcirculation and Vascular Biology (GfMVB). J Vasc Res 2011;48(Suppl.1):335

6. M. Rehberg, **M. Praetner**, C. Ferreira-Leite, F. Krombach.
Fate and effects of surface-modified quantum dots in the microvasculature.
Joint Meeting of the European Society for Microcirculation (ESM) and the German Society of Microcirculation and Vascular Biology (GfMVB) J Vasc Res 2011;48(Suppl.1):63

7. Markus Rehberg*, **Marc Praetner***, Camila Ferreira Leite, Peter Bihari, Fritz Krombach.
Fate and biological effects of systemically administered quantum dots: impact of surface modification (*equally contributing authors).
BONSAI Symposium Breakthroughs in Nanoparticles for Bio-Imaging, 8 April 2010, ENEA Research Centre of Frascati, Frascati (Rome), Italy

8. Markus Rehberg, **Marc Praetner**, Camila Ferreira Leite, Christoph Reichel, Peter Bihari, Karina Mildner, Dagmar Zeuschner, Fritz Krombach.
Quantum dots induce leukocyte adhesion and transmigration depending on their surface modification.
Joint Meeting 2009 of the Society for Microcirculation and Vascular Biology (GfMVB) and the Swiss Society for Microcirculation (SSM) Bern, Switzerland, October 8–10, 2009

9. Rehberg M, **Praetner M**, Reichel CA, Bihari P, Zeuschner D, Krombach F. Microvascular distribution and effects of surface-modified quantum dots.
4th International Conference on Nanotechnology – Occupational and Environmental Health, 26-29 August 2009, Helsinki Congress Paasitorni, Helsinki, Finland.

10. Bihari P, Holzer M, **Praetner M**, Lerchenberger M, Fent J, Reichel CA, Rehberg M, Lakatos S, Krombach F.
Single-walled carbon nanotubes augment microvascular thrombosis.
4th International Conference on Nanotechnology – Occupational and Environmental Health, 26-29 August 2009, Helsinki Congress Paasitorni, Helsinki, Finland.

11. **Praetner M**, Rehberg M, Bihari P, Lerchenberger M, Krombach F. Biodistribution and –kinetics of surface-modified quantum dots.
4th International Conference on Nanotechnology – Occupational and Environmental Health, 26-29 August 2009, Helsinki Congress Paasitorni, Helsinki, Finland.

Originalia

1. Uhl B, Zuchtriegel G, Puhr-Westerheide D, **Praetner M**, Rehberg M, Fabritius M, Hessenauer M, Holzer M, Khandoga A, Fürst R, Zahler S, Krombach F, Reichel CA.
Tissue-Type Plasminogen Activator Promotes Postischemic Neutrophil Recruitment via Its Proteolytic and Nonproteolytic Properties.
Arterioscler Thromb Vasc Biol. 2014 Apr 24. [Epub ahead of print]

2. Holzer M, Bihari P, **Praetner M**, Uhl B, Reichel CA, Fent J, Vippola M, Lakatos S, Krombach F.
Carbon-based nanomaterials accelerate arteriolar thrombus formation in the murine microcirculation independently of their shape.
J Appl Toxicol. 2014 Feb 14. doi: 10.1002/jat.2996. [Epub ahead of print]

3. Lerchenberger M, Uhl B, Stark K, Zuchtriegel G, Eckart A, Miller M, Puhr - Westerheide D, **Praetner M**, Rehberg M, Khandoga AG, Lauber K, Massberg S, Krombach F, Reichel CA.
Matrix metalloproteinases modulate ameboid-like migration of neutrophils through inflamed interstitial tissue.
Blood. 2013 Aug 1;122(5):770-80. doi: 10.1182/blood-2012-12-472944.

4. Rehberg M, **Praetner M**, Leite CF, Reichel CA, Bihari P, Mildner K, Duhr S, Zeuschner D, Krombach F.
Quantum dots modulate leukocyte adhesion and transmigration depending on their surface modification.
Nano Lett. 2010 Sep 8;10(9):3656-64.

5. **Praetner M**, Rehberg M, Bihari P, Lerchenberger M, Uhl B, Holzer M, Eichhorn ME, Fürst R, Perisic T, Reichel CA, Welsch U, Krombach F. The contribution of the capillary endothelium to blood clearance and tissue deposition of anionic quantum dots in vivo.
***Biomaterials*.** 2010 Sep;31(26):6692-700.

6. Bihari P, Holzer M, **Praetner M**, Fent J, Lerchenberger M, Reichel CA, Rehberg M, Lakatos S, Krombach F. Single-walled carbon nanotubes activate platelets and accelerate thrombus formation in the microcirculation. ***Toxicology.*** 2010 Mar 10;269(2-3):148-54.

7. Bihari P, Vippola M, Schultes S, **Praetner M**, Khandoga AG, Reichel CA, Coester C, Tuomi T, Rehberg M, Krombach F. Optimized dispersion of nanoparticles for biological in vitro and in vivo studies. ***Part Fibre Toxicol.*** 2008 Nov 6;5:14.

IV. ACKNOWLEDGMENT

Herrn Prof. Dr. med. Ulrich Pohl danke ich für die freundliche und unkomplizierte Aufnahme im Walter-Brendel-Zentrum für Experimentelle Medizin (ehem. Institut für Chirurgische Forschung), unter dessen Gesamtleitung ich die vorliegende Arbeit abschließen durfte.

Zu besonderen Dank bin ich Herrn Prof. Dr. med. vet. Dr. med. habil. Fritz Krombach für die Überlassung des Themas der vorliegenden Arbeit und die Aufnahme in seine Arbeitsgruppe verpflichtet. Sowohl seine fachlichen als auch persönlichen Qualitäten waren von fundamentaler Bedeutung für sämtliche Phasen der Dissertation und werden mir auch für meine zukünftige wissenschaftliche Tätigkeit stets als vorbildhaft in Erinnerung bleiben. Die stetige Hilfsbereitschaft und Ansprechbarkeit bei Problemen, sein ungebrochenes Interesse an den gemeinsamen Projekten und seine beispiellose Geduld zeichnen ihn neben vielen anderen Eigenschaften als einen hervorragenden Wissenschaftler und eine beeindruckende Persönlichkeit aus. Ich bin sehr dankbar, dass ich von ihm als wissenschaftlichem Mentor lernen und von seiner immensen Erfahrung profitieren durfte.

Ebenso danke ich Herrn PD Dr. rer. nat. Markus Rehberg für die einführende Betreuung sowie die Möglichkeit und Ermunterung zu eigenständiger wissenschaftlicher Arbeit.

Herrn Dr. med. Christoph A. Reichel, Herrn Dr. med. univ. Peter Bihari als auch Herrn Dr. med. Alexander Khandoga bin ich zutiefst dankbar für die zeitintensive praktische Einarbeitung in den Laboralltag. Ich danke für ihre Geduld und die kontinuierliche Unterstützung die ich erfahren durfte.

Für die problemlos umsetzbare Kooperation mit dem Anatomischen Institut bedanke ich mich sehr herzlich bei Herrn Prof. Dr. med. Dr. rer. nat. Ulrich Welsch, der mir nicht nur als herausragender Hochschullehrer, sondern auch als beispielhaft bescheidene und höfliche Persönlichkeit in Erinnerung bleiben wird. Auch bin ich den Technischen Assistentinnen, Frau Beate Aschauer und Frau Sabine Tost für die mühevolle und langwierige Durchführung der Elektronenmikroskopie zu ehrlichem Dank verpflichtet.

Ich danke Herrn Dr. hum. biol. Jürgen Peters für die fachkundige statistische Beratung und die vielen Gespräche darüber hinaus.

Den Technischen Assistenten Herrn Dieter Müller und Herrn Gerhard Adams möchte ich für ihre über die Arbeitsverhältnisse hinausgehende Hilfsbereitschaft und Freundschaft meinen besonderen Dank aussprechen.

Herausragenden Dank schulde ich jenen Kollegen, die untrennbar mit diesem Lebensabschnitt verbunden sind. Als inzwischen langjährigen Freunden danke ich Herrn Maximilian Lerchenberger, Herrn Bernd Uhl, Herrn Martin Holzer und Herrn Daniel Puhr-Westerheide für diese prägende Zeit.

Stellvertretend für die vielen weiteren Menschen, die auf unterschiedliche Weise zum Abschluss der vorliegenden Arbeit beigetragen haben, möchte ich mich bei Frau Gabriele Zuchtriegel, Frau Camila F. Leite, Frau Karina Mildner, Frau Dr. rer. nat. Dagmar Zeuschner, Herrn Prof. Dr. rer. nat. Robert Fürst, Frau Dr. rer. nat. Tamara Perisic, Herrn Dr. rer. nat. Stefan Duhr, Frau Dr. hum. biol. Siiri Lüdemann, Herrn PD Dr. med. Martin Eichhorn, Herrn Sergej Feiler, Herrn Dr. med. Seong Woong Kim, Herrn Prof. Dr. med. Markus Sperandio, Herrn PD Dr. rer. nat. Steffen Dietzel, Herrn Dr. med. vet. Eckhart Thein, Frau Silvia Münzing, Herrn Dr. rer. nat. Rolf Nitzsche, Frau PD Dr. med. Heike Künzel, Herrn Dr. rer. nat. Stephan Schultes, sowie Herrn Dr. med. Alexander Koch von ganzem Herzen bedanken.

Den Tierpflegern im Institut danke ich für die stets verantwortungsvolle Pflege der Versuchstiere und die gute Zusammenarbeit.

Zuletzt und am meisten bin ich meinen Eltern für ihre immerwährende Unterstützung und Förderung zu tiefer Dankbarkeit verpflichtet.

VI. BIBLIOGRAPHY

1. Ray, P.C., Size and shape dependent second order nonlinear optical properties of nanomaterials and their application in biological and chemical sensing. Chem Rev, 2010. **110**(9): p. 5332-65.

2. Borm, P.J., et al., The potential risks of nanomaterials: a review carried out for ECETOC. Part Fibre Toxicol, 2006. **3**: p. 11.

3. Navarro, E., et al., Environmental behavior and ecotoxicity of engineered nanoparticles to algae, plants, and fungi. Ecotoxicology, 2008. **17**(5): p. 372-86.

4. Radad, K., et al., Recent advances in benefits and hazards of engineered nanoparticles. Environ Toxicol Pharmacol, 2012. **34**(3): p. 661-72.

5. Geszke-Moritz, M. and M. Moritz, Quantum dots as versatile probes in medical sciences: synthesis, modification and properties. Mater Sci Eng C Mater Biol Appl, 2013. **33**(3): p. 1008-21.

6. Petryayeva, E., W.R. Algar, and I.L. Medintz, Quantum dots in bioanalysis: a review of applications across various platforms for fluorescence spectroscopy and imaging. Appl Spectrosc, 2013. **67**(3): p. 215-52.

7. Cheki, M., M. Moslehi, and M. Assadi, Marvelous applications of quantum dots. Eur Rev Med Pharmacol Sci, 2013. **17**(9): p. 1141-8.

8. Pinaud, F., et al., Advances in fluorescence imaging with quantum dot bioprobes. Biomaterials, 2006. **27**(9): p. 1679-87.

9. Medintz, I.L., et al., Quantum dot bioconjugates for imaging, labelling and sensing. Nat Mater, 2005. **4**(6): p. 435-46.

10. Bae, P.K., et al., The modification of quantum dot probes used for the targeted imaging of his-tagged fusion proteins. Biomaterials, 2009. **30**(5): p. 836-42.

11. Zhang, W., et al., Design and synthesis of highly luminescent near-infraredemitting water-soluble CdTe/CdSe/ZnS core/shell/shell quantum dots. Inorg Chem, 2009. **48**(20): p. 9723-31.

12. Zhu, Y., et al., Quantum dot-based nanoprobes for in vivo targeted imaging. Curr Mol Med, 2013. **13**(10): p. 1549-67.

13. Aswathy, R.G., et al., Near-infrared quantum dots for deep tissue imaging. Anal Bioanal Chem, 2010. **397**(4): p. 1417-35.

14. Bentolila, L.A., Y. Ebenstein, and S. Weiss, Quantum dots for in vivo smallanimal imaging. Journal of Nuclear Medicine, 2009. **50**(4): p. 493-6.

15. Hilderbrand, S.A. and R. Weissleder, Near-infrared fluorescence: application to in vivo molecular imaging. Curr Opin Chem Biol, 2010. **14**(1): p. 71-9.

16. Li, C., et al., In vivo real-time visualization of tissue blood flow and angiogenesis using Ag2S quantum dots in the NIR-II window. Biomaterials, 2014. **35**(1): p. 393-400.

17. Zhang, L.W. and N.A. Monteiro-Riviere, Mechanisms of quantum dot nanoparticle cellular uptake. Toxicol Sci, 2009. **110**(1): p. 138-55.

18. Lundqvist, M., et al., Nanoparticle size and surface properties determine the protein corona with possible implications for biological impacts. Proc Natl Acad Sci U S A, 2008. **105**(38): p. 14265-70.

19. Akerman, M.E., et al., Nanocrystal targeting in vivo. Proc Natl Acad Sci U S A, 2002. **99**(20): p. 12617-21.

20. Larson, D.R., et al., Water-soluble quantum dots for multiphoton fluorescence imaging in vivo. Science, 2003. **300**(5624): p. 1434-6.

21. Stroh, M., et al., Quantum dots spectrally distinguish multiple species within the tumor milieu in vivo. Nat Med, 2005. **11**(6): p. 678-82.

22. Xu, L. and C. Chen, Physiological behavior of quantum dots. Wiley Interdiscip Rev Nanomed Nanobiotechnol, 2012. **4**(6): p. 620-37.

23. Nurkiewicz, T.R., et al., Pulmonary particulate matter and systemic microvascular dysfunction. Res Rep Health Eff Inst, 2011(164): p. 3-48.

24. Nurkiewicz, T.R., et al., Systemic microvascular dysfunction and inflammation after pulmonary particulate matter exposure. Environ Health Perspect, 2006. **114**(3): p. 412-9.

25. Ryman-Rasmussen, J.P., J.E. Riviere, and N.A. Monteiro-Riviere, Surface coatings determine cytotoxicity and irritation potential of quantum dot nanoparticles in epidermal keratinocytes. J Invest Dermatol, 2007. **127**(1): p. 143-53.

26. Bihari, P., et al., Optimized dispersion of nanoparticles for biological in vitro and in vivo studies. Part Fibre Toxicol, 2008. **5**: p. 14.

27. Tang, Y., et al., The role of surface chemistry in determining in vivo biodistribution and toxicity of CdSe/ZnS core-shell quantum dots. Biomaterials, 2013. **34**(34): p. 8741-55.

28. Praetner, M., et al., The contribution of the capillary endothelium to blood clearance and tissue deposition of anionic quantum dots in vivo. Biomaterials, 2010. **31**(26): p. 6692-700.

29. Rehberg, M., et al., Quantum dots modulate leukocyte adhesion and transmigration depending on their surface modification. Nano Lett, 2010. **10**(9): p. 3656-64.

30. Lu, Y., et al., In vivo behavior of near infrared-emitting quantum dots. Biomaterials, 2013. **34**(17): p. 4302-8.

31. Geys, J., et al., Acute toxicity and prothrombotic effects of quantum dots: impact of surface charge. Environ Health Perspect, 2008. **116**(12): p. 1607-13.

32. Zhang, Y., et al., Functionalized quantum dots induce proinflammatory responses in vitro: the role of terminal functional group-associated endocytic pathways. Nanoscale, 2013. **5**(13): p. 5919-29.

33. Zhang, L.W., W. Baumer, and N.A. Monteiro-Riviere, Cellular uptake mechanisms and toxicity of quantum dots in dendritic cells. Nanomedicine (Lond), 2011. **6**(5): p. 777-91.

34. Seidel, S.A., et al., Microscale thermophoresis quantifies biomolecular interactions under previously challenging conditions. Methods, 2013. **59**(3): p. 301-15.

35. Duhr, S. and D. Braun, Why molecules move along a temperature gradient. Proc Natl Acad Sci U S A, 2006. **103**(52): p. 19678-82.

36. Perry, J.L., et al., PEGylated PRINT nanoparticles: the impact of PEG density on protein binding, macrophage association, biodistribution, and pharmacokinetics. Nano Lett, 2012. **12**(10): p. 5304-10.

37. Uskokovic, V., Dynamic Light Scattering Based Microelectrophoresis: Main Prospects and Limitations. J Dispers Sci Technol, 2012. **33**(12): p. 1762-1786.

38. Kelf, T.A., et al., Non-specific cellular uptake of surface-functionalized quantum dots. Nanotechnology, 2010. **21**(28): p. 285105.

39. Saptarshi, S.R., A. Duschl, and A.L. Lopata, Interaction of nanoparticles with proteins: relation to bio-reactivity of the nanoparticle. J Nanobiotechnology, 2013. **11**: p. 26.

40. Robe, A., et al., Quantum dots in axillary lymph node mapping: biodistribution study in healthy mice. BMC Cancer, 2008. **8**: p. 111.

41. Schipper, M.L., et al., Particle size, surface coating, and PEGylation influence the biodistribution of quantum dots in living mice. Small, 2009. **5**(1): p. 126-34.

42. Ballou, B., et al., Noninvasive imaging of quantum dots in mice. Bioconjug Chem, 2004. **15**(1): p. 79-86.

43. Wahl, R.L., P. Sherman, and S. Fisher, The effect of specimen processing on radiolabeled monoclonal antibody biodistribution. Eur J Nucl Med, 1984. **9**(8): p. 382-4.

44. Su, C.K. and Y.C. Sun, In vivo monitoring of distributional transport kinetics and extravasation of quantum dots in living rat liver. Nanotechnology, 2013. **24**(16): p. 165101.

45. Pelley, J.L., A.S. Daar, and M.A. Saner, State of academic knowledge on toxicity and biological fate of quantum dots. Toxicol Sci, 2009. **112**(2): p. 27696.

46. Frangioni, J.V., In vivo near-infrared fluorescence imaging. Curr Opin Chem Biol, 2003. **7**(5): p. 626-34.

47. Liu, N., et al., Degradation of aqueous synthesized CdTe/ZnS quantum dots in mice: differential blood kinetics and biodistribution of cadmium and tellurium. Part Fibre Toxicol, 2013. **10**(1): p. 37.

48. Qu, Y., et al., Full assessment of fate and physiological behavior of quantum dots utilizing Caenorhabditis elegans as a model organism. Nano Lett, 2011. **11**(8): p. 3174-83.

49. Summers, H.D., et al., Analysis of quantum dot fluorescence stability in primary blood mononuclear cells. Cytometry A, 2010. **77**(10): p. 933-9.

50. Fitzpatrick, J.A., et al., Long-term persistence and spectral blue shifting of quantum dots in vivo. Nano Lett, 2009. **9**(7): p. 2736-41.

51. Sadauskas, E., et al., Kupffer cells are central in the removal of nanoparticles from the organism. Part Fibre Toxicol, 2007. **4**: p. 10.

52. Choi, H.S., et al., Renal clearance of quantum dots. Nat Biotechnol, 2007. **25**(10): p. 1165-70.

53. Yu, W.W., et al., Forming biocompatible and nonaggregated nanocrystals in water using amphiphilic polymers. J Am Chem Soc, 2007. **129**(10): p. 2871-9.

54. Lee, H.A., et al., Biodistribution of quantum dot nanoparticles in perfused skin: evidence of coating dependency and periodicity in arterial extraction. Nano Lett, 2007. **7**(9): p. 2865-70.

55. Pries, A.R., T.W. Secomb, and P. Gaehtgens, The endothelial surface layer. Pflugers Arch, 2000. **440**(5): p. 653-66.

56. Aird, W.C., Phenotypic heterogeneity of the endothelium: I. Structure, function, and mechanisms. Circ Res, 2007. **100**(2): p. 158-73.

57. Nabi, I.R. and P.U. Le, Caveolae/raft-dependent endocytosis. J Cell Biol, 2003. **161**(4): p. 673-7.

58. Bendayan, M., Morphological and cytochemical aspects of capillary permeability. Microsc Res Tech, 2002. **57**(5): p. 327-49.

59. Ghitescu, L., et al., Specific binding sites for albumin restricted to plasmalemmal vesicles of continuous capillary endothelium: receptor-mediated transcytosis. J Cell Biol, 1986. **102**(4): p. 1304-11.

60. Barrett, E.J., et al., Insulin regulates its own delivery to skeletal muscle by feedforward actions on the vasculature. Am J Physiol Endocrinol Metab, 2011. **301**(2): p. E252-63.

61. Predescu, D., et al., Transcytosis of alpha1-acidic glycoprotein in the continuous microvascular endothelium. Proc Natl Acad Sci U S A, 1998. **95**(11): p. 617580.

62. Lisanti, M.P., et al., Characterization of caveolin-rich membrane domains isolated from an endothelial-rich source: implications for human disease. J Cell Biol, 1994. **126**(1): p. 111-26.

63. Farrah, T., et al., A high-confidence human plasma proteome reference set with estimated concentrations in PeptideAtlas. Mol Cell Proteomics, 2011. **10**(9): p. M110 006353.

64. Chini, B. and M. Parenti, G-protein coupled receptors in lipid rafts and caveolae: how, when and why do they go there? J Mol Endocrinol, 2004. **32**(2): p. 325-38.

65. Fujiwara, M., J.D. Baldeschwieler, and R.H. Grubbs, Receptor-mediated endocytosis of poly(acrylic acid)-conjugated liposomes by macrophages. Biochim Biophys Acta, 1996. **1278**(1): p. 59-67.

66. Xiao, Y., et al., Dynamics and mechanisms of quantum dot nanoparticle cellular uptake. J Nanobiotechnology, 2010. **8**: p. 13.

67. Al-Hajaj, N.A., et al., Short ligands affect modes of QD uptake and elimination in human cells. ACS Nano, 2011. **5**(6): p. 4909-18.

68. Clift, M.J., et al., The uptake and intracellular fate of a series of different surface coated quantum dots in vitro. Toxicology, 2011. **286**(1-3): p. 58-68.

69. Lubrano, V., et al., Beneficial effect of Lisosan G on cultured human microvascular endothelial cells exposed to oxidised low density lipoprotein. Indian J Med Res, 2012. **136**(1): p. 82-8.

70. Li, X.A., et al., High density lipoprotein binding to scavenger receptor, Class B, type I activates endothelial nitric-oxide synthase in a ceramide-dependent manner. J Biol Chem, 2002. **277**(13): p. 11058-63.

71. Yonekura, H., et al., Novel splice variants of the receptor for advanced glycation end-products expressed in human vascular endothelial cells and pericytes, and

their putative roles in diabetes-induced vascular injury. Biochem J, 2003. **370**(Pt 3): p. 1097-109.

72. Ohtani, K., et al., The membrane-type collectin CL-P1 is a scavenger receptor on vascular endothelial cells. J Biol Chem, 2001. **276**(47): p. 44222-8.

73. Campbell, L.A., et al., Chlamydia pneumoniae binds to the lectin-like oxidized LDL receptor for infection of endothelial cells. Microbes Infect, 2012. **14**(1): p. 43-9.

74. Tamura, Y., et al., FEEL-1 and FEEL-2 are endocytic receptors for advanced glycation end products. J Biol Chem, 2003. **278**(15): p. 12613-7.

75. Bentzinger, C.F., Y.X. Wang, and M.A. Rudnicki, Building muscle: molecular regulation of myogenesis. Cold Spring Harb Perspect Biol, 2012. **4**(2).

76. Quinn, L.S. and B.G. Anderson, Interleukin-15, IL-15 Receptor-Alpha, and Obesity: Concordance of Laboratory Animal and Human Genetic Studies. J Obes, 2011. **2011**: p. 456347.

77. Dimasi, D., W.Y. Sun, and C.S. Bonder, Neutrophil interactions with the vascular endothelium. Int Immunopharmacol, 2013.

78. Bevilacqua, M.P., et al., Identification of an inducible endothelial-leukocyte adhesion molecule. Proc Natl Acad Sci U S A, 1987. **84**(24): p. 9238-42.

79. Ley, K., et al., Sequential contribution of L- and P-selectin to leukocyte rolling in vivo. J Exp Med, 1995. **181**(2): p. 669-75.

80. Sperandio, M., et al., P-selectin glycoprotein ligand-1 mediates L-selectindependent leukocyte rolling in venules. J Exp Med, 2003. **197**(10): p. 1355-63.

81. Lentz, B.R., PEG as a tool to gain insight into membrane fusion. Eur Biophys J, 2007. **36**(4-5): p. 315-26.

82. Lawrence, M.B. and T.A. Springer, Leukocytes roll on a selectin at physiologic flow rates: distinction from and prerequisite for adhesion through integrins. Cell, 1991. **65**(5): p. 859-73.

83. Kunkel, E.J. and K. Ley, Distinct phenotype of E-selectin-deficient mice. Eselectin is required for slow leukocyte rolling in vivo. Circ Res, 1996. **79**(6): p. 1196-204.

84. Hidalgo, A., et al., Complete identification of E-selectin ligands on neutrophils reveals distinct functions of PSGL-1, ESL-1, and CD44. Immunity, 2007. **26**(4): p. 477-89.

85. Zarbock, A., C.A. Lowell, and K. Ley, Spleen tyrosine kinase Syk is necessary for E-selectin-induced alpha(L)beta(2) integrin-mediated rolling on intercellular adhesion molecule-1. Immunity, 2007. **26**(6): p. 773-83.

86. Dunne, J.L., et al., Control of leukocyte rolling velocity in TNF-alpha-induced inflammation by LFA-1 and Mac-1. Blood, 2002. **99**(1): p. 336-41.

87. Kunkel, E.J., et al., Absence of trauma-induced leukocyte rolling in mice deficient in both P-selectin and intercellular adhesion molecule 1. J Exp Med, 1996. **183**(1): p. 57-65.

88. Klein, L.M., et al., Degranulation of human mast cells induces an endothelial antigen central to leukocyte adhesion. Proc Natl Acad Sci U S A, 1989. **86**(22): p. 8972-6.

89. Christofidou-Solomidou, M., G.F. Murphy, and S.M. Albelda, Induction of Eselectin-dependent leukocyte recruitment by mast cell degranulation in human skin grafts transplanted on SCID mice. Am J Pathol, 1996. **148**(1): p. 177-88.

90. Setiadi, H. and R.P. McEver, Clustering endothelial E-selectin in clathrin-coated pits and lipid rafts enhances leukocyte adhesion under flow. Blood, 2008. **111**(4): p. 1989-98.

91. Zhang, J., et al., Regulation of endothelial cell adhesion molecule expression by mast cells, macrophages, and neutrophils. PLoS One, 2011. **6**(1): p. e14525.

92. Wang, Y. and H. Thorlacius, Mast cell-derived tumour necrosis factor-alpha mediates macrophage inflammatory protein-2-induced recruitment of neutrophils in mice. Br J Pharmacol, 2005. **145**(8): p. 1062-8.

93. Matzinger, P., Tolerance, danger, and the extended family. Annu Rev Immunol, 1994. **12**: p. 991-1045.

94. Land, W.G., Transfusion-Related Acute Lung Injury: The Work of DAMPs. Transfus Med Hemother, 2013. **40**(1): p. 3-13.

95. Bauernfeind, F., et al., Inflammasomes: current understanding and open questions. Cell Mol Life Sci, 2011. **68**(5): p. 765-83.

96. Said-Sadier, N. and D.M. Ojcius, Alarmins, inflammasomes and immunity. Biomed J, 2012. **35**(6): p. 437-49.

97. Bateman, R.M., et al., Endotoxemia increases the clearance of mPEGylated 5000-MW quantum dots as revealed by multiphoton microvascular imaging. J Biomed Opt, 2007. **12**(6): p. 064005.

98. Davies, L.C., et al., Tissue-resident macrophages. Nat Immunol, 2013. **14**(10): p. 986-95.

99. Hume, D.A., Macrophages as APC and the dendritic cell myth. J Immunol, 2008. **181**(9): p. 5829-35.

100. Barkauskas, D.S., et al., Extravascular CX3CR1+ cells extend intravascular dendritic processes into intact central nervous system vessel lumen. Microsc Microanal, 2013. **19**(4): p. 778-90.

101. Hume, D.A., Applications of myeloid-specific promoters in transgenic mice support in vivo imaging and functional genomics but do not support the concept of distinct macrophage and dendritic cell lineages or roles in immunity. J Leukoc Biol, 2011. **89**(4): p. 525-38.

102. Adachi, T., et al., Particle size of latex beads dictates IL-1beta production mechanism. PLoS One, 2013. **8**(7): p. e68499.

103. Fischer, H.C., et al., Exploring primary liver macrophages for studying quantum dot interactions with biological systems. Adv Mater, 2010. **22**(23): p. 2520-4.

104. Campbell, J.J., et al., Biology of chemokine and classical chemoattractant receptors: differential requirements for adhesion-triggering versus chemotactic responses in lymphoid cells. J Cell Biol, 1996. **134**(1): p. 255-66.

105. Dustin, M.L., et al., Induction by IL 1 and interferon-gamma: tissue distribution, biochemistry, and function of a natural adherence molecule (ICAM-1). J Immunol, 1986. **137**(1): p. 245-54.

106. Foy, D.S. and K. Ley, Intercellular adhesion molecule-1 is required for chemoattractant-induced leukocyte adhesion in resting, but not inflamed, venules in vivo. Microvasc Res, 2000. **60**(3): p. 249-60.

107. Kneilling, M., et al., Direct crosstalk between mast cell-TNF and TNFR1expressing endothelia mediates local tissue inflammation. Blood, 2009. **114**(8): p. 1696-706.

108. Kunder, C.A., A.L. St John, and S.N. Abraham, Mast cell modulation of the vascular and lymphatic endothelium. Blood, 2011. **118**(20): p. 5383-93.

109. Gordon, J.R. and S.J. Galli, Release of both preformed and newly synthesized tumor necrosis factor alpha (TNF-alpha)/cachectin by mouse mast cells stimulated via the Fc epsilon RI. A mechanism for the sustained action of mast cell-derived TNF-alpha during IgE-dependent biological responses. J Exp Med, 1991. **174**(1): p. 103-7.

110. Boyce, J.A., Mast cells and eicosanoid mediators: a system of reciprocal paracrine and autocrine regulation. Immunol Rev, 2007. **217**: p. 168-85.

111. Reichel, C.A., et al., Ccl2 and Ccl3 mediate neutrophil recruitment via induction of protein synthesis and generation of lipid mediators. Arterioscler Thromb Vasc Biol, 2009. **29**(11): p. 1787-93.

112. Oka, T., et al., Evidence questioning cromolyn's effectiveness and selectivity as a 'mast cell stabilizer' in mice. Lab Invest, 2012. **92**(10): p. 1472-82.